# Control of Sound Radiation From Structures with Periodic Smart Skins

Arthur Blanc

Thesis submitted to the Faculty of the
Virginia Polytechnic Institute and State University
in partial fulfillment of the requirements for the degree of

Master of Science
in
Mechanical Engineering

Chris R. Fuller, Chair
Ricardo A. Burdisso
Marty E. Johnson

July 27, 2001
Blacksburg, Virginia

Keywords: structural acoustics, periodic structures, sound radiation, smart skin

# Control of Sound Radiation From Structures with Periodic Smart Skins

By
Arthur Blanc
Committee chairman: Chris R. Fuller, Mechanical Engineering.

(ABSTRACT)

An innovative implementation of the skin concept for the reduction of the radiated sound power from a vibrating structure is proposed. The skin has a periodic structure and continuously covers a vibrating beam. Thus, this skin decouples the vibrating structure from the acoustic field by modifying the wavenumber spectrum of the radiating surface. First, structural acoustics and periodic structure theories are reviewed in order to predict how bending waves propagate along a periodic beam and how this beam radiates sound. These theories are then extended to the case of multi-layered structures in order to understand the behavior of a beam loaded with a periodic skin. In order to design the beam and skin structural periods, two different methods are used: Galois sequences and an optimization process using a real-valued genetic algorithm. Simulations are run for the case of periodic beams and beams coupled with periodic smart skins in both finite and infinite configurations. Results show that periodic beam can radiate less sound than equivalent uniform structures. Results also show the potential of periodic skin for application to the structural radiation problem for frequencies higher than approximately 100Hz with an approximately 10dB of radiated sound power attenuation.

# Acknowledgments

I appreciate Professor Chris Fuller, Professor Ricardo Burdisso and Professor Marty Johnson for serving on my committee as well as allowing me to go to see the corn grow near Purdue University.

I am very grateful to my friend Pierre Marcotte who sheltered me, fed me and even cured me during my darkest times in Blacksburg. In addition, I wish to thank Pierre for the useful, and the less useful discussions that helped me progress through this work.

Finally, my parents deserve all my gratitude for their endless moral support, their advice and for the freedom they gave me to follow my own path.

# Contents

# List of Figures

# List of Tables

# Introduction

Reducing noise emissions has become a political and economical issue as the number of polluting sound sources has constantly been increasing. Sound is usually a direct consequence of the deformation of an elastic structure undergoing some excitation. For a long time, remedies for the reduction of sound radiation were based on very simple treatments designed to alter this deformation. Mass-loading is the easiest to implement but is not viable for the aerospace industry where every added gram has a cost. Another solution is to add damping to the structure, usually by attaching a constrained viscoelastic material that will dissipate some of the vibrational energy. However, all these passive treatments have not been very effective at low frequencies ($< 500$Hz) unless much material is used. As adding more material also increases the mass of the global system, new solutions for applications where weight is a critical factor have to be found.

## Context

New developments in electronics and digital technologies have been at the origin of various approaches to actively control the sound radiated by a structure. Active noise control (ANC) is based on the principle of the destructive interference between a primary noise source and a secondary source. A controller governs the output of the secondary source to achieve the best control. Theories and techniques were compiled by Nelson and Elliott [1] and successful applications have been found in the car industry [2, 3], for heating, ventilating and air conditioning (HVAC) systems [4] or communication headsets [5] to name a few.

Although ANC has shown to be effective for controlling simple acoustic fields, it requires that actuators (speakers for example) are physically within the sound field of interest. This may not be achievable in situations such as a moving source radiating sound in an unknown environment. Thus, an alternative method is to reduce the sound radiation directly at the source. An example of this technique is called Active Structural Acoustic Control (ASAC) and was introduced by Fuller in [6]. By actively attenuating vibrational

amplitudes and changing the modal distribution of the structure, it becomes possible to attenuate the energy radiated in the acoustic sound field.

Different actuators to perform control can be used. The tuned vibration absorber (TVA) [7, 8] can be either a passive or an active-passive device. The absorber is designed for a specific frequency and cannot provide broadband control (the range of action can be "broadened" by adding damping but this will reduce the maximum attenuation at the design frequency). In addition, in order to be most effective, a TVA has to be located at an anti-node of the mode it controls. Thus, it is necessary to know the modal response of the structure as well as the frequency of excitation. This makes this device suitable only for special cases, as for example the control of the noise induced by the blade passage frequency in a propeller aircraft.

Since superposing two waves out of phase may be difficult at high frequencies ($> 1000$Hz), ASAC only gives good results at lower frequencies. Therefore, new devices have been developed to combine the advantages of both active and passive control in order to extend the bandwidth and the efficiency of the control. Active constrained layer damping (ACLD) is an actuator using viscoelastic layer sandwiched between the structure and a piezo constraining layer. The viscoelastic layer adds damping to the structure and the piezo actuator tries to maximize the energy dissipated in the viscoelastic layer by constraining that layer. While ALCD gives very good theoretical results [9], its application remains not completely convincing as a the energy input into the piezo layer is partially dissipated into the damping material.

An evolution of the TVA concept called distributed active vibration absorber (DAVA) [10] was developed at Virginia Tech. A DAVA is made of a mass layer coupled with an elastic/active layer made with a curved polymer piezoelectric sheet. The active layer acts as a distributed spring and, when a voltage is applied to the piezoelectric element, as an actuator by exciting the mass layer and applying a force to the structure. By optimizing the mass distribution of the mass layer, the mean square velocity of the structure can be minimized and thus less sound is radiated. DAVAs offer promising results for low frequencies and broadband control as long as the actuator can show authority on the structure. However, though DAVAs reduce the vibrations of the structure, the motion of the DAVA mass layer may increase the radiated sound power on the side where the treatment is applied.

In addition, there are a few drawbacks to active control. The main one is the introduction of additional energy in the system: actuators add mechanical or acoustical energy. In certain situations, such an addition may yield to an increase of the radiated sound power. The input energy is usually brought by external power supplies that adds weight to the global system. Furthermore, active control requires the design of a controller that may become unstable and create a worst situation than without control. Finally, active systems are usually expensive since one needs additional power, actuators, sensors and controller

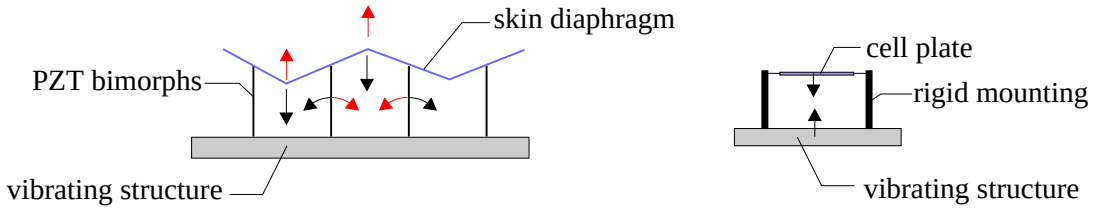


a) Active skin. From [12]. b) Passive skin. From [13].

Figure 1: Different skin concepts

and the reliability is not always guaranteed. Therefore, one may be tempted to investigate simpler passive solutions to the problem of sound radiation control.

Finally, a new approach to the problem of sound radiation control is to decouple the radiating structure from the acoustic field by adding a smart or active skin instead of modifying structural vibration. Thus, smart skins are suitable to control the radiated sound power of structures for which a large driving force would be required to achieve structural control. The main trade-off of smart skin approach is that the skins need to cover all the radiating surfaces. Gentry *et al.* [11] designed a smart foam skin made of acoustic foam and a curved PVDF element. The foam acts as a passive treatment for high frequencies ($>$ 1000Hz) while the active element is used to control lower frequencies by reducing the normal motion of the skin element. These smart skins showed good results for controlling the sound radiated from a plate in the low and high-frequency range. Johnson and Fuller [12] developed an active skin made of independent skin cells that modify the impedance radiation of a clamped plate. Each skin element is a small acoustic transducer made with piezoelectric (PZT) bimorphs that can move a diaphragm with a normal motion with respect to the vibrating structure (see figure 1-a). The PZT bimorphs are actively controlled to minimize an acoustic cost function. This design showed good broadband attenuation of the radiated sound power. Finally, Ross and Burdisso [13] investigated a passive skin element. It is a single degree of freedom (SDOF) system (the mass is a rigid plate, see figure 1-b). Above its resonance frequency, a SDOF system vibrates out of phase with respect to the excitation. Therefore, if the skin element mass vibrates out of phase with the excitation base, the coupled structure behaves like a weak sound radiator (an acoustic dipole is a less efficient sound radiator than a piston). Conceptually, if a large vibrating structure is divided into small partitioned areas that behave as pistons, an array of weak radiating cells can be distributed on each of these partitioned areas. Therefore, the coupled structure behaves as a distribution of dipoles instead of a distribution of monopoles and the overall sound radiated by the structure is minimized.

In this thesis, we intend to investigate a new smart skin based upon periodic structures and designed to minimize sound radiation by affecting the component wavenumbers of the beam response.

## Objectives

The scope of this research is the study of a light weight passive treatment based on periodic structures to reduce sound radiation: a light continuous periodic skin with a poor radiation efficiency is coupled to the vibrating structure. This is illustrated in figure 2. We want to investigate that if the motion of the skin is mainly governed by the skin dynamics, the coupled structure will become a poor radiating structure. This approach is thus equivalent to the theoretical concept of arrays of weak radiating elements [13] since it is passive and the vibration of the skin motion will determine how much sound is radiated. However, it also differs from the weak radiating cells since the skin is a continuous medium, it is conceptually less complex and the motion of the skin may not necessarily be out of phase compared to the motion of the vibrating structure in order to be a poor sound radiator.

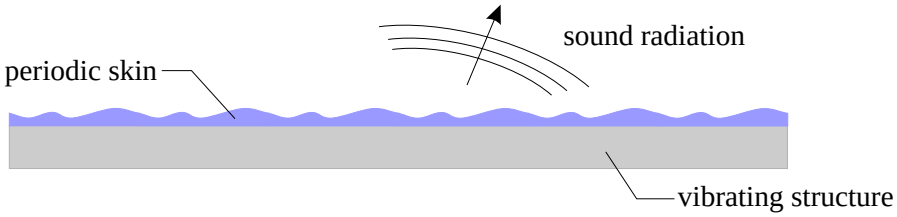


Figure 2: Concept of a periodic skin for sound radiation control

In order to achieve these objectives, numerical methods have to be developed to predict if the bending wavenumbers in a periodic structure can be modified to ensure that the structure is subsonic, i.e. the periodic structure should be made a poor sound radiator in the design region. The current research also investigates how the sound radiation of a simply supported beam can be modified by repeating a structural pattern in order to alter its radiating efficiency. As it may not be possible to alter the response of the vibrating structure, multi-layered structure configurations (e.g. the original structure is loaded with a periodic skin) are investigated in order to decouple the sound field from the vibrating structure.

## Organization

The thesis is arranged as follows. The first chapter is a brief review of structural acoustics. It introduces the basic concepts about bending wave and sound radiation. The second chapter presents the various theoretical principles about periodic structures that were used in the thesis. The third chapter introduces real-valued genetic algorithm optimization technique as a mean to design the periodic structures. The fourth chapter investigates

how single layered structure can be modified in order to reduce wave propagation if they are infinite or radiated sound power if they are finite. Finally, the fifth chapter presents a theoretical investigation of bending waves in multi-layered structure, and more specifically of a 2-layer structure for sound radiation control. This chapter introduces the passive skin approaches based on periodic structure and investigates their potential. The thesis ends with conclusions and recommendations for future work.

# Chapter 1

# Structural Acoustic Fundamentals

This chapter presents the main acoustic and vibration theoretical tools needed to understand the work presented in this thesis. The derivation of the bending wave equation of a uniform beam with constant cross-sectional area $S$ and moment of inertia $I$ is presented. A brief review of sound radiation for finite and infinite beams is included.

## 1.1 The bending wave equation

The vibration of a beam can be decomposed as the sum of three different kinds of waves: compressive, rotational and bending waves. Since sound radiation is our only concern, we shall only focus on the transversal waves. The following derivation of the equation for bending waves is based upon that presented in [14] by Junger and Feit.

The Bernoulli-Euler theory for beams assumes that there is no deformation of the cross-section (i.e. the beam has an infinite high shear stiffness) and that rotational inertia can be ignored. Such assumptions are only valid if the bending wavelength is much larger than the thickness of the beam.

The longitudinal displacement $u(x,t)$ can be written as a function of $w(x,t)$ and $\xi$, where $\xi$ is the distance between the neutral axis and the point of evaluation as presented on figure 1.1:

$$u(x,t) = -\xi \frac{\partial w(x,t)}{\partial x} \tag{1.1}$$

Substituting $u(x,t)$ from the previous equation into Hooke's law ($\sigma = E\frac{\partial u(x,t)}{\partial x}$) gives the

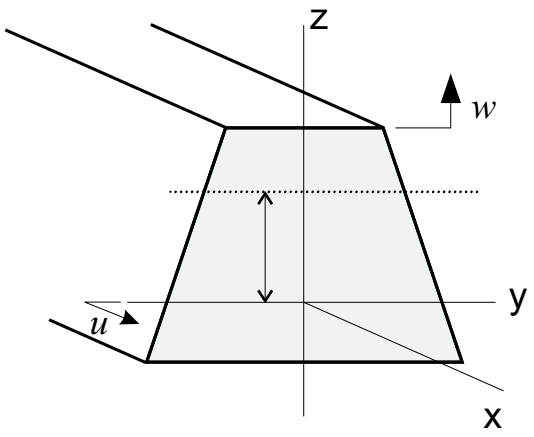


Figure 1.1: Cross-section of a beam at position x

expression of the stress in the beam:

$$\sigma = -\xi E \frac{\partial^2 w(x,t)}{\partial x^2} \tag{1.2}$$

The expression of the bending moment in a beam as a function of the stress is given by:

$$M(x,t) = \iint_S \xi \sigma \mathrm{d}S \tag{1.3}$$

$$\Rightarrow M(x,t) = -E \frac{\partial^2 w(x,t)}{\partial x^2} \iint_S \xi^2 \mathrm{d}S \tag{1.4}$$

The cross-sectional area moment of inertia $I(x)$ is defined as $I(x) = \iint_S \xi^2 \mathrm{d}S$. Therefore, the bending moment due to a bending deformation is:

$$M(x,t) = -EI(x) \frac{\partial^2 w(x,t)}{\partial x^2} \tag{1.5}$$

If a small distant $\Delta x$ is considered, the expressions for $M(x+\Delta x,t)$ and $F(x+\Delta x,t)$ can be expanded about $x$ using Taylor's expansion. Neglecting the second and higher order terms, this yields

$$F(x+\Delta x,t) = F(x,t) + \frac{\partial F(x,t)}{\partial x} \tag{1.6}$$

$$M(x+\Delta x,t) = M(x,t) + \frac{\partial M(x,t)}{\partial x} \tag{1.7}$$

The moment equilibrium equation at point $P$ (see figure 1.2) is:

$$M(x+\Delta x,t) - M(x,t) + F(x+\Delta x,t)\Delta x - [q(x,t)\Delta x]\frac{\Delta x}{2} = 0 \tag{1.8}$$

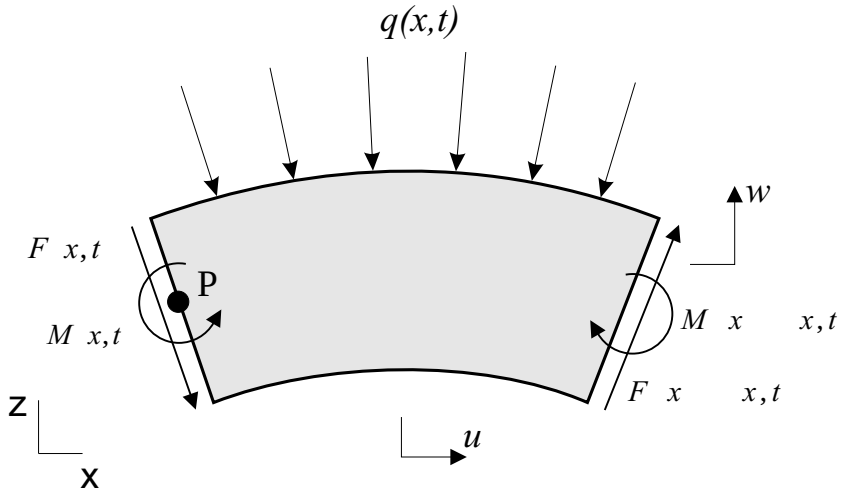


Figure 1.2: Forces and moments on a bar element of length $\Delta\ x$

where $q(x,t)$ is the distributed load along the considered element. Substituting equation (1.6) and equation (1.7) in equation (1.5) yields

$$\left[\frac{\partial M(x,t)}{\partial x} + F(x,t)\right]\Delta x + \left[\frac{\partial F(x,t)}{\partial x} - \frac{q(x,t)}{2}\right]\Delta x^2 = 0 \tag{1.9}$$

Considering that $\Delta x$ is very small, the second term can be neglected. However, because $\Delta x$ is not equal to zero, $\left[\frac{\partial M(x,t)}{\partial x} + F(x,t)\right] = 0$ has to be true. Therefore

$$F(x,t) = -\frac{\partial M(x,t)}{\partial x} \tag{1.10}$$

Substituting equation (1.5) into the previous equation yields

$$F(x,t) = EI\frac{\partial^3 w(x,t)}{\partial x^3} \tag{1.11}$$

Applying Newton's second law to the beam element yields

$$F(x+\Delta x,t) - F(x,t) - q(x,t)\Delta x = \rho S(x)\Delta x\frac{\partial^2 w(x,t)}{\partial x^2} \tag{1.12}$$

Finally, the bending wave equation is

$$\frac{\partial^2}{\partial x^2}\left[EI(x)\frac{\partial^2 w(x,t)}{\partial x^2}\right] + \rho S(x)\frac{\partial^2 w(x,t)}{\partial t^2} = -q(x,t) \tag{1.13}$$

Up to this point in the derivation, the cross section of the beam $S(x)$ could possibly vary as a function of the position $x$. For example, this allows us to analyze beams where the

cross-sectional area moment of inertia $I$ is a periodic function. However, if $S(x)$ remains constant along a beam element with homogeneous physical properties, i.e. $EI$ is also constant with regard to $x$, equation (1.13) can be simplified

$$EI\frac{\partial^4 w(x,t)}{\partial x^4} + \rho S\frac{\partial^2 w(x,t)}{\partial t^2} = -q(x,t) \tag{1.14}$$

If no force distribution is applied on the beam, equation (1.14) reduces to:

$$EI\frac{\partial^4 w(x,t)}{\partial x^4} + \rho S\frac{\partial^2 w(x,t)}{\partial t^2} = 0 \tag{1.15}$$

### 1.1.1 Solution of the bending wave equation

The bending wave equation is a fourth order differential equation and therefore differs from the acoustic wave equation (second order differential equation). However, we can seek a solution to equation (1.15) by setting:

$$w(x,t) = Ae^{j(-kx+\omega t)} \tag{1.16}$$

This yields

$$EIk^4 - \rho S\omega^2 = 0 \tag{1.17}$$

We can now solve for the bending wave number:

$$k^4 = \frac{\omega^2 \rho S}{EI} \tag{1.18}$$

Equation(1.18) has four solutions:

$$k_{propagative(+,-)} = \pm k_b$$
$$k_{evanescent(+,-)} = \pm jk_b$$

where

$$k_b = \left|\sqrt{\omega}\sqrt[4]{\frac{\rho S}{EI}}\right| \tag{1.19}$$

The global solution of equation (1.15) can be written as a sum of all the four solutions of equation (1.18)

$$w(x,t) = [Ae^{-jk_b x} + Be^{-k_b x} + Ce^{jk_b x} + De^{k_b x}]e^{j\omega t} \tag{1.20}$$

where $A$, $B$, $C$ and $D$ are complex constants. Because of the different notations used around the world, we choose the following convention:

- the $A$ term is for the waves propagating in the positive direction
- the $B$ term is for the evanescent waves going in the positive direction
- the $C$ term is for the waves propagating in the negative direction
- the $D$ term is for the evanescent waves going in the negative direction

This is summarized in figure 1.3

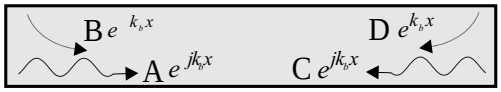


Figure 1.3: Convention used for directions of waves in a beam

The evanescent waves cannot be neglected if there is any change of impedance on the beam (point force, boundaries,...).
If we consider finite beam, or a finite beam element, equation (1.20) can be rewritten as:

$$w(x,t) = [C_1 \cosh k_b x + C_2 \sinh k_b x + C_3 \cos k_b x + C_4 \sin k_b x] e^{j\omega t} \tag{1.21}$$

where $C_1$, $C_2$, $C_3$ and $C_4$ are real constants. Such a formulation is very practical because $w(x,t)$ is real and allows easier computations. However, some physical meaning is lost in such a description since it is not clear what propagates and what disappears in the far field.

### 1.1.2 Bending wave velocity

Equation(1.19) shows that there is not a linear relation between the wave number $k$ and the circular frequency $\omega$. The velocity $c$ is given by

$$c = f\lambda = \frac{\omega}{2\pi}\frac{2\pi}{k} = \frac{\omega}{k} \tag{1.22}$$

Substituting $k$ in the previous equation by equation (1.19) yields

$$c_b = \sqrt{\omega}\sqrt[4]{\frac{EI}{\rho S}} \tag{1.23}$$

where $c_b$ is the bending wave velocity. This velocity depends on frequency since it follows the square root of the circular frequency. Such a wave type is called dispersive.

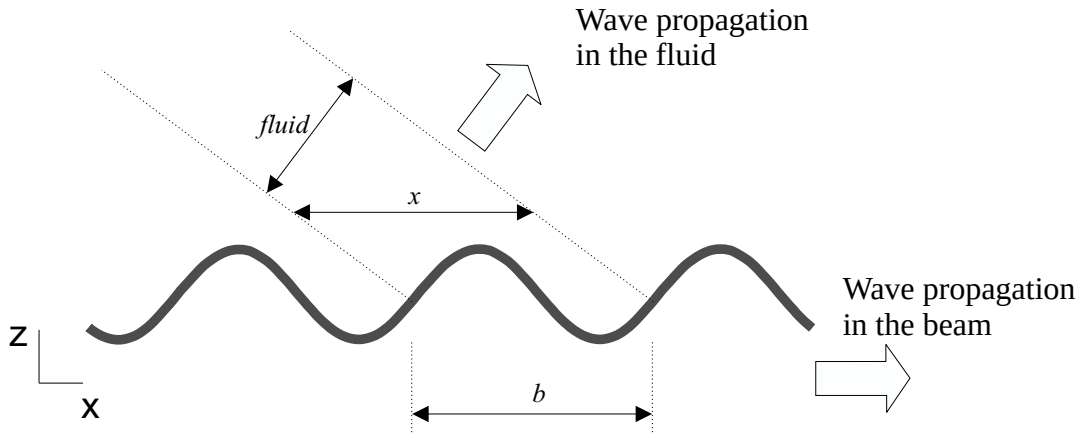


Figure 1.4: Wavelength projection

## 1.2 Sound radiation

### 1.2.1 Infinite structure

An infinite beam is considered as a one-dimension waveguide, i.e. the bending waves propagate along one dimension. The corresponding bending wave number has therefore only one directional component ([1×1] vector). The fluid is a two-dimension domain([2×1] vector). The wave number in the fluid can be decomposed as:

$$\vec{k}_{fluid} = \vec{k}_x + \vec{k}_z \tag{1.24}$$

$$\Rightarrow k_z = \pm\sqrt{k_{fluid}^2 - k_x^2} \tag{1.25}$$

The boundary condition on the surface of the beam is the normal velocity of the beam has to be equal to the particle velocity of the fluid. This is equivalent to say that the particle displacement has to be the same at the interface between the two media. Therefore, the axial wavelength in the beam has to be equal to the projected wavelength component $\lambda_x = \lambda_b$ (see figure 1.4). The wave number is related to the wavelength by

$$k = \frac{2\pi}{\lambda} \tag{1.26}$$

Therefore, at the interface, $k_x = k_b$. Replacing $k_x$ in equation (1.25) yields

$$k_z = \pm\sqrt{k_{fluid}^2 - k_b^2} \tag{1.27}$$

Equation (1.27) admit two different kinds of solutions:

- if the wave number in the beam $k_b$ is smaller than the wave number in the fluid $k_{fluid}$ then $k_z$ is a real number. Therefore, a wave will propagate within the fluid and the beam will be a strong sound radiator. The pressure becomes

$$p(x,z,t) = \omega\rho_0 \frac{\parallel \dot{w} \parallel}{\sqrt{k_{fluid}^2 - k_b^2}} e^{-jk_x x} e^{-j\sqrt{k_{fluid}^2 - k_b^2}z} e^{j\omega t} \tag{1.28}$$

  The frequency range where such a case applies is called the *supersonic* region.

- if the wave number in the beam $k_b$ is bigger than the wave number in the fluid $k_{fluid}$, then $k_z$ is purely imaginary ($k_z = \pm j\sqrt{k_b^2 - k_{fluid}^2}$). No acoustic waves will propagate since the results corresponds to an evanescent wave but a near field will be present. The pressure becomes

$$p(x,z,t) = j\omega\rho_0 \frac{\parallel \dot{w} \parallel}{\sqrt{k_{fluid}^2 - k_b^2}} e^{-jk_x x} e^{-\sqrt{k_{fluid}^2 - k_b^2}z} e^{j\omega t} \tag{1.29}$$

  The frequency range where such a case applies is called the *subsonic* region.

The case where $k_{fluid} = k_b$ is called the cutoff frequency. These supersonic and subsonic regions as a function of frequency and the wave numbers are presented in figure 1.5. One of the goals of sound radiation control is to make the cut-off frequency as high as possible in order to have a a wide frequency range where the radiation efficiency is low.

Another way of considering the problem is to look at the particle velocity in the different media. If, for a given frequency range, the waves in the beam travel slower than the waves in the fluid, this is a subsonic region. The comparison of the velocity of bending waves and the speed of sound in air is illustrated in figure 1.6 (note: the velocities have been normalized with respect to the velocity of waves in air). Finally, we say that a medium $M$ is acoustically slow with respect to a medium $N$ if the propagating waves in $M$ are slower than the propagating waves in $N$.

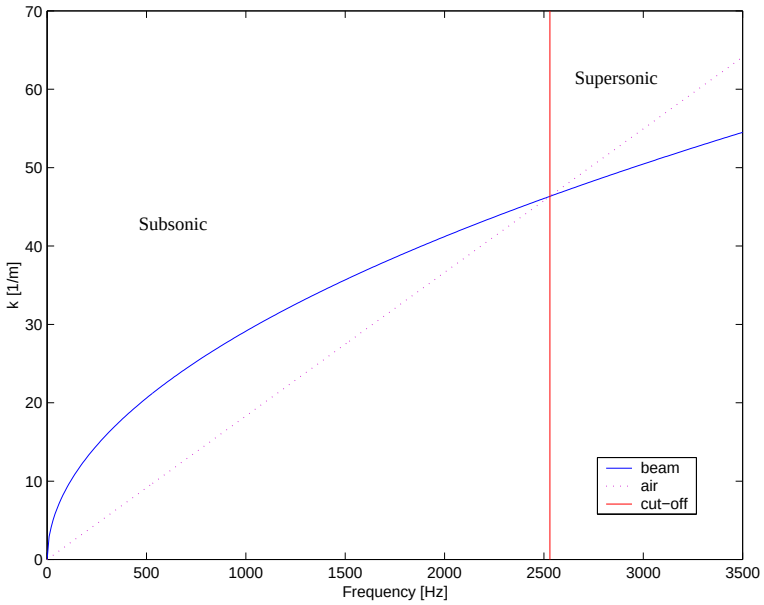


Figure 1.5: Wave number in air and in a beam

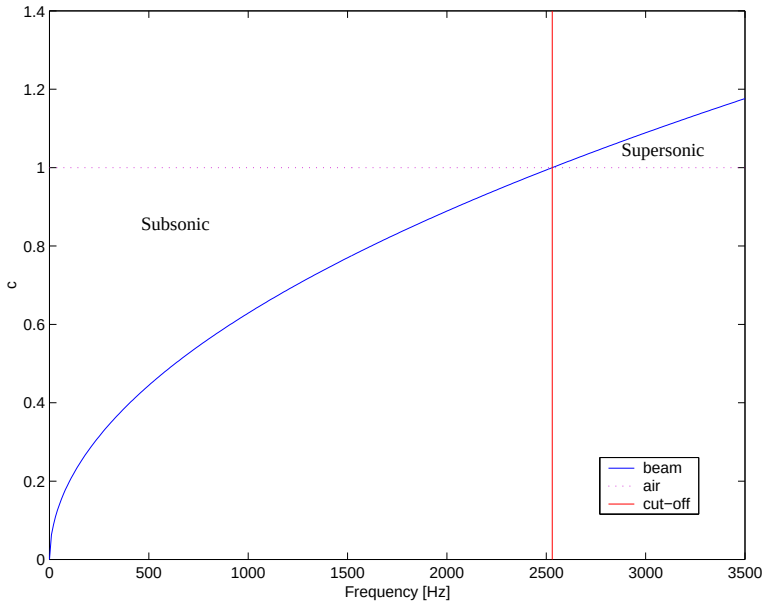


Figure 1.6: Wave velocities normalized with respect to the speed of sound

### 1.2.2 Finite structure

#### Rayleigh's integral

In order to compute the pressure field radiated by a structure, the easiest way to proceed is to use the Rayleigh's integral, or its discrete formulation. Instead of considering a vibrating structure, we assume we have an infinitely rigid structure in front of which there is a distribution of monopoles. The source strength of each monopole is found by evaluating the volume of air displaced by the real structure. If we add the contribution of each equivalent sources, we get the sound pressure field at a point $M$ (see figure 1.7) using

$$p(R,t) = j\omega\rho_0 \sum_p \frac{\dot{w}(x)S_p}{2\pi r} e^{-jk_{fluid}r} e^{j\omega t} \tag{1.30}$$

with $r = \mid R - r_s \mid$ and $S_p$ the surface of each equivalent piston source.

If we have a continuous field of sources, we can rewrite equation (1.30) as the Rayleigh's integral formulation:

$$p(R,t) = j\omega\rho_0 \int_S \frac{\dot{w}(r_s)}{2\pi r} e^{-jk_{fluid}r} dS e^{j\omega t} \tag{1.31}$$

Equation (1.30) and equation (1.31) only give accurate results if the wavelength is much bigger than the piston dimension and if the observer point is in the far field (the near field component cannot be reproduced by the single sum of elementary sources). We also assume that the radiator is in a baffle so that no acoustic shortcut can occur.

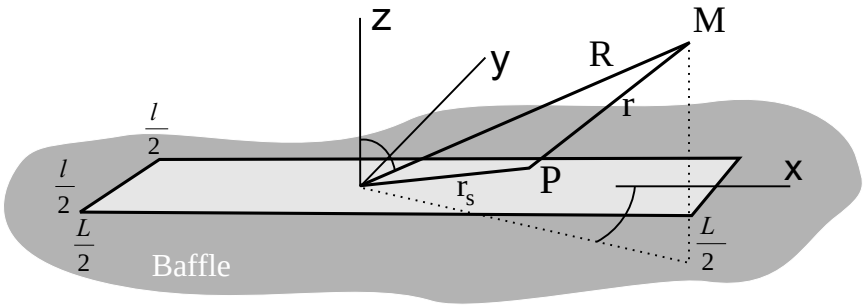


Figure 1.7: Coordinate system for the finite beam

**Radiated acoustic power**

Integrating the mean square of the pressure in the far-field over a hemisphere gives the total acoustic power $\Pi$ radiated by the structure:

$$\Pi = \frac{1}{2\rho_0 c} \int_S \mid p(R,\theta,\phi) \mid^2 dS \tag{1.32}$$

Such a formula assumes that we either have an expression for the pressure as a function of the position $(R,\theta,\phi)$ or that we have an estimate of $p$ at several points in space using the Rayleigh's integral. However, since we are also interested in the spectral content of the beam, the computation of the radiated power $\Pi$ can be done using the wavenumber transform as it is presented by Fahy in [15].

For the case of the beam with no cross-section deformation and harmonic excitation, we can get a far-field approximation of the radiated acoustic pressure [16]:

$$p(R,k_x,k_y) = -\frac{\omega^2\rho_0}{2\pi}\frac{e^{-jk_{fluid}R}}{R}\hat{W}(k_x,k_y) \tag{1.33}$$

where $\hat{W}(k_x,k_y)$ is the 2D wavenumber transform of the beam displacement and $k_x$ and $k_y$ are the components of the structural wavenumber along the $x$ and $y$-axis such that

$$k_x = k_{fluid}\cos\theta\sin\phi \tag{1.34}$$

$$k_y = k_{fluid}\sin\theta\sin\phi \tag{1.35}$$

and where $R$, $\theta$ and $\phi$ are the spherical coordinates of the observer point $M$ (see figure 1.7). Using the fact that the displacement of the beam along the $y$-direction remains constant, we can simplify the expression of $\hat{W}(k_x,k_y)$ with

$$\hat{W}(k_x,k_y) = \frac{2\sin(\frac{k_y l}{2})}{k_y}\int_{-L/2}^{L/2} w(x)e^{-jk_x x}dx \tag{1.36}$$

where $l$ is the beam width and $L$ is the beam length. Since the beam is baffled, the term $\hat{W}(k_x) = \int_{-L/2}^{L/2} w(x)e^{-jk_x x}dx$ in equation (1.36) is equivalent to the wavenumber transform of the beam displacement along the $x$ axis. Thus, equation (1.36) is rewritten as

$$\hat{W}(k_x,k_y) = \frac{2\sin(\frac{k_y l}{2})}{k_y}\hat{W}(k_x) \tag{1.37}$$

Substituting equation (1.33) in equation (1.32) and taking into account that only supersonic structural waves radiate sound in the far field yields

$$\Pi = \frac{\rho_0\omega^3}{8\pi^2}\int_{-k_{fluid}}^{k_{fluid}}\int_{-\sqrt{k_{fluid}^2-k_x^2}}^{\sqrt{k_{fluid}^2-k_x^2}} \frac{\mid \hat{W}(k_x,k_y) \mid^2}{\sqrt{k^2-k_x^2-k_y^2}}dk_y dk_x \tag{1.38}$$

The previous equation is the general solution for a plate. Substituting equation (1.37) in equation (1.38) yields

$$\Pi = \frac{\rho_0 \omega^3}{8\pi^2} \int_{-k_{fluid}}^{k_{fluid}} \int_{-\sqrt{k_{fluid}^2 - k_x^2}}^{\sqrt{k_{fluid}^2 - k_x^2}} \left( \frac{2\sin(\frac{k_y l}{2})}{k_y} \right)^2 \frac{\mid \hat{W}(k_x) \mid^2}{\sqrt{k^2 - k_x^2 - k_y^2}} dk_y dk_x \tag{1.39}$$

For a narrow beam ($\mid k_y \frac{l}{2} \mid \ll 1$), we can rewrite previous equation as

$$\Pi = \frac{\rho_0 \omega^3}{8\pi^2} \int_{-k_{fluid}}^{k_{fluid}} \int_{-\sqrt{k_{fluid}^2 - k_x^2}}^{\sqrt{k_{fluid}^2 - k_x^2}} l^2 \frac{\mid \hat{W}(k_x) \mid^2}{\sqrt{k^2 - k_x^2 - k_y^2}} dk_y dk_x \tag{1.40}$$

Noting that $\int \frac{dX}{\sqrt{a^2 - X^2}} = \arcsin \frac{X}{a}$ and making the change of variables $X = k_y$ and $a^2 = k^2 - k_x^2$, equation (1.40) can be rewritten as

$$\Pi = \frac{\rho_0 \omega^3 l^2}{8\pi^2} \int_{-k_{fluid}}^{k_{fluid}} \left[ \arcsin \frac{k_y}{\sqrt{k_{fluid}^2 - k_x^2}} \right]_{k_y = -\sqrt{k_{fluid}^2 - k_x^2}}^{\sqrt{k_{fluid}^2 - k_x^2}} \mid \hat{W}(k_x) \mid^2 dk_x \tag{1.41}$$

$$= \frac{\rho_0 \omega^3 l^2}{8\pi^2} \int_{-k_{fluid}}^{k_{fluid}} \left[ \frac{\pi}{2} + \frac{\pi}{2} \right] \mid \hat{W}(k_x) \mid^2 dk_x \tag{1.42}$$

Thus, the acoustic power radiated by a narrow beam is given by

$$\Pi = \frac{\rho_0 \omega^3 l^2}{8\pi} \int_{-k_{fluid}}^{k_{fluid}} \mid \hat{W}(k_x) \mid^2 dk_x \tag{1.43}$$

Using equation 1.43, we can get the sound power radiated by a simply supported beam as a function of frequency. Let us consider a beam which is 0.8m long, 0.024m wide and 0.003m thick. It is made out of steel (Young's Modulus $E = 210$GPa and damping factor $\eta = 0.005$). The beam is excited by a unit point force at the point x=0.232m, y=0m (the coordinate system was introduced in figure 1.7). The radiated sound power is presented in figure 1.8 . The numbers on the plot correspond to the modal order of the beam response, i.e. the number 1 is for the first mode, etc.

At low frequencies, i.e. where the excitation frequency is below the critical frequency and where the wavelength is not very small with respect to the beam length ($\mid k_{fluid} l \mid \ll 1$), it appears clearly that odd modes usually radiates more sound than even ones. This can be explained by considering how air is displaced in front of the beam. Successive out-of-phase areas (represented by + and − on figure 1.9) cancel out and therefore, lower the global volume of air displaced by the beam. However, volume displaced by the cells at the edges remain partly uncancelled by the nearest out-of-phase cell. Two different cases can occur:

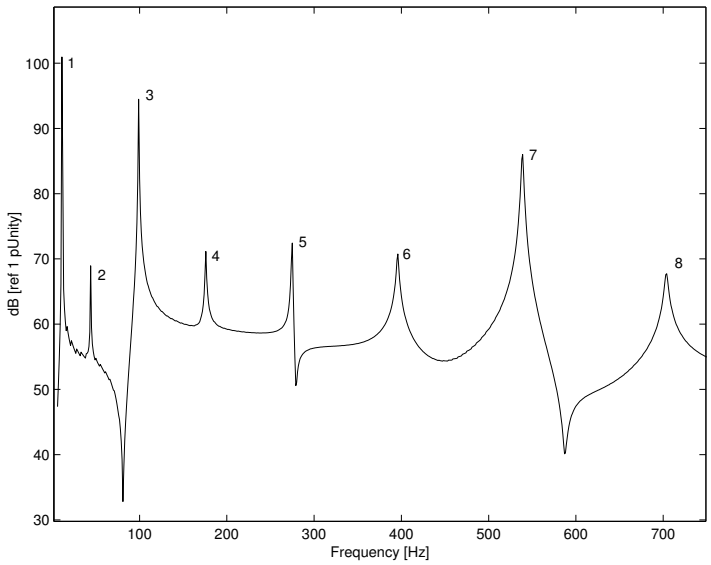


Figure 1.8: Sound power radiation from a simply supported beam

- Even modes have an antisymmetric vibrational pattern. The non-cancelling regions at the edges have volume velocities out-of-phase. This is a less effective sound radiator than the previous case since cancellation between the air displaced by the edges will occur.
- Odd modes have a symmetric vibrational pattern. The non-cancelling regions at the edges have volume velocities in phase.

This effect is very pronounced between the first and second mode.

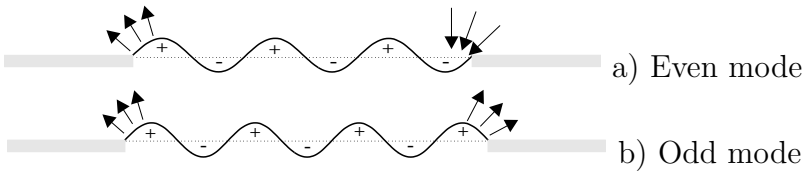


Figure 1.9: Intercell cancellation and edge radiation pattern at low frequencies

At higher frequencies ($kl > 1$), the cells radiate independently.

**Sound radiation control strategy**

It should be clear by now that modifying the vibrational pattern of a beam can help in reducing its overall sound radiation at low frequencies. Firstly, the beam should be acoustically slow on a frequency band as wide as possible. In the case of an infinite structure, we have seen that no sound is radiated in the far field below the critical frequency. For a finite structure, we computed power by integrating the energy spectrum $\mid \partial w(k_x/\partial t \mid^2$, only considering the energy spectrum for bending wavenumbers $k_x$ below the acoustic wavenumber $k$. If we plot the energy spectrum (see figure 1.10) for a baffled beam, the power is proportional to the integration of the energy spectrum (c.f. equation 1.43). We notice that most energy is concentrated around the structural cutoff frequency (the corresponding wavenumber is noted $k_c$). In order to avoid radiating a lot of sound, we should try to have a structure excited lower than the cutoff frequency or try to reject the cutoff frequency as high as possible, i.e. make the beam acoustically slow.

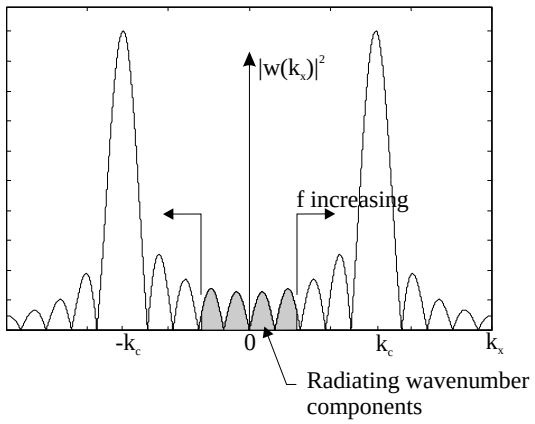


Figure 1.10: Identification of radiating wavenumber components. From Fahy [15].

Secondly, the beam displacement should be as small as possible in order to minimize the normal velocity at the surface of the beam. An example of two different envelops is shown in figure 1.11. The displacement envelop of beam 1 is much larger than the envelop of beam 2. The power radiated is directly related to the displacement ($\Pi$ is proportional to $\mid w(x) \mid^2$). Thus, if the displacement envelop along the beam is doubled, the radiated power increases by 6dB.

Finally, we can consider the radiation efficiency [17] of a baffled beam as a function of its modal order $n$. The radiation efficiency $\sigma$ is defined as:

$$\sigma = \frac{\Pi(f)}{\rho c S <\mid \dot{w}(f) \mid^2>} \tag{1.44}$$

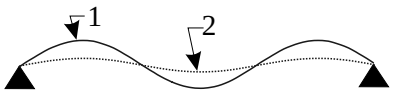


Figure 1.11: Minimization of the beam displacement envelops

where $\Pi$ is the radiated power by the $n^{th}$ mode at a frequency $f$ and $<|\ \dot{w}(f)\ |^2>$ denotes the mean-square velocity averaged over the surface of the beam. $\sigma$ measure how efficient with respect to an equivalent piston source (a very efficient sound radiator), one structural mode radiates sound. It appears that below the cutoff frequency $f_c$, odd modes are more efficient sound radiator than even modes. This is presented on the radiation efficiency plot (see figure 1.12). The index $n$ indicates the mode order, i.e. $n = 1$ is for the first mode, etc. Thus, another control strategy for a finite beam is to shift some structural energy from efficient (odd) modes to poor radiating (even) modes if the structure is excited below $f_c$.

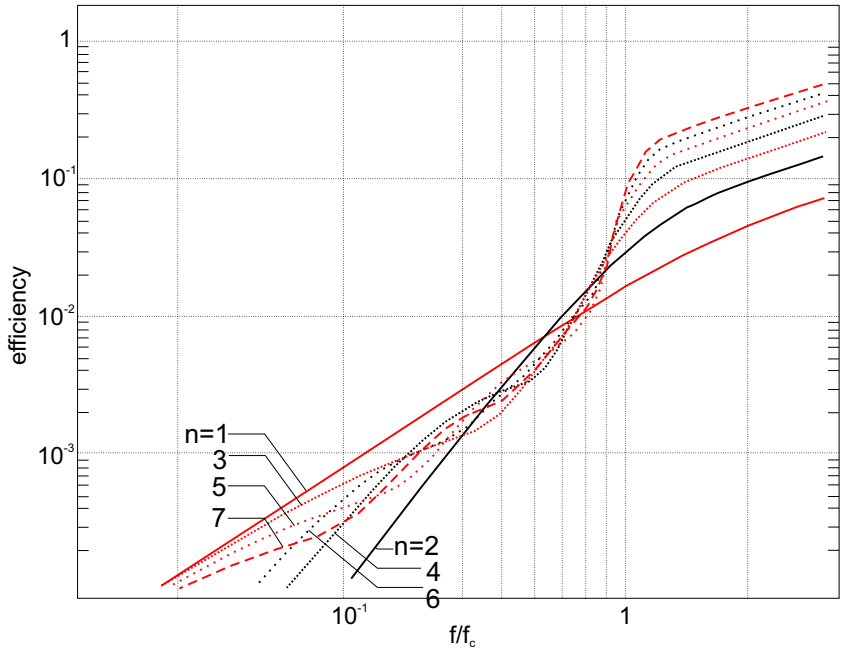


Figure 1.12: Radiation efficiency of a baffled beam. From Wallace [17]

# Chapter 2

# Periodic Structures

A structure is considered periodic if it can be described by only one repeated element that is connected to identical elements in an identical manner. Each element corresponds to one structural period. This is illustrated in figure 2.1.

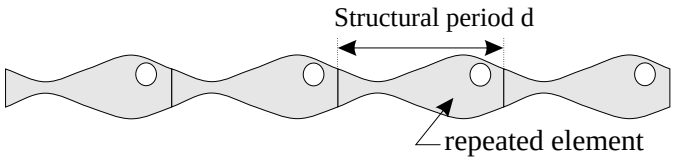


Figure 2.1: Illustration of a periodic structure

In this research, periodic structures are investigated as a means to control sound radiation. However, since periodic structures do not remain geometrically uniform over a structural period, theories reviewed in chapter 1 about bending wave propagation are not fully appropriate. Thus, new scientific tools for the study of wave propagation in periodic structure are briefly introduced in the case of flexural waves along periodic beams.

### Terminology

The following terms or expressions are defined:

- A $n$-segment entity is defined as an entity made of $n$ sub-elements where each of the sub-elements has constant physical properties. For example, a 15-segment beam is shown on figure 2.2.

- Sequential structure. The design of large and complicated structures may require that boundary conditions along a uniform beam cannot be described as a repetitive succession of conditions. This is refereed as a "disordered structure" in the literature. However, since in this thesis, physical alterations made to the beam are intentional, controlled and repetitive, the expression "sequential structure" will be used to describe a periodic beam with a repetitive pattern based on a $n$-segment sequence. For example, the beam presented on figure 2.2 is based on a 5-segment sequence.

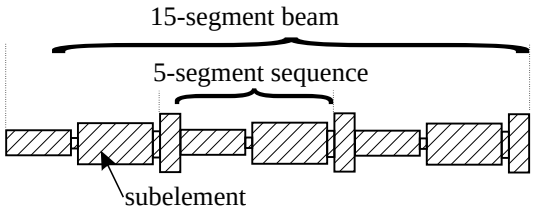


Figure 2.2: Illustration of a 15-segment beam based on a 5-segment sequence

- Stopping bands. Periodic beams are non uniform structures. If a wave propagates along a periodic beam, the variations of impedance create reflected wave fields. At certain frequencies, the reflected waves interfere with the incoming waves and create a standing wave within a structural period. Thus, if we consider one structural period, the adjacent structural periods vibrate in phase or out of phase. As a result of standing waves, energy does not propagate along the structure. The frequency regions where this phenomena happen are called stopping bands.

  On the other hand, the frequency band where the structure does not interfere with wave propagation is called a passing band.

  For the case of flexural waves in an infinite periodic beam, stopping and passing bands are mathematically described by considering the bending wavenumber $k_b$ over one structural period. If we consider a wave such of the form $w(x,t) = Ae^{-jk_b x}e^{j\omega t}$ along the structure

  - $k_b$ is real. The wave propagates without being attenuated. This is a passing band.
  - $k_b$ is complex and $Im[k_b] \neq 0$. The wave is evanescent as the exponential term $e^{Im[k_b x]}$ attenuates the wave amplitude $A$.

  Thus, stopping and passing bands can be found by plotting the wavenumber $k_b$. An example is presented in figure 2.3.

  In this research, stopping bands are used as a means to reduce sound radiation: if no waves propagate in an infinite structure, no sound is radiated in the far field.

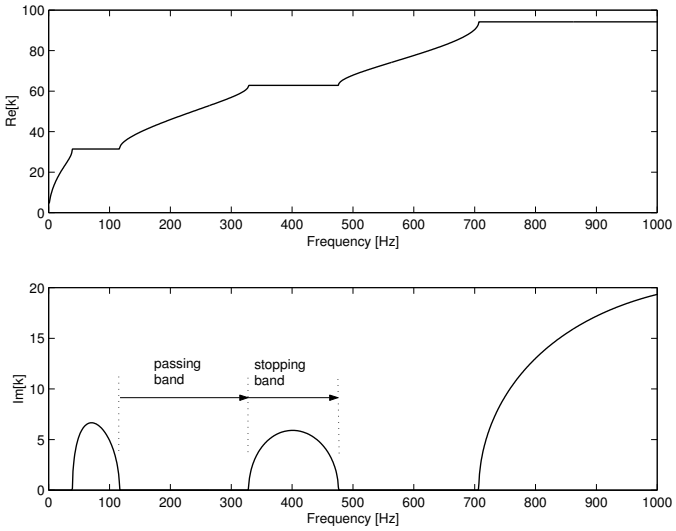


Figure 2.3: Stopping and passing band representation

## 2.1 Review

The theory of periodic structures was partly developed for applications and research in the fields of electricity, optics and quantum physics. The main reference is a book by Léon Brillouin [18]. The author makes a review, mainly regarding the standard wave equation, lattices of particles and electric circuits. Elachi [19] also made a general review of periodic structure theory with developments in a large variety of periodic media applications.

Investigations of periodic structures can be traced as far back as Newton's attempt to predict the wave velocity in air. As a matter of fact, he modelled the fluid as a succession of discrete masses $m_i$ equally spaced by weightless springs $s_i$ as presented in figure 2.4.

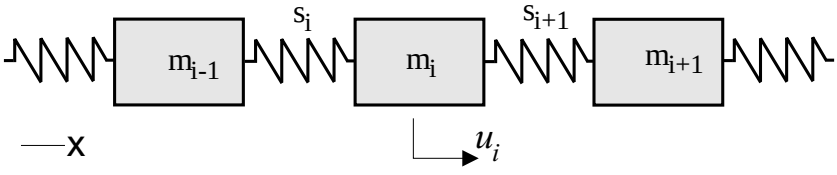


Figure 2.4: Newton's model of air

Unfortunately, Newton used the isothermal bulk modulus of air for the stiffness and this yielded to a smaller theoretical value than the experimental one. However, Newton's model of air gives better result if the springs take the values of adiabatic elastic constants.

Rayleigh carried out the first investigation of wave propagation in continuous periodic structure in 1887. In [20], he studied the transverse vibration of a stretched string with a periodic and continuous variation of density. Using Hill's equation [21], Rayleigh derived the basis for wave propagation governed by a second order differential equation in any periodic structure.

The study of bending wave propagation has principally been investigated for structures with periodic impedances [22] and periodic supports [23]. The wave propagation pattern was computed using receptance and transfer matrix methods. Recently, Mead [24] provided an extensive overview of the contributions made by researchers at the University of Southampton.

Numerical methods and results on bending waves propagating in beams with varying cross-sections appeared more recently. Various methods have been developed. Hawwa [25] investigated the reflection characteristics of a beam with a weak sinusoidal variation of the beam cross-section along its axis. In order to find the flexural wave propagation in the beam, he expanded equation (1.13)(i.e. the bending equation in a periodic beam) and used a power series to compute the inverse of the moment of inertia and perturbations techniques to solve the resulting system. Floquet's theory, as it is presented and used in this research, was used by Tassilly in [26]. Its study is limited to a 2-segment case with constant cross-section, damping and stiffness along each element of the sequence. Lee *et al.*, [27] looked at the bending wave propagation in a periodic structure with continuously varying cross-section and decomposed the wave fields into the superposition of two pairs of waves propagating in opposite directions.

Finally, the alteration of wave propagation by disordered structures has given promising results. Bouzit and Pierre [28] experimentally showed that in a multi-span beam, bending wave propagation in the passing bands is greatly altered if the support are randomly spaced. In addition, they also found that in the passbands, the introduction of damping in an ordered beam was having less effect for spatial decay than the introduction of disorder. However, length disorders can also be used to broaden the passband regions [29].

## 2.2 Formulation for discrete systems

Let us consider a structure such as Newton's model of air (see figure 2.4). This is a 1-segment structure, i.e. each element and its neighbors are identical. Applying Newton's second principle on the $i^{th}$ mass yields:

$$m_i\ddot{u}_i(t) + [s_i + s_{i+1}]u_i(t) - s_i u_{i-1}(t) - s_{i+1}u_{i+1}(t) = 0 \tag{2.1}$$

where $u_i(x,t)$ is the relative displacement of the $i^{th}$ mass along the x-axis. Considering that a free-wave propagates along the structure, the displacements of the $i^{th}$ and $(i+1)^{th}$

masses can be written as:

$$u_{i-1} = u_i(t)e^{jkd} \tag{2.2}$$
$$u_{i+1} = u_i(t)e^{-jkd} \tag{2.3}$$

where $k$ is the wavenumber of the propagating wave in the structure, $d$ the distance between each masses at equilibrium position and $u_i(t)$ describes the time dependance function of all masses. Assuming the structure is excited at a single frequency ($u_i(t) = e^{j\omega t}$) and substituting equation (2.2) and equation (2.3) in equation (2.1) yields:

$$-\omega^2 m_i = -2s_i + s_i e^{jkd} + s_i e^{-jkd} \tag{2.4}$$

Rearranging previous equation gives an expression for $k$:

$$k = \frac{1}{d}\arccos(1 - \frac{\omega^2 m_i}{2s_i}) \tag{2.5}$$

where $k$ is defined as modulus $\frac{2\pi}{d}$.

Note: The arccos (inverse cosine) function is define as

$$\arccos(z) = -j\ln\left[z + j\sqrt{1-z^2}\right] \tag{2.6}$$

where $z$ is a complex number. If $z < -1$, $\arccos(z)$ will be a complex number with a non-zero imaginary part. Thus, in the Newton's model, if $\frac{\omega^2 m_i}{2s_i} > 2$, the wavenumber $k$ will be complex and will corresponds to non-propagating waves.

## 2.3 Floquet's theory

In the real world, structures are not always modelled as a sum of mass-spring systems. However their vibration behavior can be described using differential equations. The following is a quick review of how Floquet's theory helps solving second order differential equations having periodic coefficients. For example, it could be used to show acoustic waves propagates in a pipe with a varying cross-section. Floquet's theory will be later applied to the case of bending waves as the governing equation for flexural waves is a fourth order differential equation.

### Wave equation

Let us consider a wave that can be described by a second order differential equation, a compressive wave for example. If this wave propagates along a periodic structure, the

following equation applies:

$$\frac{\partial^2 u(x,t)}{\partial x^2} + \omega^2 \Psi(x) u(x,t) = 0 \tag{2.7}$$

where $\Psi(x)$ is a periodic function describing the change of physical properties along the structure and $u(x,t)$ is the field displacement as a function of time and position.

Mathieu's equation [30] is a special case of equation 2.7 if $\Psi(x)$ is given by:

$$\Psi(x) = \alpha + \beta \cos kx \tag{2.8}$$

where $\alpha$ and $\beta$ are constant. Thus, Mathieu's equation can be written as:

$$\frac{\partial^2 u(x,t)}{\partial x^2} + \omega^2 \left[\alpha + \beta \cos 2\pi x\right] u(x,t) = 0 \tag{2.9}$$

**Floquet's solution to Mathieu's equation**

The general solution to Mathieu's equation was found by Floquet [31] and can be written as:

$$u(x) = C_1 \Upsilon(x) e^{-jkx} + C_2 \Xi(x) e^{jkx} \tag{2.10}$$

where $C_1$ and $C_2$ are arbitrary constant and where $\Upsilon(x)$ and $\Xi(x)$ are periodic functions of $x$ with a period $2\pi$. In order to solve the problem, it is generally assumed that the frequency of excitation is known and therefore a solution for the corresponding wavenumber $k$ can be found. It is also assumed that $u(x,t)$ is an harmonic wave, i.e. $u(x,t) = e^{j\omega t} u(x)$. Equation (2.10) describes two waves propagating (or being attenuated if $k$ is a complex number) in both directions. If we only keep one of these waves, we can rewrite equation (2.10) as:

$$u(x) = \Upsilon(x) e^{-jkx} \tag{2.11}$$

**Hill's equation**

Hill's equation [21] is a more general case of Mathieu's equation where the sinusoidal function is replaced by any kind of periodic function along $x$. This can be written as

$$\frac{\partial^2 u(x,t)}{\partial x^2} + [\alpha + \beta \Psi(x)] u(x,t) = 0 \tag{2.12}$$

General solutions to Hill's equation can be found but each of them depends on the nature of the $\Psi(x)$ function.

In this research, the function $\Psi(x)$ will always be a $n$-segment sequence. For that case, solutions of Hill's equation have the form of equation (2.10) [18]. However, if the $\Psi(x)$ function has a period $d$, the function $\Upsilon(x)$ and $\Xi(x)$ also have a period $d$. Thus, we can rewrite equation (2.11) as:

$$\begin{aligned} u(x+d) &= \Upsilon(x+d)e^{-jk(x+d)} && (2.13)\\ \Rightarrow u(x+d) &= e^{-jkd}\Upsilon(x)e^{-jkx} && (2.14)\\ \Rightarrow u(x+d) &= e^{-jkd}u(x) && (2.15) \end{aligned}$$

where $k$ is unknown. Equation (2.15) tells us that if for a periodic structure we know the displacement field $u(x)$, the displacement field at $(x+d)$ is only a function of $k$ and the structural period $d$. In this research, equation (2.15) is referred to as the equation defining Floquet's theory.

## 2.4 Floquet's theory applied to the bending wave equation

Floquet's theory was found by solving second order differential equations. It can also be extended to the case of the fourth order differential equation [26, 27]. Thus, we can write the Floquet theory for a bending wave as:

$$w(x+d) = e^{-kd}w(x) \tag{2.16}$$

If we define $X$ as $X = e^{-jk_b d}$ where $k_b = k$, we can rewrite equation (2.16) as

$$w(x+d) = Xw(x) \tag{2.17}$$

If we differentiate three times the previous equation with respect to $x$, we get the following system:

$$\begin{aligned} w(x+d,t) &= Xw(x,t)\\ \frac{\partial w(x+d,t)}{\partial x} &= X\frac{\partial w(x,t)}{\partial x}\\ \frac{\partial^2 w(x+d,t)}{\partial x^2} &= X\frac{\partial^2 w(x,t)}{\partial x^2}\\ \frac{\partial^3 w(x+d,t)}{\partial x^3} &= X\frac{\partial^3 w(x,t)}{\partial x^3} \end{aligned} \tag{2.18}$$

where $\frac{\partial^2 w(x,t)}{\partial x^2}$ and $\frac{\partial^3 w(x,t)}{\partial x^3}$ are respectively proportional to the moment and the force applied to the beam. Thus, the equation system 2.18 is used to describe the physics of a structural period end as a function of the physics of the other end and the bending wavenumber in the periodic structure. Therefore, if the behavior of the structural period is known at its two ends, the wavenumber in the periodic structure can be found.

### 2.4.1 Bending wavenumber computations

Two methods have been used in order to determine the wave propagation in a periodic structure. The first one is rather slow for large sequences since it requires the determinant computation of a large matrix. It is presented here as a preview for multi-layered system and as how large matrices describing a finite or infinite bending structures are constructed. The second method was used to efficiently compute wavenumbers in infinite periodic beams.

#### The determinant approach

The determinant approach is a method using a wave field description (as defined on page 10): at each interface between two sub elements (see figure 2.5), one can write equilibrium equations (displacement, slope, moment and force) as a function of the unknown coefficients (A, B, C and D) of each sub element.

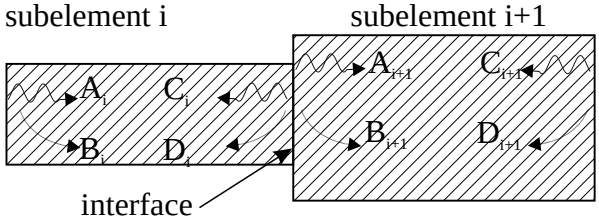


Figure 2.5: Interface between two sub elements

In order to ease notations, we introduce $\mathbb{E}$ as:

$$\mathbb{E}_i(x_i) = \begin{bmatrix} 1 & 1 & 1 & 1 \\ -jk_{bi} & -k_{bi} & jk_{bi} & k_{bi} \\ -\frac{k_{bi}^2}{E_iI_i} & \frac{k_{bi}^2}{E_iI_i} & -\frac{k_{bi}^2}{E_iI_i} & \frac{k_{bi}^2}{E_iI_i} \\ \frac{jk_{bi}^3}{E_iI_i} & -\frac{k_{bi}^3}{E_iI_i} & -\frac{jk_{bi}^3}{E_iI_i} & \frac{k_{bi}^3}{E_iI_i} \end{bmatrix} \begin{bmatrix} e^{-jk_{bi}x} & 0 & 0 & 0 \\ 0 & e^{-k_{bi}(x-x_{i-1})} & 0 & 0 \\ 0 & 0 & e^{jk_{bi}x} & 0 \\ 0 & 0 & 0 & e^{jk_{bi}(x-x_i)} \end{bmatrix} \tag{2.19}$$

Thus, the continuity equations at any point of a sub element can be written as

$$\begin{bmatrix} w_i(x_i) \\ \frac{\partial w_i(x_i)}{\partial x} \\ \frac{1}{E_iI_i}\frac{\partial^2 w_i(x_i)}{\partial x^2} \\ \frac{1}{E_iI_i}\frac{\partial^3 w_i(x_i)}{\partial x^3} \end{bmatrix} = \mathbb{E} \begin{bmatrix} A_i \\ B_i \\ C_i \\ D_i \end{bmatrix} \tag{2.20}$$

Therefore, at the interface between two sub elements, we can write the equilibrium equations in a matrix form:

$$\begin{bmatrix} \mathbb{E}_i(x_i) & -\mathbb{E}_{i+1}(x_i) \end{bmatrix} \begin{bmatrix} A_i \\ B_i \\ C_i \\ D_i \\ A_{i+1} \\ B_{i+1} \\ C_{i+1} \\ D_{i+1} \end{bmatrix} = \begin{bmatrix} 0 \\ 0 \\ M_{ext} \\ F_{ext} \end{bmatrix} \tag{2.21}$$

where $M_{ext}$ and $F_{ext}$ are respectively the external moments and external forces applied at the interface. Thus, for a $n$-segment beam (see the extracted beam on figure 2.6), we can describe the system in a matrix form by considering the equilibrium equations at each interface. This is written as:

$$\begin{bmatrix} -\mathbb{E}_1(x_0) & 0 & 0 & 0 & 0 & 0 & 0 \\ \mathbb{E}_1(x_1) & -\mathbb{E}_2(x_1) & 0 & 0 & 0 & 0 & 0 \\ 0 & \mathbb{E}_2(x_2) & \ddots & 0 & 0 & 0 & 0 \\ 0 & 0 & \ddots & -\mathbb{E}_i(x_{i-1}) & 0 & 0 & 0 \\ 0 & 0 & 0 & \mathbb{E}_i(x_i) & -\mathbb{E}_{i+1}(x_i) & 0 & 0 \\ 0 & 0 & 0 & 0 & \mathbb{E}_{i+1}(x_{i+1}) & \ddots & 0 \\ 0 & 0 & 0 & 0 & 0 & \ddots & -\mathbb{E}_n(x_{n-1}) \\ 0 & 0 & 0 & 0 & 0 & 0 & \mathbb{E}_n(x_n) \end{bmatrix} \begin{bmatrix} \mathbb{A}_i \end{bmatrix} = \begin{bmatrix} \mathbb{F}_i \end{bmatrix} \tag{2.22}$$

where $\mathbb{A}_i$ are the $\{A_i, B_i, C_i, D_i\}, (i = 1 \dots n)$ coefficients and $\mathbb{F}_i$ is the vector representing external inputs to the beam. If we consider an infinite periodic structure based on a $n$-segment sequence, we need to extract one structural period. This is shown on figure 2.6. Assuming no external excitation ($\mathbb{F}_i = 0$) and applying Floquet's theory at the end sub elements of the extracted beam ($\mathbb{E}_1(x_0) = X\mathbb{E}_n(x_n)$), we can rewrite equation (2.22) as:

$$\begin{bmatrix} \mathbb{E}_1(x_1) & -\mathbb{E}_2(x_1) & 0 & 0 & 0 \\ 0 & \mathbb{E}_2(x_2) & \ddots & 0 & 0 \\ 0 & 0 & \ddots & -\mathbb{E}_{n-1}(x_{n-2}) & 0 \\ 0 & 0 & 0 & \mathbb{E}_{n-1}(x_{n-1}) & -\mathbb{E}_n(x_{n-1}) \\ -\mathbb{E}_1(x_0) & 0 & 0 & 0 & X\mathbb{E}_n(x_n) \end{bmatrix} \begin{bmatrix} \mathbb{A}_i \end{bmatrix} = [0] \tag{2.23}$$

Since waves in the beam must have a non zero amplitude, $\mathbb{A}$ cannot be a null vector

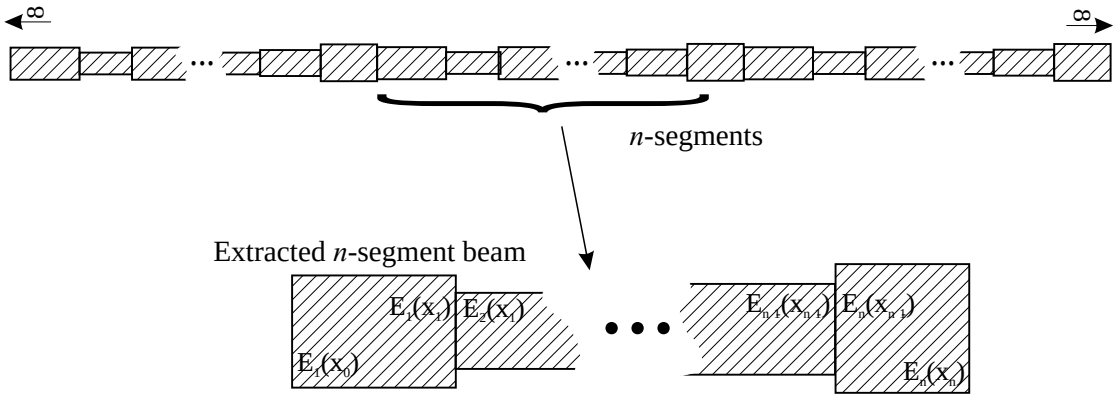


Figure 2.6: Extraction of the $n$-segment beam defining the periodic structure

($\mathbb{A} \neq 0$). Therefore, the following equation has to be satisfied:

$$\begin{vmatrix} \mathbb{E}_1(x_1) & -\mathbb{E}_2(x_1) & 0 & 0 & 0 \\ 0 & \mathbb{E}_2(x_2) & \ddots & 0 & 0 \\ 0 & 0 & \ddots & -\mathbb{E}_{n-1}(x_{n-2}) & 0 \\ 0 & 0 & 0 & \mathbb{E}_{n-1}(x_{n-1}) & -\mathbb{E}_n(x_{n-1}) \\ -\mathbb{E}_1(x_0) & 0 & 0 & 0 & X\mathbb{E}_n(x_n) \end{vmatrix} = 0 \tag{2.24}$$

The determinant of the previous equation can be rewritten in a polynomial form $p(X) = X^4 + pX^3 + qX^2 + rX + t$ where $p$, $q$ $r$ and $t$ are real or complex coefficients. In the case of a 2-segment beam, an expression for these coefficients was given by Tassilly [26]. For higher sequential beams, $p$, $q$, $r$ and $t$ are found numerically. Thus, equation (2.24) is rewritten as

$$p(X) = 0 \tag{2.25}$$

Taking the natural logarithm (see note below) of the roots of equation (2.25) gives four solutions $k_{b1,2,3,4}$. The displacement field in the beam segment can be written as a superposition of these four solutions:

$$w(x,t) = \left[C_1 e^{jk_{b1}x} + C_2 e^{jk_{b2}x} + C_3 e^{jk_{b3}x} + C_4 e^{jk_{b4}x}\right] e^{j\omega t} \tag{2.26}$$

where $C_1$, $C_2$, $C_3$ and $C_4$ are constants to be determined.

Note: If $X = e^{jk_b d}$ is a complex number, $k_b$ is found by using the natural logarithm (ln)[32]: $k_b = \frac{\ln(X)}{jd}$. This yields

$$\mathrm{Re}[k_b] = \frac{\arctan\left(\mathrm{Im}[X]/\mathrm{Re}[X]\right)}{d} \tag{2.27}$$

$$\mathrm{Im}[k_b] = \frac{\ln\left(\mathrm{Re}[X]^2 + \mathrm{Im}[X]^2\right)}{2d} \tag{2.28}$$

It should be noticed that the real part of $k_b$ is defined as *modulus* $2\pi/d$.

### Lee and Ke algorithm

The Lee and Ke algorithm [27, 33] is an efficient technique to compute the bending wavenumber for a periodic infinite structure. The algorithm is much faster than the previous method in the case of an infinite periodic beam as it does not involve the computation of the determinant of a large matrix. Therefore, a $n$-segment sequence, where $n$ is a large number, can be investigated. This allows the study of periodic structures with continuously varying cross-section (this is achieved by discretizing the structures as a succession of small elements with constant cross-sections).

The solution of the bending wave equation in each element $i$ of the sequence is decomposed on a set of linearly independent functions $W_{j,i}$ $(j = 1, 2, 3, 4)$. This is written as $w_i(x,t) = Q_i W_{1,i}(x) + R_i W_{2,i}(x) + S_i W_{3,i}(x) + T_i W_{4,i}(x)$ where $Q_i$, $R_i$, $S_i$ and $T_i$ are complex constants (these constants are not important to the algorithm since they are only to be found if one needs to know the displacement $w_i$ along the $i^{th}$sub element). A few criteria have to be fulfilled at one end of the sequence (chosen at $x = 0$ here):

- the cross-section variation is continuously differentiable at $x = 0$, meaning that $EI(0) = EI(d)$.
- the cross-section at $x = 0$ is at a local extremum, i.e. the slope is zero ($\frac{\partial W(0)}{\partial x} = \frac{\partial W(d)}{\partial x} = 0$).
- The set of $W_j$ functions on the first element has to satisfy:

$$\begin{bmatrix} W_1(0) & W_2(0) & W_3(0) & W_4(0) \\ \frac{\partial W_1(0)}{\partial x} & \frac{\partial W_2(0)}{\partial x} & \frac{\partial W_3(0)}{\partial x} & \frac{\partial W_4(0)}{\partial x} \\ \frac{\partial^2 W_1(0)}{\partial x^2} & \frac{\partial^2 W_2(0)}{\partial x^2} & \frac{\partial^2 W_3(0)}{\partial x^2} & \frac{\partial^2 W_4(0)}{\partial x^2} \\ \frac{\partial^3 W_1(0)}{\partial x^3} & \frac{\partial^3 W_2(0)}{\partial x^3} & \frac{\partial^3 W_3(0)}{\partial x^3} & \frac{\partial^3 W_4(0)}{\partial x^3} \end{bmatrix} = \begin{bmatrix} 1 & 0 & 0 & 0 \\ 0 & 1 & 0 & 0 \\ 0 & 0 & 1 & 0 \\ 0 & 0 & 0 & 1 \end{bmatrix} \tag{2.29}$$

  Therefore, the Wronskian [32] of $[W_1(x)W_2(x)W_3(x)W_4(x)]$ at $x = 0$ is one ($\mathbb{W}(0) = 1$).

In order to find the $W_i$'s, the following set of functions is defined:

$$\begin{aligned} \tilde{W}_{1,i+1}(x - x_i) &= \left[\cosh\left(k_{i+1}(x - x_i)\right) + \cos\left(k_{i+1}(x - x_i)\right)\right]/2 \\ \tilde{W}_{2,i+1}(x - x_i) &= \left[\sinh\left(k_{i+1}(x - x_i)\right) + \sin\left(k_{i+1}(x - x_i)\right)\right]/2k_{i+1} \\ \tilde{W}_{3,i+1}(x - x_i) &= \left[\cosh\left(k_{i+1}(x - x_i)\right) - \cos\left(k_{i+1}(x - x_i)\right)\right]/2k_{i+1}^2 \\ \tilde{W}_{4,i+1}(x - x_i) &= \left[\sinh\left(k_{i+1}(x - x_i)\right) - \sin\left(k_{i+1}(x - x_i)\right)\right]/2k_{i+1}^3 \end{aligned} \tag{2.30}$$

where $x_i$ is the coordinate of the interface between the $i^{th}$ and $(i+1)^{th}$ elements. Along the first element, the solutions are defined using equations (2.30) and $i = 0$ ($x_0$ is set to zero).

The set of fundamental solutions in each element is found using the following iteration:

$$\begin{aligned} W_{j,i+1}(x) &= \tilde{W}_{1,i+1}(x-x_i)W_{j,i}(x_i) + \tilde{W}_{2,i+1}(x-x_i)\frac{\partial W_{j,i}(x_i)}{\partial x} + \\ &+ \frac{E_i I_i}{E_{i+1} I_{i+1}}\left[\tilde{W}_{3,i+1}(x-x_i)\frac{\partial^2 W_{j,i}(x_i)}{\partial x^2} + \tilde{W}_{4,i+1}(x-x_i)\frac{\partial^3 W_{j,i}(x_i)}{\partial x^3}\right] \end{aligned} \quad (2.31)$$

where $\tilde{W}_{j,i}$ are the fundamental solutions as defined in equation (2.30) and $j = 1, 2, 3, 4$.

Using the iteration, a numerical value for the $W_j(d)$ can be found. Rewriting equation (2.18) yields

$$\begin{vmatrix} W_1(d) - X & W_2(d) & W_3(d) & W_4(d) \\ \frac{\partial W_1(d)}{\partial x} & \frac{\partial W_2(d)}{\partial x} - X & \frac{\partial W_3(d)}{\partial x} & \frac{\partial W_4(d)}{\partial x} \\ \frac{\partial^2 W_1(d)}{\partial x^2} & \frac{\partial^2 W_2(d)}{\partial x^2} & \frac{\partial^2 W_3(d)}{\partial x^2} - X & \frac{\partial^2 W_4(d)}{\partial x^2} \\ \frac{\partial^3 W_1(d)}{\partial x^3} & \frac{\partial^3 W_2(d)}{\partial x^3} & \frac{\partial^3 W_3(d)}{\partial x^3} & \frac{\partial^3 W_4(d)}{\partial x^3} - X \end{vmatrix} = 0 \quad (2.32)$$

This can be written in a polynomial form $p(X) = X^4 + pX^3 + qX^2 + rX + t$ with

$$p = r = -W_1(d) - \frac{\partial W_2(d)}{\partial x} - \frac{\partial^2 W_3(d)}{\partial x^2} - \frac{\partial^3 W_4(d)}{\partial x^3} \quad (2.33)$$

$$\begin{aligned} q &= \begin{vmatrix} W_1(d) & W_2(d) \\ \frac{\partial W_1(d)}{\partial x} & \frac{\partial W_2(d)}{\partial x} \end{vmatrix} + \begin{vmatrix} W_1(d) & W_3(d) \\ \frac{\partial^2 W_1(d)}{\partial x^2} & \frac{\partial^2 W_3(d)}{\partial x^2} \end{vmatrix} + \begin{vmatrix} W_1(d) & W_4(d) \\ \frac{\partial^3 W_1(d)}{\partial x^3} & \frac{\partial^3 W_4(d)}{\partial x^3} \end{vmatrix} + \\ &+ \begin{vmatrix} \frac{\partial W_2(d)}{\partial x} & \frac{\partial W_3(d)}{\partial x} \\ \frac{\partial^2 W_2(d)}{\partial x^2} & \frac{\partial^2 W_3(d)}{\partial x^2} \end{vmatrix} + \begin{vmatrix} \frac{\partial W_2(d)}{\partial x} & \frac{\partial W_4(d)}{\partial x} \\ \frac{\partial^3 W_2(d)}{\partial x^3} & \frac{\partial^3 W_4(d)}{\partial x^3} \end{vmatrix} + \begin{vmatrix} \frac{\partial^2 W_3(d)}{\partial x^2} & \frac{\partial^2 W_4(d)}{\partial x^2} \\ \frac{\partial^3 W_3(d)}{\partial x^3} & \frac{\partial^3 W_4(d)}{\partial x^3} \end{vmatrix} \end{aligned} \quad (2.34)$$

$$t = 1 \quad (2.35)$$

It can be shown that the roots of equation 2.25 are:

$$X_{1,2} = \frac{1}{2}\left[H_1 \pm \sqrt{H_1^2 - 4}\right] \quad (2.36)$$

$$X_{3,4} = \frac{1}{2}\left[H_2 \pm \sqrt{H_2^2 - 4}\right] \quad (2.37)$$

where $H_{1,2} = \frac{1}{2}\left[p \pm \sqrt{p^2 - 4(q-2)}\right]$.

All solutions are to be considered and have a physical interpretation. It has been proved [27] that

- if $\mid H_1 \mid < 2$, $X_1$ and $X_2$ are complex conjugate. Thus, the corresponding wavenumbers $k_{b1}$ and $k_{b2}$ will be real and such that $k_{b1} = -k_{b2}$. Therefore, this corresponds to passing-bands.
- if $\mid H_1 \mid > 2$. $X_1$ and $X_2$ are both real numbers. Thus, the corresponding wavenumbers $k_{b1}$ and $k_{b2}$ will be complex numbers. Therefore, waves will be attenuated along the sequence in both directions. This corresponds to stopping-bands.
- if $\mid H_1 \mid = 2$, there will either be a standing wave, i.e. the group velocity is equal to zero, or propagating waves in both directions (the group velocity is not equal to zero).

Note: $\mid H_2 \mid$ is always bigger than 2 if the beam is excited. All the previous remarks in the case of $\mid H_1 \mid > 2$ apply , i.e. $k_{b3}$ and $k_{b4}$ always describe evanescent waves in the sequence. Therefore, only $k_{b1}$ and $k_{b2}$ determine if the structure allows wave propagation.

# Chapter 3

# Sequence design and optimization

The design of periodic beams and periodic skin is done by only considering one structural period of the structure. Thus, mathematical functions have to be defined to describe these structural periods. In this thesis, these functions are only based on $n$-segment sequences. Each value of these sequences is used to determine the length and/or the thickness of a sub-element of a $n$-segment beam. First, Galois sequences are briefly introduced as a tool to create a periodic function. However, mathematical tools to design an appropriate function that meets the control needs (e.g. attenuation of the radiated sound power) may be difficult to find. Thus, real-valued genetic algorithms are also presented as a technique to find optimum sequences for the problem.

## 3.1 Galois sequences

A good review of Galois sequences was made by Schroeder [34]. Various applications are also presented, one of them being in room acoustics where Schroeder's diffusors are used to scatter broadly incident acoustic waves. In physics, these diffusors are called *reflection phase-grating* as they scatter incident acoustic waves and reflects them "without absorbing them and with a minimum of specular reflection". Thus, we propose to apply these sequences to periodic beams and skins to scatter bending waves as much as possible along the structure.

### Mathematical definition

Galois series are defined with respect to a prime number $p$ (for example, $p = 2, 3, 5, 7, 11, ...$). This number $p$ also defines the number of points in the sequence $(p-1)$. In this research,

we use the following Galois series:

$$\sigma_n = n^2 \mod p \tag{3.1}$$

where $n$ goes from 1 to $p-1$ and mod is the *modulo* operator. An example of such a sequence is presented in table 3.1.

Table 3.1: Galois sequence for $p = 7$

| $n$ | 1 | 2 | 3 | 4 | 5 | 6 |
|---|---|---|---|---|---|---|
| $\sigma_n$ | 1 | 4 | 2 | 2 | 4 | 1 |

## 3.2 Optimization technique using the genetic algorithm

It may be difficult to theoretically find, or even guess, a mathematical sequence describing the geometry of a structure that would best fit the application of sound radiation control over a certain frequency band. Therefore, optimization techniques are used to look for the best possible solution in the design region. The following section presents a real-valued genetic algorithm that will be later used for the design of optimized periodic beams and smart skins.

### 3.2.1 Concept

Genetic algorithms [35] are a powerful means of finding optimal solutions to problems. The algorithm tries to find the optimal solution based on a survival or the fittest selection routine. From a large population of possible solutions, individual solutions are evaluated against an error criterion. An individual is the representation of a set of bounded or unbounded parameters to be optimized where each of these parameters is encoded on a basis as a different gene. Genes will have to be decoded to be used. Their expressions in the problem domain are called phenotypes.

The simulation of evolution is run on a population of individuals: children are created by using cross-overs and mutations over the genetic material of the parents. Then, the siblings are reinserted in the population. These steps are repeated over a given number of generation or until a satisfactory fitness of the population is achieved. The first generation of individuals is chosen randomly.

The optimization algorithms are used in this research to find a $n$-segment sequence that performs well on some user-defined criteria (these criteria are later defined. See page 37). A $n$-segment sequence is represented as an individual. Each sub-element of the sequence is a combination of genes that can be altered. These genes are the representations of the sub-element lengths $l_i$, the sub-element thicknesses $h_i$ and the suspending springs $s_i$ in the case of a multi-layered structure. An example is shown on figure 3.1. Using a mathematical package, parameters are usually stored in a matrix form where each line of the matrix corresponds to the the genetic material for one sub-element.

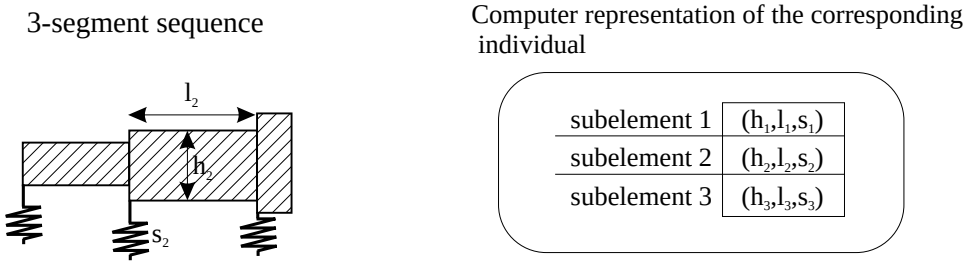


Figure 3.1: Computer description of an individual

Values for the genetic parameters are constrained to be in defined ranges in order to preserve a realistic beam. For example, each sub-element can only have a thickness between 0.002m and 0.003m, insuring that the overall weight of the structure is not above a certain weight. This prevents the algorithms to look for solutions that would not suite the application (e.g. the structure could be too heavy). Constraining the gene value is also done when the first individuals are generated: each gene gets a random value picked in the allowed range.

Note: In nature, genes are encrypted by sequences of 4 different nucleotides, whereas in basic genetic algorithms, genes are encoded on a binary basis. However, these descriptions are not very practical in most problems since real-valued parameters are considered (this would require to convert genes to phenotypes and *vice versa*). Therefore, genes will be considered and encoded as real numbers to avoid time consuming conversion and loss of precision in the phenotype values.

### Cross-over

Cross-over is the basic operation in creating new chromosomes by recombining the genetic materials of two parents into two children. Each child will have some of its parents material. Wright [36] explained how crossovers are performed in the case of real-valued genes. The simplest case is when the crossover point is exactly between two genes as

shown in figure 3.2. In this example, individuals have two genes (**x** and **y**). The genotype of parents 1 and 2 are respectively ($x_1$,$y_1$) and ($x_2$,$y_2$). Since the cross-over does not happen within a gene, each child get non modified genes from their parents. However, each child will get a gene **x** from one parent and the gene **y** from the other parent.

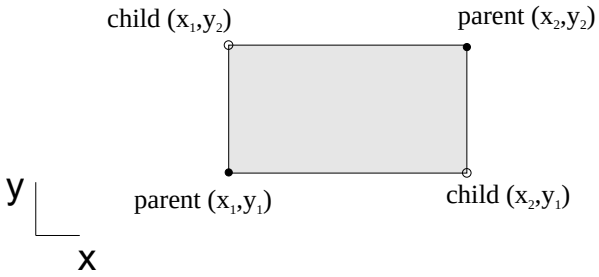


Figure 3.2: Crossover with real valued genes from Wright [36]

If the crossover points are located within a gene, a child obtains the significant part (the first digits) of the parameters from one parent, and a less important part (the last digits) from the other. The latter contribution can be seen as a perturbation of the first parent genetic material. Of course, this perturbation is limited by the allowed range that can be taken by the gene. An example is given in figure 3.3.

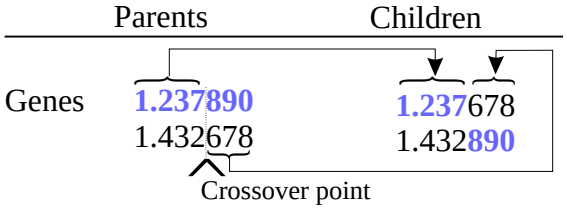


Figure 3.3: Crossover within the code of a real-valued gene

### Mutation

Mutation is a a random process where an allele of a gene is replaced by another. This creates a new genetic structure with a different phenotype. In the case of a real valued representation, mutations are achieved by either perturbing the gene values or selecting a new gene value within the allowed range. The main purpose of mutation in genetic algorithm is to ensure that the extrema found is not local.

### 3.2.2 Reinsertion

Once new individuals have been generated, they have to be inserted in the population. However, in order to preserve the subpopulation size, a selection of individuals has to be done. Different strategies can be applied. The "survivor" model is to replace the oldest individuals of a population by the new generated members. This follows evolution but a more efficient method is used in this research: the elitist approach. It compares individuals performance and only conserves the most fit individuals, without any age restriction.

### 3.2.3 Migration

It has been shown [37] that the quality of genetic algorithm results can be improved by using a multiple populations representation instead of just studying the evolution of one single population. This is achieved by running the genetic algorithm on different subpopulations that evolve at the same time. However, in order to introduce diversity in each subpopulation, from time to time individuals are picked randomly and migrate between each subpopulation. So a migrant from a population that rapidly became fit will help its new population to become fitter.

There are various models of migrations such as neighborhood migration topology (individuals can only migrate from the neighbor subpopulations) or unrestricted migration topology as illustrated in figure 3.4. For example, in the restricted model, an individual from subpopulation 1 will only be able to migrate to subpopulation 2 or 5 whereas in the unrestricted model, an individual from subpopulation 1 can migrate to any other subpopulation. The unrestricted migration topology will be used in the different cases involving genetic algorithm in the present research.

### 3.2.4 Objective functions

In a elitist reinsertion model, the performance of each individual in a subpopulation has to be evaluated before any selection can be made. An individual is fit if it minimizes a cost function, also called an objective function. These functions are built by considering user-defined criteria important in defining a good fitness, i.e. one must create a function with variables that will describe how well an individual performs with respect to the main objective.

In this research, two different types of structures are investigated (i.e. finite and infinite structures). Thus, an objective function for each of these types of structure has to be defined. The genetic algorithm will try to minimize these functions by modifying the

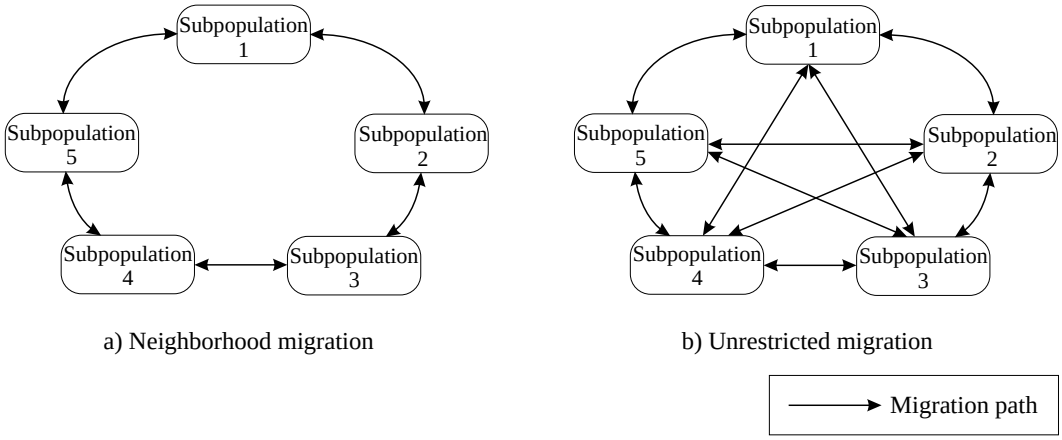


Figure 3.4: Different models of migration

parameter of the $n$-segment sequences the structures are based on.

### Infinite beams

An infinite beam radiates sound in the far field only if there is a *supersonic* wave propagating along the structure. Therefore, if no waves propagate, no sound is radiated. We have seen that flexural waves are evanescent if the imaginary part of the corresponding bending wavenumber is nonzero ($Im[k_b] \neq 0$). Thus, the objective is to have stopping bands in the frequency band of interest. In order to consider a frequency band behavior, we look at the sum of the imaginary parts of the wavenumbers over that band. If this sum is zero, the considered frequency band is a passing band. Otherwise, there are some frequencies for which the structure is a stopping band. Thus, a simple cost function for infinite structure can be written as:

$$o = \frac{1}{\epsilon + \sum_{f=f_1}^{f_2} \mid Im[k_b(f)] \mid} \tag{3.2}$$

where $\epsilon$ is a small number to prevent any singularity of the previous equation, $k_b(f)$ are the estimates of the wavenumber in the structure as a function of frequency and $f_1$ and $f_2$ are the frequency band limits. If we consider an infinite periodic beam based on a $n$-segment sequence, the $k_b$'s are evaluated using Lee and Ke algorithm (see page 30).

However, less material, and therefore less weight, can be an important criteria to consider if one wants to design a light structure. Thus, equation (3.2) is modified in order to take

into account the mass $m$ of the sequence. We define the objective function for the infinite structure as:

$$o = \frac{m^{\alpha}}{\epsilon + \sum_{f=f_1}^{f_2} \mid Im[k_b(f)] \mid} \tag{3.3}$$

where $m$ is the mass of the sequence, $\alpha$ is a weighting factor to determine whether the main goal is to have a light structure ($\alpha$ is big) or a fast stopping band media.

Note: In equation (3.3), $m$ should be bigger than 1 in order to have $m^{\alpha} > m$ if $\alpha > 1$. Therefore, $m$ will be in grams when evaluating objective functions.

### Finite beams

For a finite structure, the main objective of this research is to reduce the radiated sound power over a frequency band. Thus, the simplest way of building an effective cost function is to sum the radiated sound power at different spectral lines in that frequency band. This is written as:

$$o = \sum_{f=f_1}^{f_2} \Pi(f) \tag{3.4}$$

where $f_1$ and $f_2$ are the frequency band limits and $\Pi(f)$ is the radiated sound power as a function of frequency as computed in equation (1.43).

As mass loading of a structure is an easy remedy to reduce sound radiation, we have to take into account the weight of the optimized structure. Thus, the cost function for a finite structure is defined as:

$$o = m^{\beta} \left[ 10 \log \left( \frac{\sum_{f=f_1}^{f_2} 10\Pi(f)}{10^{-12}} \right) \right]^{\alpha} \tag{3.5}$$

where $m$ is the mass of the structure, $\alpha$ and $\beta$ are weighting factors. In previous equation, $10 \log \left( \frac{\sum_{f=f_1}^{f_2} 10\Pi(f)}{10^{-12}} \right)$ represents the power radiated in decibel (dB) and is greater than 1. Assuming that $m$ is also greater than 1 (this is always possible if a change in the weight units is done), $\alpha$ and $\beta$ are changed to accommodate the designs needs. For example, if we want a poor sound radiator without big restriction on the structure weight, we can choose $\alpha = 4$ and $\beta = 1$. On the other hand, if weight is the main concern, $\beta$ will be chosen greater than $\alpha$.

# Chapter 4

# Sound radiation control by periodic beams

Sound power radiation and wave propagation reduction is usually achieved by adding active or passive external devices to the system. However, the governing idea in this chapter is that sound radiation control can also be performed by modifying the geometry of the structure. Instead of considering a beam with a uniform cross-section, we investigate the case of periodic beam with a structural period based on $n$-segment sequence. Alterations to the uniform beams are schematically represented in figure 4.1.

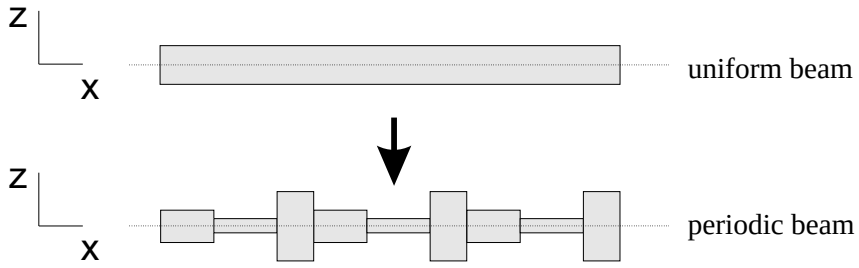


Figure 4.1: Periodic modifications of a uniform beam

This chapter is divided in two distinct sections. The first one investigates how infinite beams can be modified into periodic structures in order to avoid or reduce sound radiation. The second section focuses on finite beams and how a periodic variation of the beam thickness can alter the radiated sound power. In both sections, design of the structural period is either done using the Galois sequences or by using the genetic algorithm optimization technique.

## 4.1 Infinite beam

We have seen in chapter 1 whether sound radiates in the far field or not for infinite structure only depends on the bending wavenumbers propagating along the beam. Structural damping usually is the main factor for the attenuation of a propagating wave along an infinite and uniform structure. In order to only take into account the effects of the structure periodicity, the structural damping $\eta$ is assumed to be zero in this section. All the bending wavenumbers for infinite periodic beams were calculated using the Lee and Ke algorithm (see section 2.4.1).

### 4.1.1 Galois Sequences

#### Thickness computation

Galois sequences were introduced in section 3.1. These sequences are used to compute the thickness of each sub-element of a $n$-segment beam such as the one presented on figure 4.2. After choosing the prime number $p$ that fully describes the coefficients of the

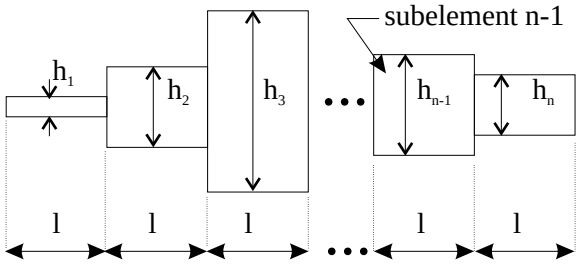


Figure 4.2: Representation of a structural period based on a Galois sequence

Galois sequence , we can compute the sequence $\sigma_n$ (see equation (3.1)). We define the thickness $h_i$ of the $i^{th}$ beam sub-element as the product of the $i^{th}$ coefficient of the Galois sequence times a minimum thickness $h_{min}$. This is written:

$$h_i = \sigma_i \times h_{min} \tag{4.1}$$

where $h_{min}$ corresponds to the minimum thickness a sub-element can have ($h_{min}$ should be chosen large enough to ensure that the structure does not break while being used). An example of thickness computation is presented in table 4.1 ($h_{min} = 0.0002$m and the prime $p$ is 11).

Note: No sub-element will have a null or smaller height than $h_{min}$ since Galois sequence guarantees the smallest residue is 1 (*c.f* equation (3.1)).

Table 4.1: Height computation for a Galois sequence

| $n$ | 1 | 2 | 3 | 4 | 5 | 6 | 7 | 8 | 9 | 10 |
|---|---|---|---|---|---|---|---|---|---|---|
| $\sigma_n$ | 1 | 4 | 9 | 5 | 3 | 3 | 5 | 9 | 4 | 1 |
| Sub-element thickness $h_n$ $10^{-3}$.[m] | 0.2 | 0.8 | 1.8 | 1 | 0.6 | 0.6 | 1 | 1.8 | 0.8 | 0.2 |

**Simulations**

Several infinitely long aluminium beams ($\rho = 2700\text{kg.m}^{-3}$ and $E = 71\text{GPa}$) with thicknesses which vary based on Galois sequences have been investigated. If the prime number $p$ defining the sequence is large, the ratio between the thickest and the thinnest sub-element will be large. For example, if $p = 53$, this ratio is 52. Thus, very high order Galois sequences require thicknesses to be in a very wide range that may not be practical or feasible. Therefore, we choose the prime number $p$ to be small. $p$ are 5, 7, 11. We choose $h_{min} = 0.0002\text{m}$ (a very thin aluminium beam) and arbitrarily set each sub-element length $l$ to 0.01m. Thus, the linear weight of the beams based on a 5-, 7- and 11-segment sequences are respectively 2.175, 2.030 and 3.828 $\text{kg.m}^{-1}$. The resultant beams are presented in figure 4.3.

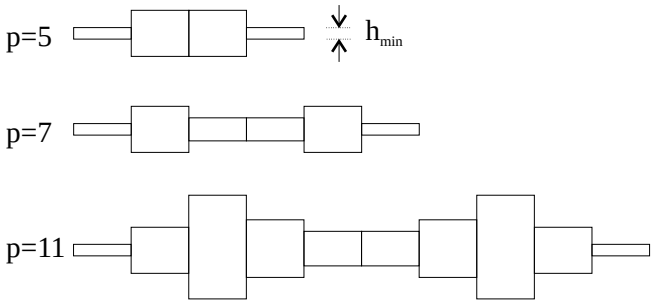


Figure 4.3: Beam profiles for various prime numbers $p$

The wavenumber solutions for the beam were calculated using the Lee and Ke algorithm (see section 2.4.1). Results for the wavenumber predictions are presented in figure 4.4.

Note: Both the complex and imaginary parts of the wavenumber estimates are presented when considering an infinite structure. If the imaginary part of a wavenumber is non zero, the corresponding wave does not propagate, i.e. it is in a stopping band. The rate of decay depends on the value of the wavenumber imaginary part: if $\mid Im[k] \mid$ is large, the wave decays "fast", if $\mid Im[k] \mid$ is small, the rate of decay will be low. Furthermore, in these bands, it can be seen that the real part of the wavenumber remains constant.

**Remarks**

As the prime number $p$ becomes large, i.e. the number of sub-elements in a sequence becomes large, a few distinct phenomena occur (see figure 4.4). First of all, the real part of the bending wavenumber become lower, i.e. waves will become supersonic at lower frequencies. This is mainly due to the increase of the average thickness of the beam. On the other hand, the imaginary part of the bending wavenumber obtains higher values in the stopping bands, meaning that in these regions, the bending waves decay faster away from excitation points.

In addition, as the number of sub-elements in a sequence becomes large ($p$ becomes large),

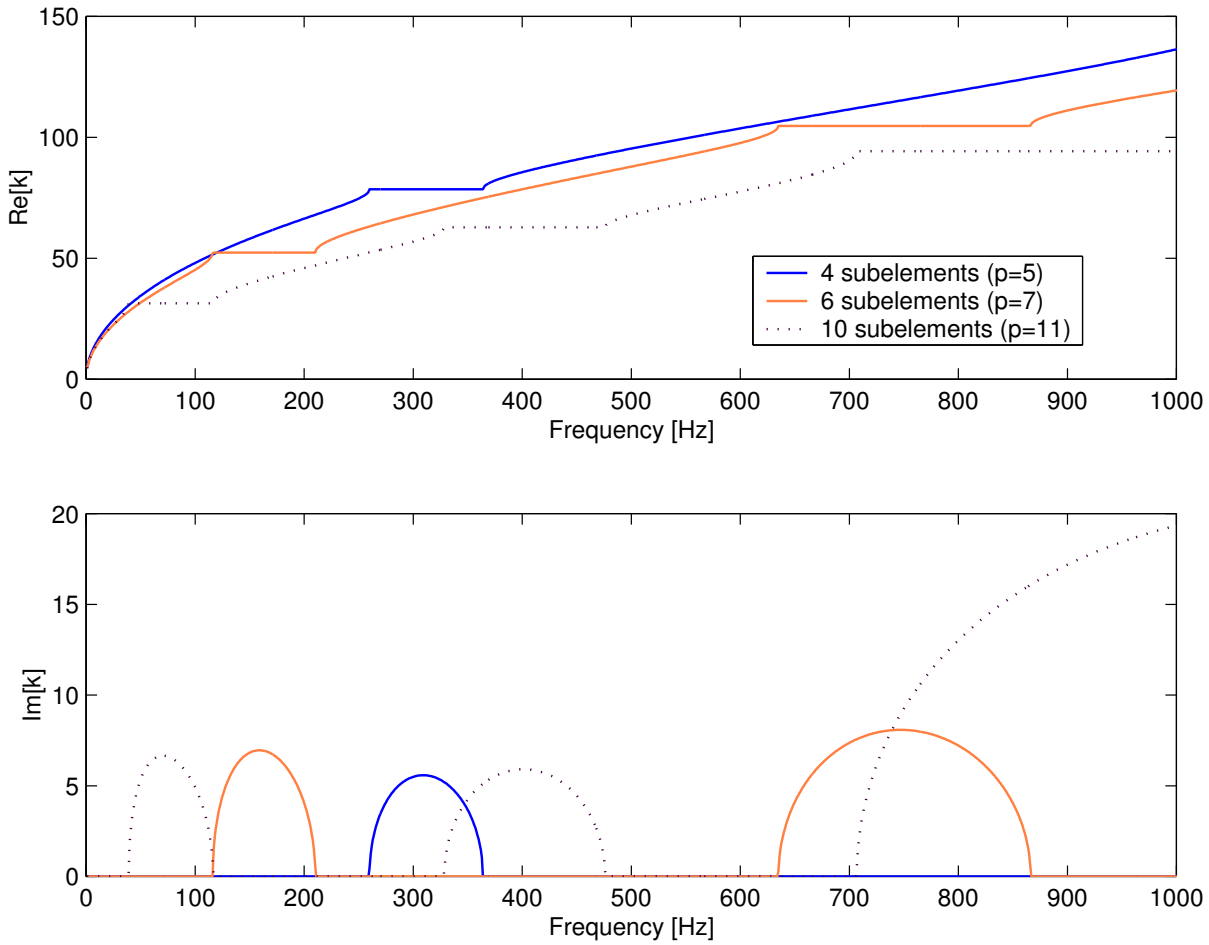


Figure 4.4: Wavenumber in infinite beams with cross sections based on different Galois series

the number of stopping bands for a given frequency band increases. For example, in the [0-1000]Hz region, a 10-segment beam has 3 stopping bands whereas a 4-segment only has one. This is not specific to Galois sequence, but to periodic structure in general with a large number of sub-elements in each sequence. Another interesting feature is that the width of these stopping bands also increases with $p$.

Finally, with large values of $p$, reduction of wave propagating at low frequencies becomes a possibility. For $p = 11$, a stopping band exists as low as 40Hz whereas no attenuation (for the chosen $h_{min}$) can be achieved if $p = 5$ below 260Hz. However, a few factors are not taken into account in that specific situation, especially the length of the sequence. For example, if the sequence is short, no stopping bands will exist at low frequencies regardless of the number of sub-elements (as shown later).

The results show that Galois sequences, also used in acoustic diffusion problems, have passing bands and stopping bands characteristics in beam elements. These stopping bands can be a useful feature to prevent bending wave propagation along a structure and resultant sound radiation. Therefore, it could be used as a bending wave insulator if an "infinitely" long beam is inserted between two structures.

### 4.1.2 Optimized infinite structure

Though infinite beams with periodic discontinuities based on Galois sequences have large stopping-bands, it may be tricky to have an attenuation of propagating waves in a specified frequency band. Besides, the rapid change of cross-section along the beam may not be acceptable for all applications: there are stress concentration points that may require $h_{min}$ to be large enough so that the beam does not break under possible external load. In addition, having a large prime number $p$ would yield to a large linear mass. Therefore, in this section, genetic algorithms are used to design periodic beams with a smaller range of height variations. The use of real-valued genetic algorithms for optimization have been previously discussed in section 3.2.

A periodic aluminium beam with a structural period based on sequences with different number of sub-elements has been optimized. The length $l_i$ and thickness $h_i$ of each element can be modified (see figure 4.5). The parameter $l_i$ is restricted to have values between 0.001m and 0.02m and $h_i$ is in the $0.5.10^{-3}$m to $1.5.10^{-3}$m range.

#### Wide band design

The genetic algorithm (see section 3.2) is run to optimize two infinite beams with structural periods based on 3-segment and 50-segment sequences. The objective was to have as

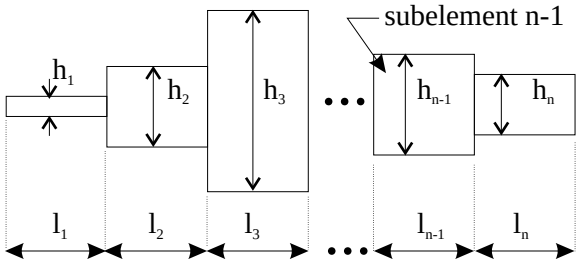


Figure 4.5: Representation of a structural period

large stopping bands as possible in the [0-500] Hz frequency range. The resultant beams are presented on figure 4.6. The bending wavenumbers estimates calculated using the theory of section 2.4.1 are shown in figure 4.7.

Once again, the beam with the larger number of sub-elements has more and wider stopping bands. For the structural period with 50 sub-elements ($n = 50$), there are narrow stopping bands in the [92-103]Hz, [148-158]Hz and [213-226]Hz frequency bands. These stopping bands do not attenuate wave propagation fast (the rate of decay is low as $Im[k_b]$ is small). However, control of bending wave propagation is mainly achieved at frequencies higher than 300 Hz in both cases with a high rate of decay (values of $Im[k_b]$ are high).

If control is to be achieved primarily at lower frequencies and on a large frequency band, the objective function (see page 39) has to be modified. For example, the imaginary part of the bending wavenumber could be weighted by a factor inversely proportional to the frequency. Thus, the genetic algorithm would take more into account attenuation of bending waves at low frequencies.

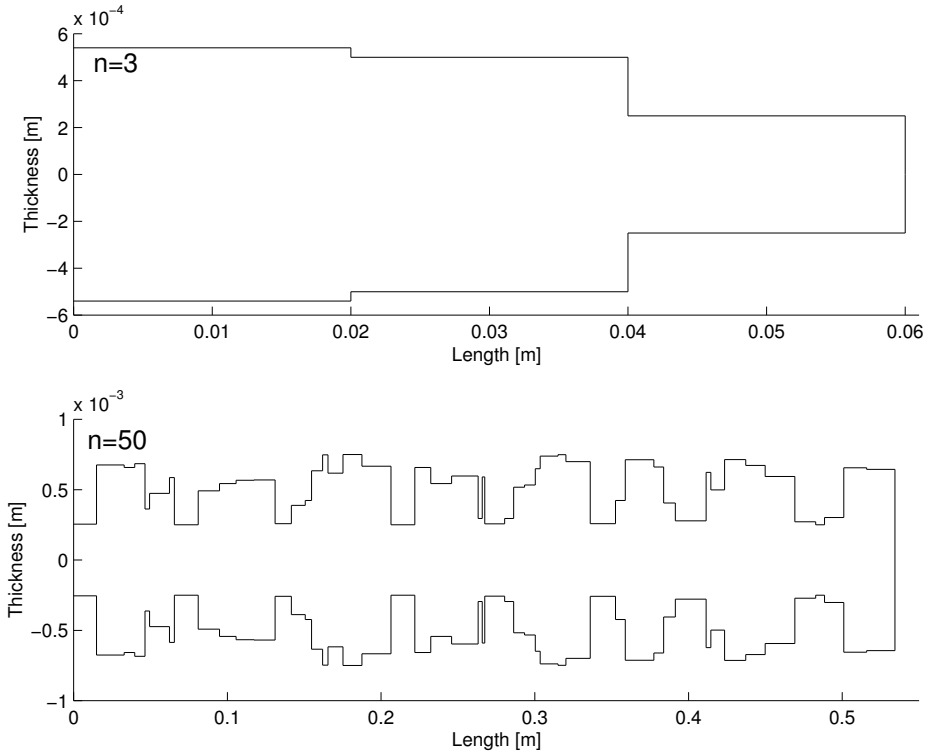


Figure 4.6: Resultant structural periods with $n$ sub-elements - wide band design

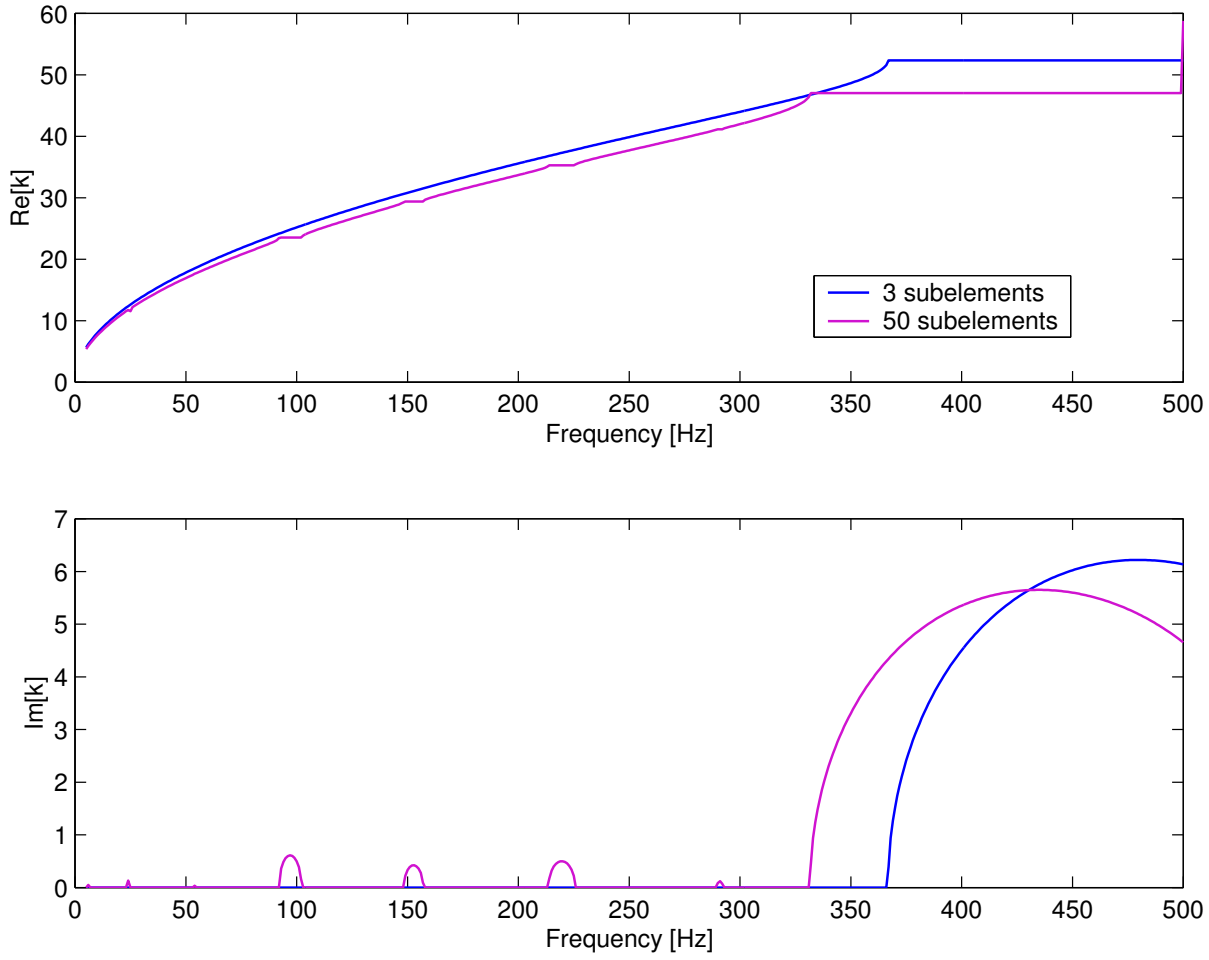


Figure 4.7: Wavenumber in infinite beams with cross sections optimized for the [0-500] Hz range

**Narrow band low-frequency design**

This simulation was run to show how effectively periodic structures can filter bending waves at low frequencies. The design criteria was to have as effective structure as possible to stop bending wave propagation in the [0-15]Hz frequency band. The 20-, 30-, and 50-sub-element sequences were optimized on both the length and the height of each sub-element. The resultant beams are presented on figure 4.8.

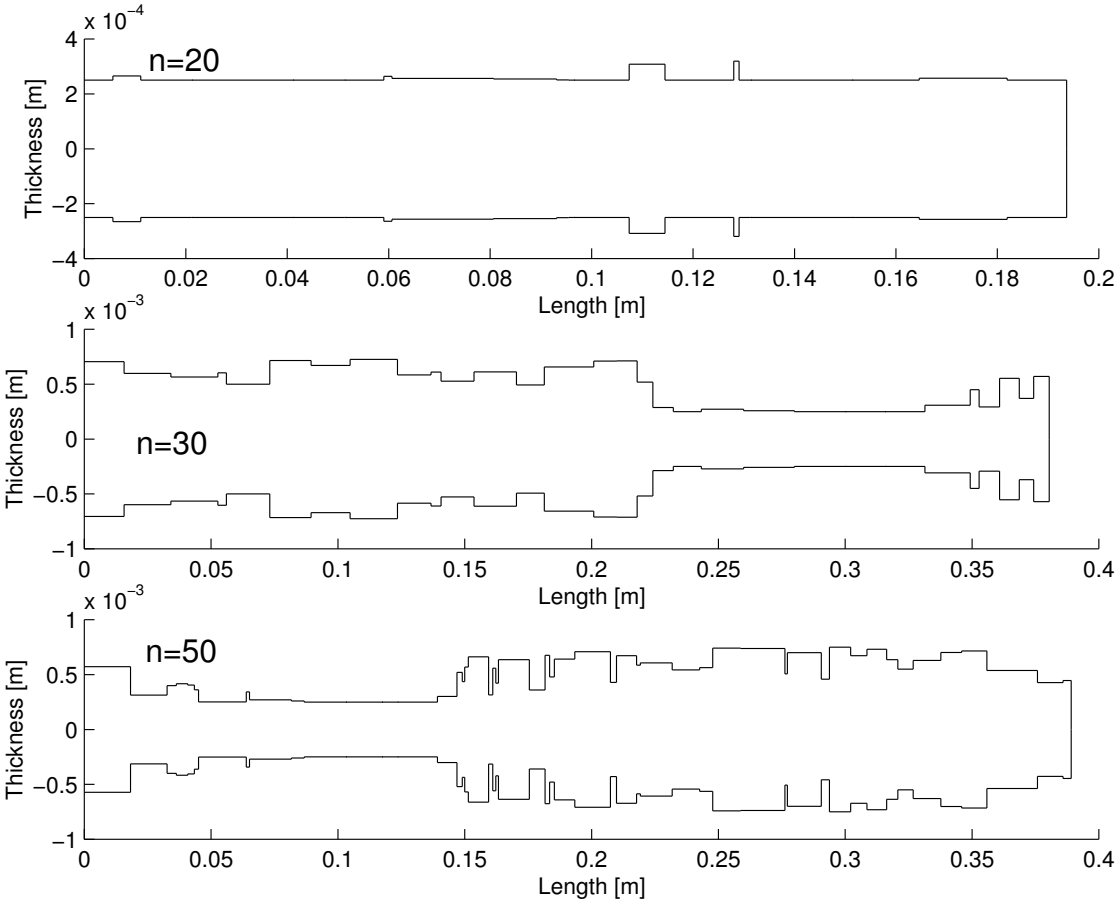


Figure 4.8: Resultant structural periods with $n$ sub-elements - narrow band low-frequency design

The bending wavenumber estimates using the Lee and Ke algorithm (see section 2.4.1) for these sequences are presented in figure 4.9.

While the 20-segment structures has no effect on wave propagation in the design area, both the 30- and 50-segment structures can achieve filtering with similar performance in

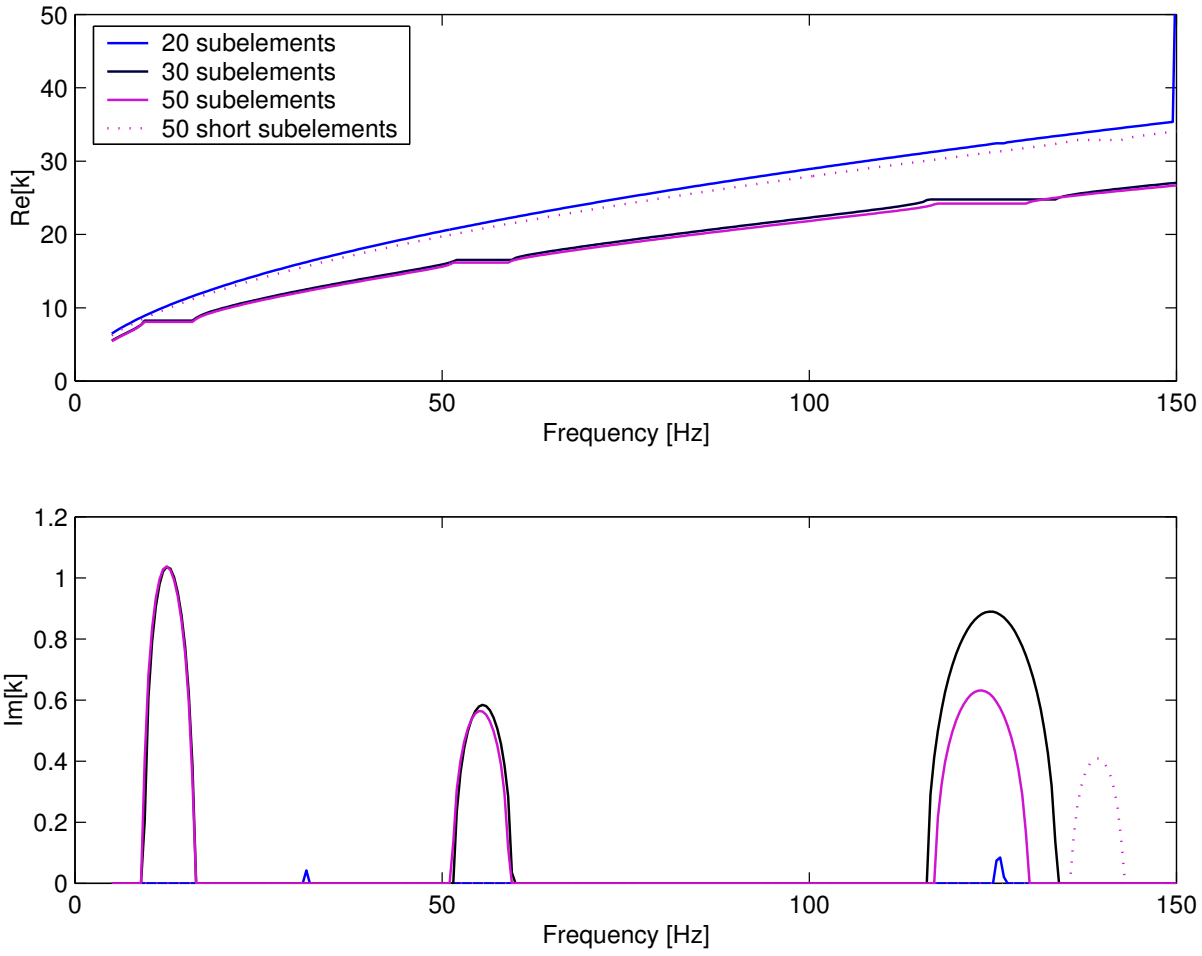


Figure 4.9: Wavenumber in infinite beams with cross sections optimized on the 5 to 15Hz band

the targeted control region. However, in the [0-150]Hz range, the 30-segment structure has the best performance since it has a larger stopping band between 100 and 150 Hz than any other presented case. This is because the genetic algorithm only optimized the sequence behavior in the design region.

An additional case is also presented on figure 4.9: a 50-segment sequence noted "50 short sub-elements". This sequence is made of 50 sub-elements but with a restriction on the overall length of the sequence: it as to be the same length as the 20-sub-element case. In that case, no control can be achieved in the design area. Thus, the overall sequence length is a factor in stopping low frequencies.

## 4.2 Finite beam

As most real-life structures cannot be considered as infinite structure, we also have to investigate how periodic finite beams radiate sound. In this section, we investigate finite periodic beams with structural periods based on a Galois sequence and on optimized designs. As our main objective is to to turn a structure into a poor sound radiator, it is useful to compute the radiated sound power $\Pi$ (see equation (1.43)).

#### Computation of radiated sound power attenuation

In order to evaluate the performance of a periodic structure over a frequency band, we compute the radiated sound power attenuation $H$. $H$ is found by comparing the radiated power from the periodic beam to the radiated power from a reference structure. We define $H$ (in dB) as:

$$H = 10 \log \left( \frac{\int_{f_1}^{f_2} \Pi_{ref}(f) - \Pi_p(f) df}{10^{-12}} \right) \tag{4.2}$$

where $\Pi_{ref}$ is the radiated power by the reference beam, $\Pi_p$ is the radiated power by the periodic beam and $f_1$ and $f_2$ are the frequency band limits ($f_1 \leq f_2$). In this thesis, the reference structures are the equivalent beams (see section 4.2.1).

In this section, all beams are made out of aluminium (with a loss factor $\eta$ of 0.005), are simply supported, measure 1m long and 0.025m wide. They are excited by a 1N point force at $x = 0.23$m.

### 4.2.1 Equivalent beam

The vibrational behavior of a beam is greatly affected by its overall weight. Thus, the sound power radiated by a periodic beam will be compared to the sound power radiated by an "equivalent beam" with a constant cross-section, with the same weight and with the same material properties as the periodic structure. The modal frequencies of a simply supported beam are defined as [14]:

$$f_n = \frac{n^2}{4L^2} \sqrt{\frac{Eh^2}{12\rho}} \tag{4.3}$$

where $n$ i the mode order, $h$ is the beam thickness and $L$ the beam length.

### 4.2.2 Beam based on a Galois sequence

#### Simulations

The beam is based on a Galois sequence with $p = 11$ where the minimum height $h_{min}$ is $2.10^{-4}$m and each sub-element has a length of 0.01m. The different heights along the sequence were computed in table 4.1 and one structural sequence was presented on figure 4.3. Since one structural period is 0.1m long, the finite beam is made of 10 sequences. Figure 4.10 illustrates the setup used in this section. The response of the beam is computed using the method presented in Appendix A.

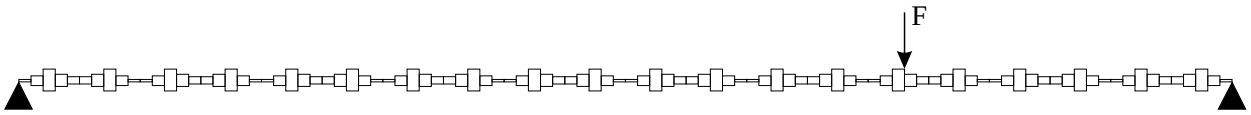


Figure 4.10: Simply supported beam based on Galois sequence ($p = 11$)

The sound power radiated is computed using equation (1.43) and presented in figure 4.11.

#### Remarks

The stopping bands of an infinite beam constructed with the same structural period were presented in figure 4.4. These bands were located between 38hz and 117 Hz and between 328Hz and 477Hz. For the case of a finite periodic beam, no strong peaks of radiated sound power occur in these stopping bands (see figure 4.11) while they do for the equivalent uniform beam. If we look at the shape of the beam responses (see figure 4.12), we can see that at frequencies in the stopping bands ($f = 51$Hz, $f = 110$Hz and $f = 400$Hz), the displacement decays faster away from the excitation point ($x = 0.23$) for the periodic beam than for the equivalent beam. However, for $f = 110$Hz, the periodic beam is a more efficient sound radiator than the equivalent beam because of a larger amplitude of displacement.

Out of the stopping bands, i.e in the passing bands, the power radiated by the periodic structure has peaks and dips. In these passing bands (see figure 4.12 for $f = 163$Hz, $f = 230$Hz and $f = 295$Hz, the displacement of the periodic beams do not decay fast away from the excitation. At $f = 163$Hz, the two beams have about the same displacement amplitude and radiate the same amount of power (76dB). Otherwise, the structure with the larger beam displacement radiates the more sound: at $f = 230$Hz, the periodic beam radiates 2dB more than the equivalent beam whereas at $f = 295$Hz, the periodic structure radiates 10dB less than the uniform structure.

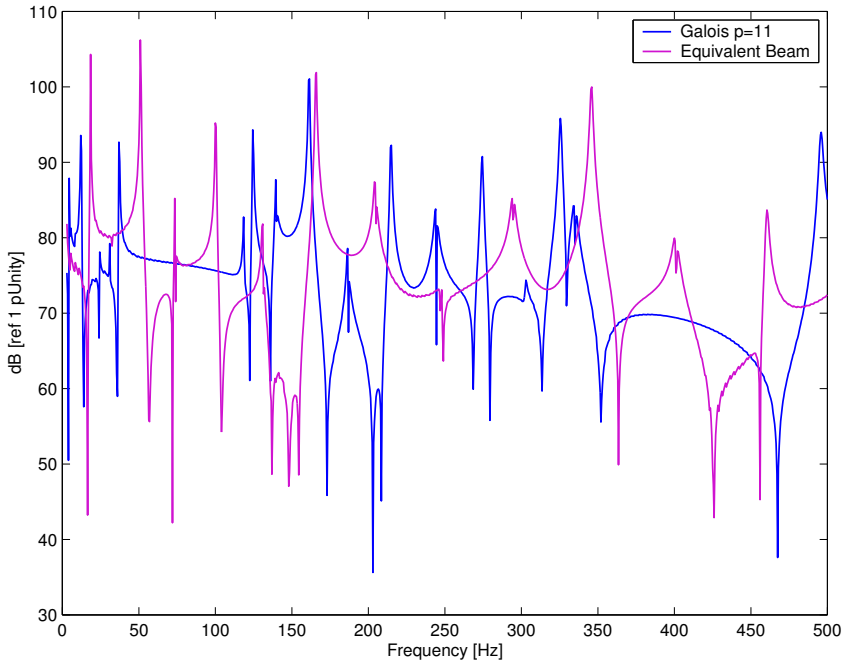


Figure 4.11: Sound power radiated by a simply supported beam based on Galois sequence ($p = 11$)

Using equation 4.2, we compute attenuations in the stopping bands, as well as on the [0-500]Hz band. Results are summarized in table 4.2. In the first stopping band ([38hz-117]Hz), the attenuation is about 10dB but most of this attenuation comes from the reduction of the power radiated around 51Hz and 100Hz. In the second stopping band ([328-477]Hz), attenuation is 10.8dB. Overall ([0-500]Hz), the attenuation is 2.8dB (this number does not reflect amplification in the radiated power at some discrete frequencies, at $f = 244$Hz or $f = 274$Hz for example).

Table 4.2: Sound power attenuation for a simply supported beam based on Galois sequence ($p = 11$)

| Frequency band [Hz] | 38-117 | 328-477 | 0-500 |
|---|---|---|---|
| Attenuation [dB] | 10.0 | 10.8 | 2.8 |

In this case, if the behavior of the infinite sequence is known, the beam cross section may be designed using the infinite model as long as the stopping bands have significant rate of attenuation, i.e. the imaginary part of the bending wavenumber is not small in these regions. Therefore, if a finite structure is excited in these stopping bands, the

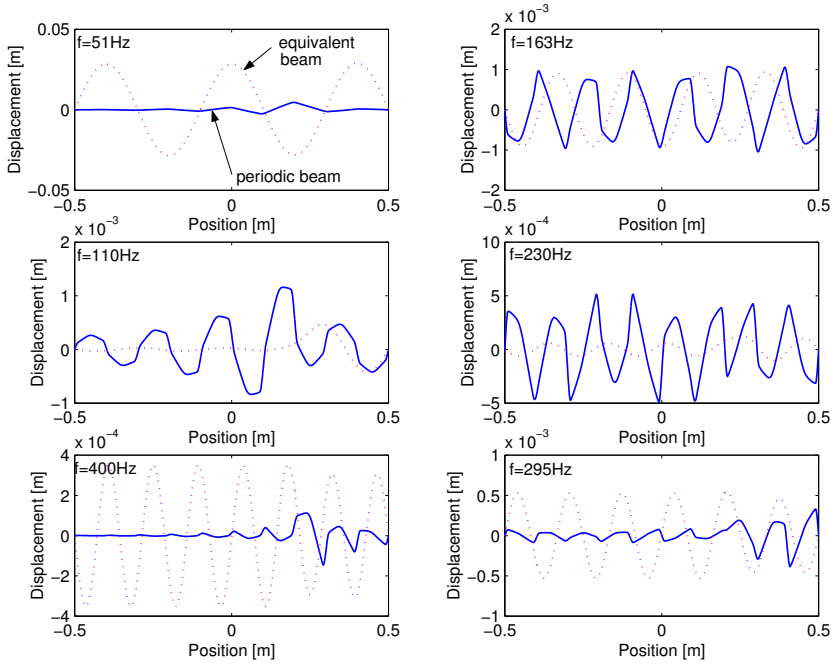


Figure 4.12: Responses at various frequencies for a beam based on a Galois sequence ($p = 11$)

corresponding bending waves are evanescent and do not have a large influence on the beam response away from the excitation point.

### 4.2.3 Optimized finite beams

The objective is to reduce the radiated sound power in the [5-50]Hz frequency band by different sets of periodic beams by designing the corresponding structural periods using the genetic algorithm. Two different kinds of optimization are run. Each sub-element thickness $h_i$ (see figure 4.5) has its value between 0.0016m and 0.0032m.

#### 1-parameter optimization

This case only involves the finding of the thickness of each sub-element of a 25-segment sequence by the genetic algorithm outlined in section 3.2. Each sub-element has a length of 0.01m, thus the beam is the repetition of 4 sequences. The beam is schematically represented on figure 4.13.

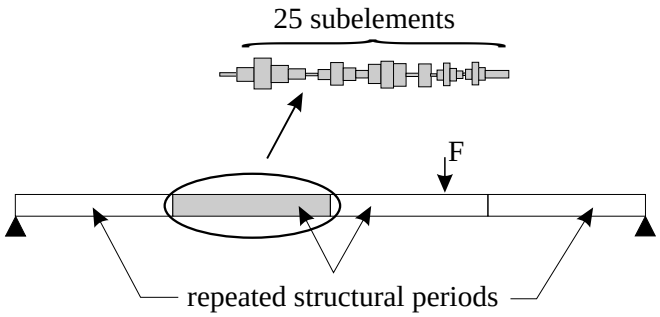


Figure 4.13: Beam with 4 repeated structural periods with 25-sub-element sequences

The first five modal frequencies of the equivalent beam are computed using equation (4.3) and presented in table 4.3.

Table 4.3: Equivalent beam modal frequencies

| Mode | 1 | 2 | 3 | 4 | 5 |
|---|---|---|---|---|---|
| Modal frequency [Hz] | 4.7 | 19.1 | 43.0 | 76.4 | 119.5 |

The sound power radiated is computed using equation (1.43) and presented in figure 4.14. Attenuation between the periodic beam and the equivalent beam is 16.9dB in the [5-50]Hz frequency band. The first mode (approximately around 4.7Hz) is below the minimum frequency of design. Therefore, the periodic structure is not appropriately design for sound reduction of this mode. The reduction is mainly achieved for the third resonance of the beam (43Hz). However, the periodic beam has its peak of radiated sound power 5Hz lower as the $3^{rd}$ mode of the periodic structure is shifted down . Both beam responses are computed at 38Hz and 43Hz and are presented on figure 4.15. At 38Hz, the periodic beam has a large displacement envelope with a $3^{rd}$ mode pattern. It is very similar to the pattern of the equivalent beam third mode (43Hz). This shows that the third mode of the periodic beam is lower than the third mode of the equivalent beam accounting for the peak in the radiated power at that frequency.

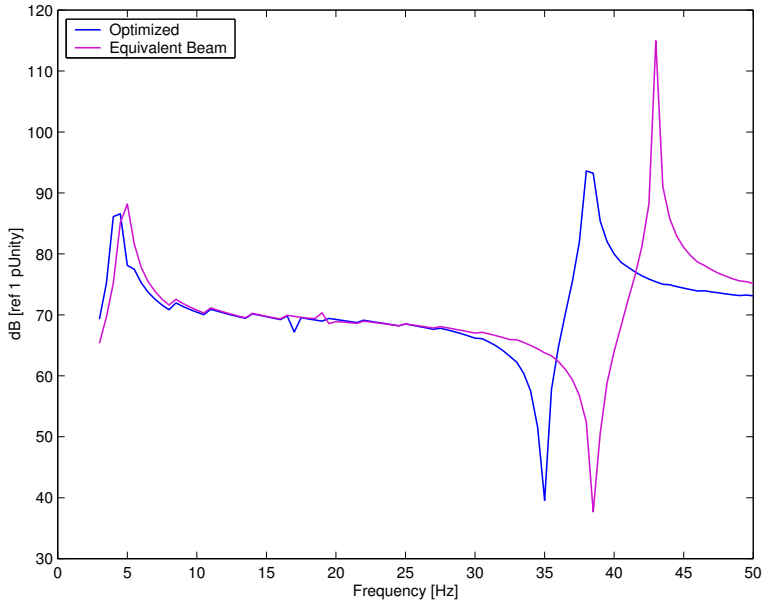


Figure 4.14: Sound power radiated by a beam with a 1-parameter optimized 25-sub-element sequence

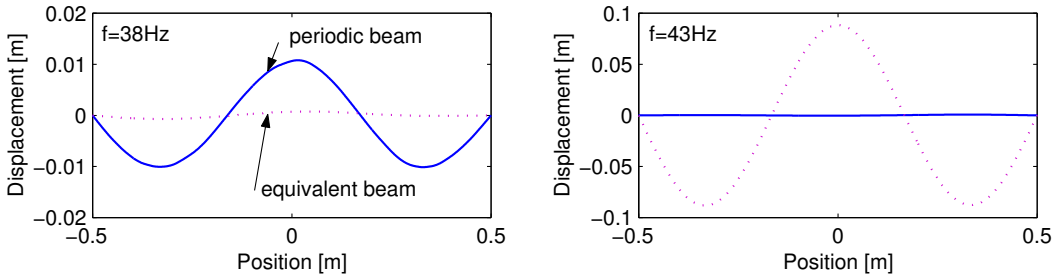


Figure 4.15: Beam displacements at various frequencies

**2-parameter optimization**

Two different cases are investigated: one beam is made of 10 identical 10-segment sequences (i.e the structural period $d$ is 0.1m long), the other is made of 4 identical 25-segment sequences (i.e the structural period $d$ is 0.25m long). The genetic algorithm can modify the sub-element lengths $l_i$ ($l_i$ has its value between 0.001m and 0.05m) and the sub-element thicknesses $h_i$ ($h_i$ has its value between 0.0016m and 0.0032m).

The first six modal frequencies of the equivalent beams are computed and presented in table 4.4.

Table 4.4: Equivalent beam modal frequencies

| Mode | 1 | 2 | 3 | 4 | 5 | 6 |
|---|---|---|---|---|---|---|
| Modal frequency (10-sub-element sequence) [Hz] | 4.4 | 17.8 | 40.1 | 71.4 | 111 | 160 |
| Modal frequency (25-sub-element sequence) [Hz] | 4.9 | 19.9 | 44.9 | 79.9 | 124 | 179 |

First, we consider the case for a beam with a structural period based on a 10-sub-element sequence. The radiated sound power corresponding to the design region is shown in figure 4.16. From table 4.4, we know that the first mode of the equivalent beam (4.4Hz) is not in the design region. Besides, as for the 1-parameter optimization, it appears that the peak of maximum radiated sound power are at lower frequencies for the periodic structure. The first peak is located around 4Hz and the second one around 35Hz (the equivalent beam has its third resonance mode at 40Hz and has a peak of radiated sound power at that frequency).

In order to investigate the shifting of resonance frequencies, the sound power radiated by the the periodic beam and the equivalent structure are presented on figure 4.17. If we consider the first six modal frequencies of the equivalent beam (see table 4.4), the equivalent beam has peaks of radiated sound power at the first six modal frequencies except the second one (17.8Hz). The periodic beam does not have peaks in its radiated power response at the same frequencies, but it appears that for frequencies below 200Hz, the power responses have a similar trend, except that peaks of radiated sound power by the periodic beam are at lower frequencies (4Hz, 35Hz, 63Hz, 98Hz and 141Hz). Assuming that the periodic beam has maxima of radiated sound power at its modal frequencies, we compare the beam responses of the equivalent beam and the periodic beam at for the third, the fourth, the fifth and the sixth modal frequencies. The vibrational shapes of both the equivalent beam and the periodic beam are presented in figure 4.18. For the supposed modal frequencies (35Hz, 63Hz, 98Hz and 141Hz), the periodic beam has mode shapes

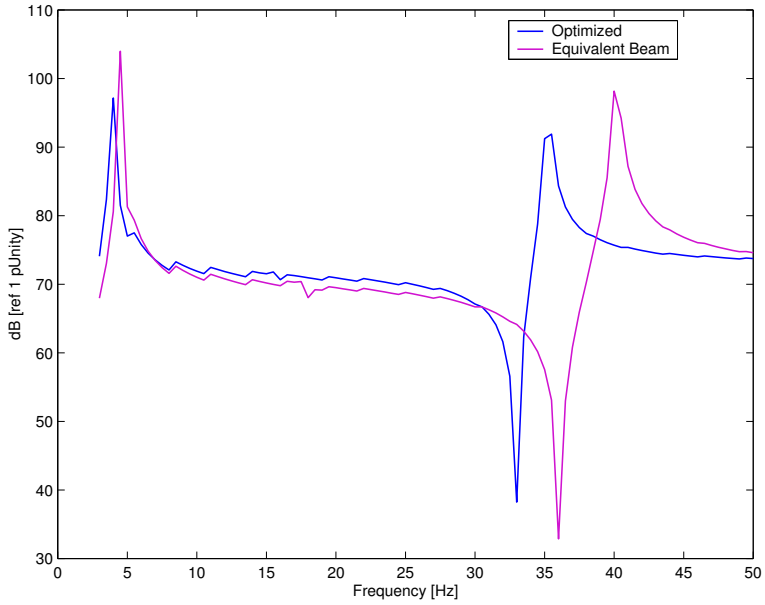


Figure 4.16: Sound power radiated by a beam with a 2-parameter optimized 10-sub-element sequence

similar to the modes shapes of the equivalent beam at its own modal frequencies (40Hz, 71Hz, 111Hz and 160.5Hz). We can also notice that for any of these modal frequencies, the beam with the larger displacement amplitude is the most efficient sound radiator.

Finally, the radiated sound power curve for the the periodic beam (see figure 4.17) shows no zones with a possible stopping band (c.f. the stopping band effects on the radiated power on figure 4.11). This can be verified by plotting the bending wavenumber for an infinite periodic structure with a structural period based on the 10-parameter optimized sequence. Results are presented on figure 4.19. There are no stopping bands in the [0-500]Hz frequency bands ($Im[k_b] = 0$), and thus no stopping bands in the design region. Therefore, control of the radiated sound power can be achieved without a stopping band in the [0-50]Hz frequency band.

Next, a beam made with four periodical structures based on 25-sub-element sequences is also optimized. This beam is constructed similarly to the beam schematically presented on figure 4.13 except that the length $l_i$ of each sub-element can be optimized by the genetic algorithm. The radiated sound power corresponding to the design region is shown on figure 4.20. Once again, the first mode of the equivalent beam is out of the design region. However, we can notice a 28.7dB peak attenuation around the first modal frequency (4.5Hz) ( as a comparison, the beam based on a 10-segment sequence only achieves 6.8dB peak attenuation for the peak corresponding to the first modal frequency. See figure 4.16).

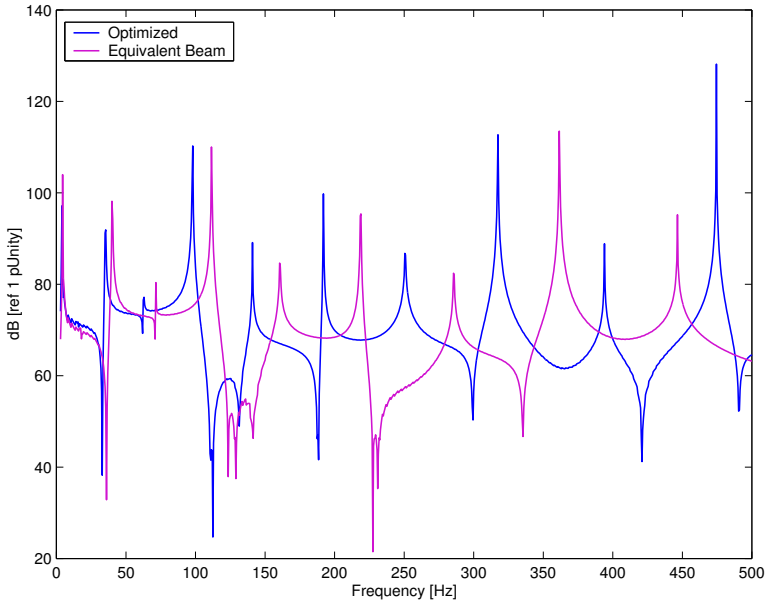


Figure 4.17: Sound power radiated by a beam with a 2-parameter optimized 10-sub-element sequence

Once again, the optimization reduced the radiated power for the third mode (44.9Hz for the equivalent beam and 38Hz for the periodic beam).

Achieved overall attenuations for the two optimized periodic beams are summarized in table 4.5. Both designs gives attenuation in the design region. However, the structure based on the 25-sub-element sequence has a much better performance (24.4 dB attenuation). However, on the [0-500]Hz frequency bands, both periodic structures radiate more sound than the equivalent beams (approximately 12dB amplification) because periodic beams have higher levels of radiated sound power for structural resonances above 100Hz.

Table 4.5: Sound power attenuation for beams with 2-parameter optimized 10- and 25-sub-element sequences

| Frequency band [Hz] | 5-50 | 0-500 |
|---|---|---|
| 10 sub-elements [dB] | 3.7 | -12.2 |
| 25 sub-elements [dB] | 24.4 | -12.5 |

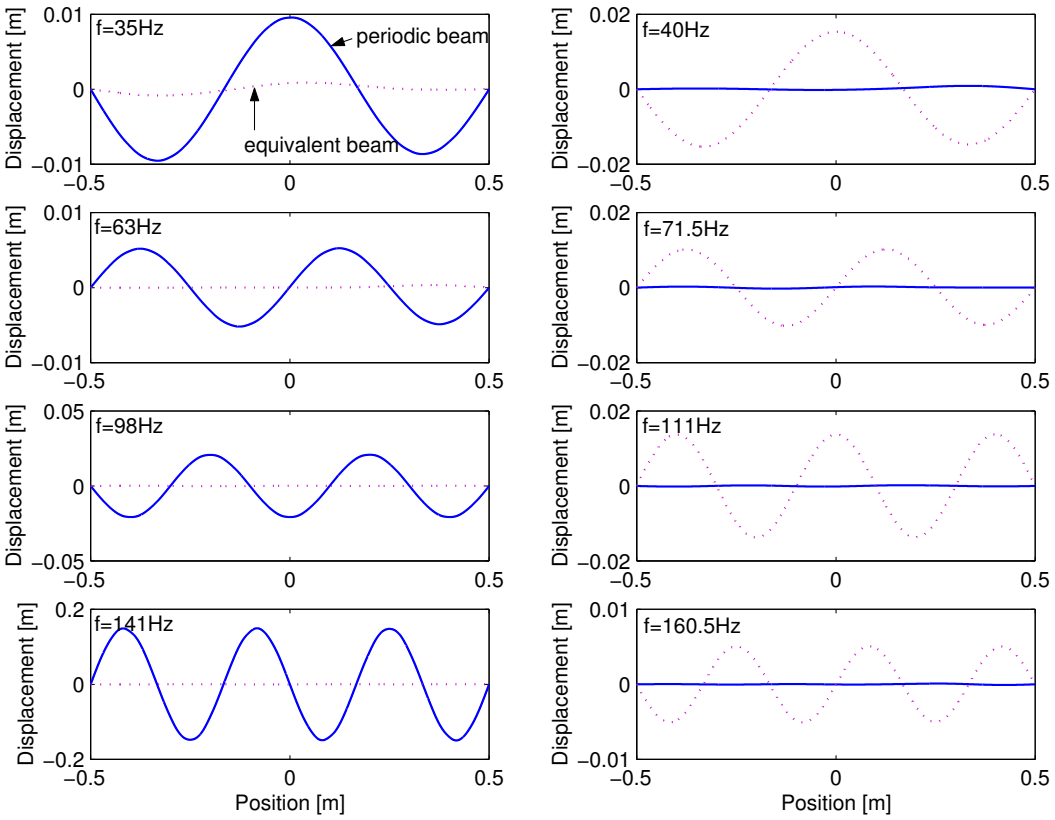


Figure 4.18: Beam displacements at various frequencies (2-parameter optimized 10-sub-element sequence)

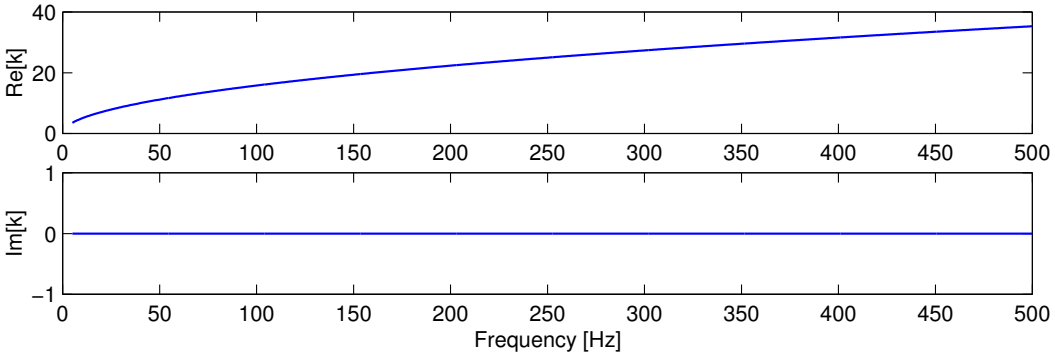


Figure 4.19: Bending wavenumbers for the infinite beam using the 2-parameter optimized 10-sub-element sequence

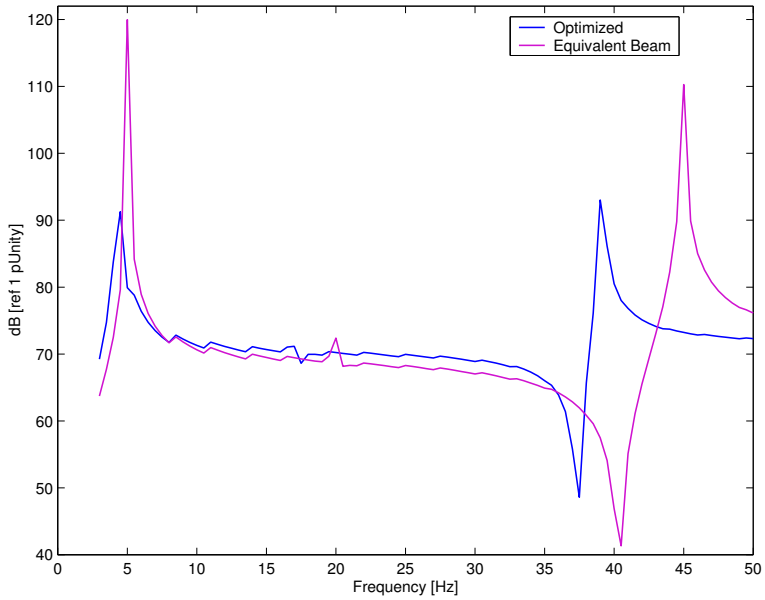


Figure 4.20: Sound power radiated by a beam with a 2-parameter optimized 25-sub-element sequence

**Remarks**

For the same number of sub-elements in the sequence, the 2-parameter optimization gives a better reduction in the targeted range than the 1-parameter optimization (7.5dB). Moreover, it is preferable to have long sequences with a large number of sub-elements to get better reduction in radiated sound as the 1-parameter 25-segment sequence optimization has a better performance than the 2-parameter 10-segment sequence optimization (13.2dB).

On all optimized cases, vibrational modes are shifted down in frequency compared to equivalent beams as a result of the change of morphology of the beam.

Finally, while control of radiated sound power can be achieved for a narrow band at low frequencies, in the [0-500]Hz frequency band, the sequential structures usually radiates more sound than the equivalent beams. This can be of concern if the structure is excited over a wide frequency band.

## 4.3 Summary

In this chapter, the design of finite and infinite periodic beams was investigated for the control of sound radiation. Structures were designed by either using Galois sequences or real-valued genetic algorithms. For both finite and infinite structures, radiation control was achieved when structures were excited within a stopping band. For finite beams, modifying the structure dynamics showed some potential for reducing the radiated sound power at low frequencies at which the structure has no stopping bands. Thus, these two ways of reducing the sound radiated from a finite periodic beam will be useful to design periodic smart skins considered in the next chapter.

# Chapter 5

# Sound radiation control by layered structures

The geometry of existing structures may not easily be modified to achieve a better control of sound radiation. Therefore, many passive treatments have become widely available to modify the structure vibrational responses to attenuate the radiated sound power. In this chapter, we introduce a new type of treatment based on periodic structures. A periodic smart skin is coupled with a beam (see figure 5.1) in order to change the bending wave components at the radiating surface of the coupled structure. Thus, the acoustic field is decoupled from the beam while the coupled structure is designed to be a worse sound radiator.

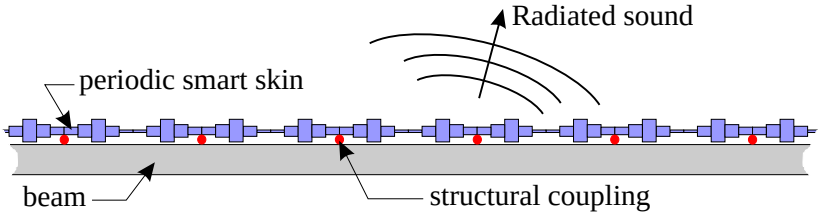


Figure 5.1: Periodic smart skin concept

This chapter is organized as follows. Firstly, the concepts of *subsonic* skins for sound radiation control are quickly reviewed for both finite and infinite structures. Then, additional numerical models for the evaluation of the bending wavenumber spectrums in an infinite beam loaded with an infinite smart periodic skin are introduced. The chapter ends with the investigation of smart skins for sound radiation control when coupled to finite beams.

## 5.1 Subsonic skin concepts

A structure made of two layers is a coupled waveguide in which multiple waves exist at one frequency. Therefore, we want to take advantage of the multiple waves in the structure to reduce the radiated sound power. In this section, we introduce the concepts of subsonic skins to decrease the structure radiation efficiency for both finite and infinite structures.

Note: A first definition of *subsonic* and *supersonic* regions was introduced in section 1.2.1: frequency regions where the bending waves velocity is lower than the wave velocity in air are defined as *subsonic* regions. In this section, we define a *subsonic* skin as a structure that as a lower bending wave velocity than the wave velocity in the reference structure.

### 5.1.1 Infinite structure

An infinitely long beam is coupled with a light subsonic skin as shown in figure 5.2. If the beam is structurally excited, most of the energy is in the beam path. However, since the skin is coupled to the beam, energy leaks from the beam to the skin. In order to satisfy the skin dynamics, some of the transferred energy is transformed into bending waves propagating with the skin wavenumber. These phenomena are schematically presented on figure 5.2. Thus, at the surface of the skin, the normal motion is a combination of two different waves: the skin wave and the beam wave. If the skin can "suck" enough energy from the beam, the skin wave will start to dominate the total normal motion of the coupled structure and thus reduce the radiated sound power since it's a weaker radiator.

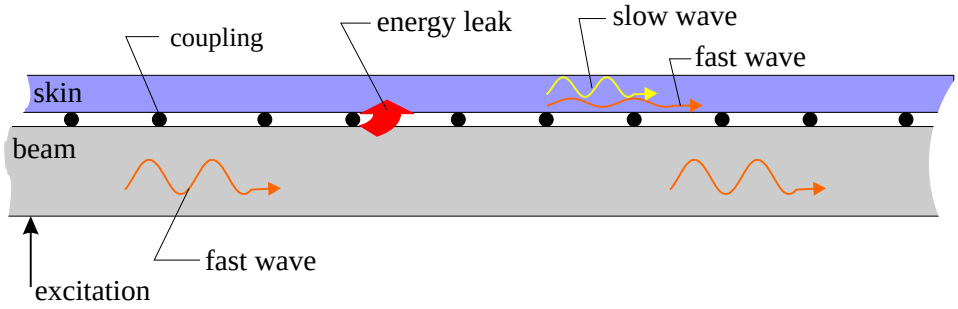


Figure 5.2: Subsonic skin concept for an infinite structure

### 5.1.2 Finite structure

The vibrational response of a finite system can be described by a sum of modes. However, not all modes have the same radiation efficiency: for a simply supported beam, odd modes are more efficient sound radiators than even modes at frequencies below the cut-off frequency (see figure 1.12). Thus, if a beam is excited at a frequency that corresponds to an efficient mode, a strategy for reducing the power radiated by the beam coupled with a smart skin is to modify the vibrational response of the coupled system into a less efficient radiating mode shape. An example is given in figure 5.3. In this example, we consider a simply supported finite beam excited at its third resonances (an efficient radiating mode shape). At that frequency, we also consider a skin that has its $4^{th}$ mode of vibration (an inefficient radiating mode shape). If the beam and the skin are coupled, the response of the structure is a combination of the motions off each layer. Thus, not all the energy in the system is used to establish the $3^{rd}$ mode shape of the coupled structure and energy leaks into the $4^{th}$ mode shape of the skin. Therefore, the modal amplitude of the efficient radiating mode is decreased and the modal amplitude of an inefficient radiating mode is increased. Thus, the coupled structure is a less efficient sound radiator than the beam alone.

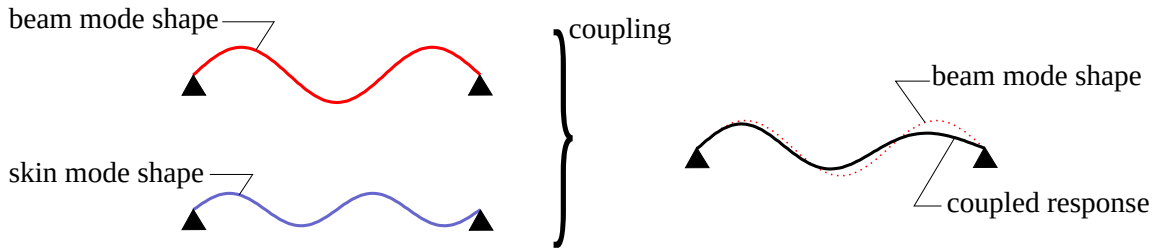


Figure 5.3: Alteration of the beam modal response with a smart skin

Note: The concept of smart skin can also be inverted and used to increase the radiation efficiency of a structure by moving energy from inefficient radiating modes to efficient radiating modes.

## 5.2 Solutions for the infinite problem

Methods for computing the wavenumber of bending waves in an infinite periodic beam were introduced in chapter 2. However, these techniques do not apply to infinite periodic multi-layered structures. Since a beam loaded with a periodic smart skin is a structure made with two different layers, a new way of computing the bending wavenumbers along

each medium has to be found before considering the problem of sound radiation for the infinite case.

### 5.2.1 Determinant problem

In section 2.4.1, the bending wavenumbers along a periodic infinite beam are found by computing the determinant of a matrix that fully describes one structural period. This method can be extended to the more general case of a periodic structure with many layers (one structural period of a periodic multi-layered structure is presented in figure 5.4).

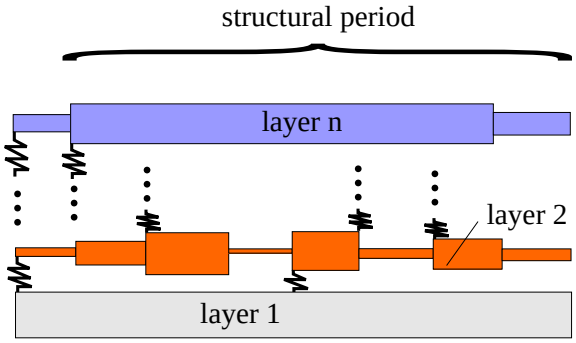


Figure 5.4: Structural period of a periodic multi-layered structure

Note: To be able to compute the wavenumbers for an infinite periodic multi-layered structure, one must find a common structural period to all layers.

Let us consider each periodic layer $\lambda$ independently. Thus, using equation (2.23), we can define a matrix $\mathbb{M}_\lambda$ that describes the infinite periodic layer $\lambda$:

$$\mathbb{M}_\lambda = \begin{bmatrix} \mathbb{E}_1(x_{1,\lambda}) & -\mathbb{E}_2(x_{1,\lambda}) & 0 & 0 & 0 \\ 0 & \mathbb{E}_2(x_{2,\lambda}) & \ddots & 0 & 0 \\ 0 & 0 & \ddots & -\mathbb{E}_{n-1}(x_{n-2,\lambda}) & 0 \\ 0 & 0 & 0 & \mathbb{E}_{n-1}(x_{n-1,\lambda}) & -\mathbb{E}_n(x_{n-1,\lambda}) \\ -\mathbb{E}_1(x_{0,\lambda}) & 0 & 0 & 0 & X_\lambda \mathbb{E}_n(x_{n,\lambda}) \end{bmatrix} \tag{5.1}$$

where $X_\lambda$ describes the wave propagation in the layer $\lambda$ and where the general form of the $\mathbb{E}_i$ matrix was defined in equation (2.19). Thus, for a structure made of $n$ layers, we have $n$ $\mathbb{M}$ matrices. Up to this point of the derivation, we only considered independent layers. However, layers are interconnected to form a multi-layered structure and coupling occurs.

If only discrete contacts between layers are considered, coupling is introduced in two different ways:

- an inter-layer coupling. Layer $i$ will have an influence on layer $j$. This is described by the matrix $\mathbb{T}_{i\to j}$. $\mathbb{T}_{i\to j}$ is made using rows of $\mathbb{M}_i$.
- a self-induced coupling. For example, the displacement of a layer constrained by a spring will create a force on that same layer. This self-induction effect is represented by matrix $\mathbb{S}$.

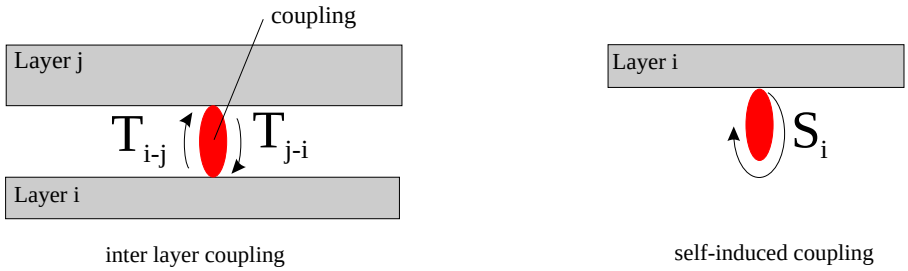


Figure 5.5: Schematic representations of matrix coupling

These couplings are schematically represented on figure 5.5.

Thus, we can assemble a matrix describing a multi-layer structure with the matrices $\mathbb{M}_\lambda$, $\mathbb{T}_{\lambda\to\gamma}$ and $\mathbb{S}_\lambda$. Assuming no external excitation on the multi-layered structure, the determinant formulation of the problem is written:

$$\begin{vmatrix} [\mathbb{M}_1+\mathbb{S}_1] & \mathbb{T}_{2\to1} & \dots & \mathbb{T}_{n\to1} \\ \mathbb{T}_{1\to2} & [\mathbb{M}_2+\mathbb{S}_2] & \ddots & \vdots \\ \vdots & \ddots & \ddots & \mathbb{T}_{n\to n-1} \\ \mathbb{T}_{1\to n} & \dots & \mathbb{T}_{n-1\to n} & [\mathbb{M}_n+\mathbb{S}_n] \end{vmatrix} = 0 \tag{5.2}$$

Thus, equation (5.2) can be written in a polynomial form

$$p(X_1,...,X_n) = 0 \tag{5.3}$$

Taking the natural logarithm of the set of roots $\{X_1,...,X_n\}$ satisfying previous equation will give the wavenumbers in the corresponding layers.

### Solutions to the determinant problem

For a multi-layered structure, the determinant problem is equivalent to finding the roots of polynomial $p$ with $n$ variables (see equation (5.3)). Let us consider a structure only

made with 2 layers. Thus, we need to solve the equation $p(X_1, X_2) = 0$. Solutions to this problem can be found graphically by considering the intersection(s) between the plane $p = 0$ and the surface $\Sigma$ described by $p(X_1, X_2)$. There are three different cases:

- There is no intersection between $\Sigma$ and the plane $p = 0$. Thus, there are no sets of solutions $\{X_1, X_2\}$. This is not a valid case since there would be no propagating or evanescent waves in any layer of the structure.
- $\Sigma$ has a finite number of extreme points that satisfies $p = 0$. Thus, there is a finite number of sets of solutions $\{X_1, X_2\}$.
- The surface $\Sigma$ cuts the plane $p = 0$. Thus, the intersection between the plane $p = 0$ and the surface $\Sigma$ is a curve and there is an infinite number of sets of solutions $\{X_1, X_2\}$.

For example, we consider an infinite periodic structure made with two uniform layers periodically interconnected by springs every 0.11m. One layer is a 0.001m thick magnesium beam, the other layer is a 0.003m thick aluminium beam. One structural period of the system is presented in figure 5.6.

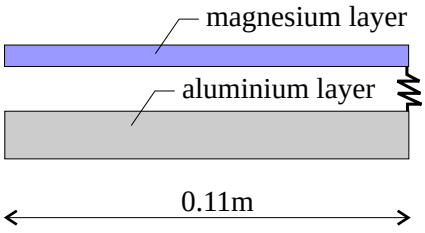


Figure 5.6: Structural period for a two layer structure

For that example, the surface $\Sigma$ is presented in figure 5.7 at one frequency ($f = 10$Hz). In order to ease the interpretation, the norm of $p(X_1, X_2)$ is considered: the roots of the system are the points along the rejection curve (i.e. the curve where the norm operator forces the polynomial $p$ to be positive or null). Thus, in the example, there is an infinite number of sets of bending wavenumbers that can satisfy equation (5.3) at one particular frequency.

Solutions for a structure with more than 2 layers cannot be drawn easily as the representation of polynomial $p$ is a complex hyperplane depending on more than 2 dimensions.

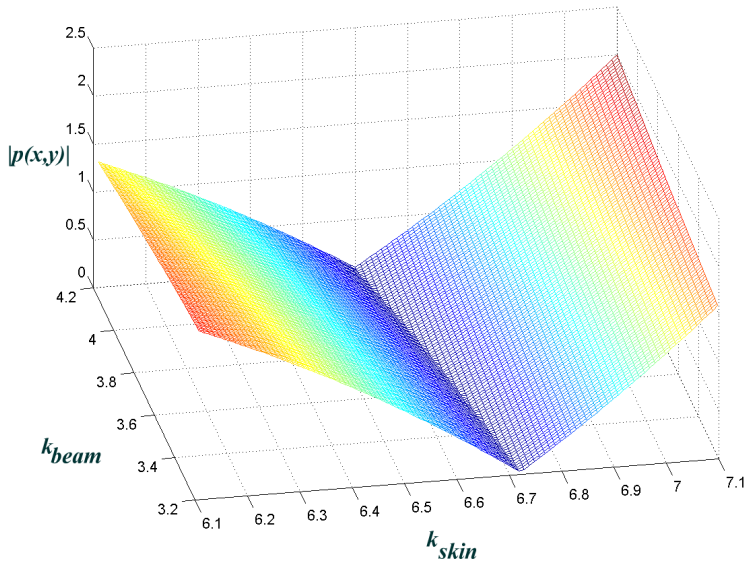


Figure 5.7: Representation of $p(X_1, X_2)$ for a two layer structure

### 5.2.2 Approximation

If a multi-layered structure is excited at one frequency, only a few bending wavenumbers dominate the structural response. Since there mathematically exists an infinite sets of solution to equation (5.3) as seen on page 66, a different method for evaluating the dominating bending wavenumbers in a 2-layer periodic infinite structure is introduced.

The technique is illustrated on figure 5.8. Let us consider a finite periodic structure $M$ made with $m$ structural periods of the infinite structure of interest. Since the structure is finite, bending waves are reflected at each end of the layers. Thus, in order to remove reflections at each layer end, we connect a semi-infinite element at each layer end (each semi-infinite element has the properties of the sub-element it is connected to). Therefore, waves are no longer reflected at the previous finite ends and propagate towards infinity. Thus, if we consider a number $m$ of structural period large enough, the finite structure $M$ will behave like an infinite structure. In order to find the wavenumber in each layer, we first need to compute the normal displacement $w$ in each layer. This is done using the method presented in the appendix A. The structure is either excited by an incoming wave from one of the semi-infinite ends or by a force $F$ at one end of the structure $M$. Once the displacement in each layer is known, the bending wavenumbers in each layer are computed using the wavenumber transform (see note page 68).

Note: a quick review of the wavenumber transform

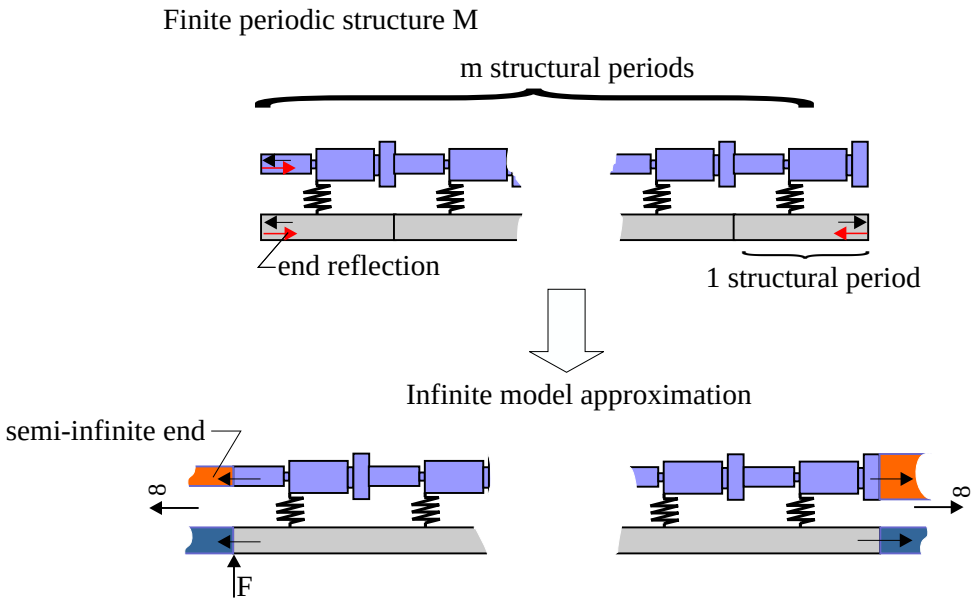


Figure 5.8: Finite number of periods in infinite structure

The wavenumber transform is a Fourier transform (FT) of the beam displacement [15]. It is defined as:

$$w(k) = \int_{\infty}^{+\infty} w(x,t)e^{-jkx}dx \tag{5.4}$$

where $w(x,t)$ is a continuous function describing the beam displacement and $k$ is the wavenumber. When a FT is applied to a spatial domain, the resulting domain is the wavenumber domain. If $w(x,t)$ is real, $w(k)$ is a complex number such that $w(-k) = w(k)^*$ ($^*$ is the complex conjugate operator). Thus, solutions in the wavenumber domain are represented as two different waves going in opposite directions. If k is real, the wave propagates. If $k$ is complex ($Im[k] \neq 0$), the wave is evanescent.

If the displacement of the beam is only known at a finite number of points, also called the sampling points (see figure 5.9), a discrete Fourier transform (DFT) [38] has to be used. In this research, we only use the following discrete Fourier transform property: in order to increase the wavenumber resolution $\Delta k$, the displacement of the structure should be considered on a length as long as possible. This is equivalent to the analysis in the frequency domain where to increase the frequency resolution, the measured time data is made as long as possible [38].

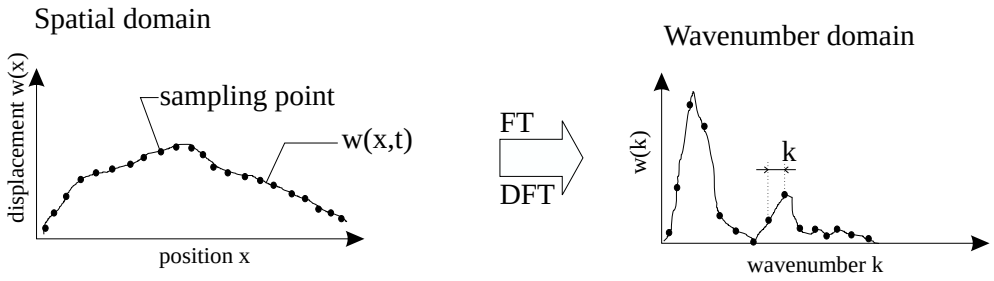


Figure 5.9: The wavenumber transform

### 5.2.3 Parameter sensitivity for a 2-layer infinite structure

Using the approximation method described in section 5.2.2, one can study the influence of changes of Young's modulus in one of the layer or change of the suspension springs. Investigations are done on a 2-layer medium, as the one presented in figure 5.10. 50 structural periods are considered in the infinite approximation. One of the layers is a uniform beam (it is made of aluminium, $E = 71$GPa and has a thickness of 0.003m), the other layer is a light skin based on a 2-sequence structure. The skin geometry is the same for all cases. The skin weight remains constant in all simulations and is just 18% of the beam weight. The four different skins are:

- The reference skin. It is made of extruded magnesium ($E = 44$GPa) and the springs are chosen with an arbitrarily value of 1000N.m$^{-1}$.
- The weakly coupled skin. It is the same skin except that the coupling springs are 1N.m$^{-1}$.
- The "soft" skin. The skin is made with a material with a small Young' modulus ($E = 0.44$GPa). Coupling springs are 1000N.m$^{-1}$.
- The "stiff" skin. The skin is made with a material with a small Young' modulus ($E = 4400$GPa). Coupling springs are 1000N.m$^{-1}$.

The coupled structure is excited through the beam by a force as presented on figure 5.8.

As a reference, the wavenumbers for corresponding infinite uncoupled skins and the beam are computed using the Lee and Ke algorithm (see section 2.4.1). Results are presented on figure 5.11. In the [0-700]Hz frequency band, the skins and the beam are subsonic with respect to air. The skin with a large Young's modulus is acoustically faster than the beam. The reference skin has a stopping band in the [360-598]Hz frequency band. The

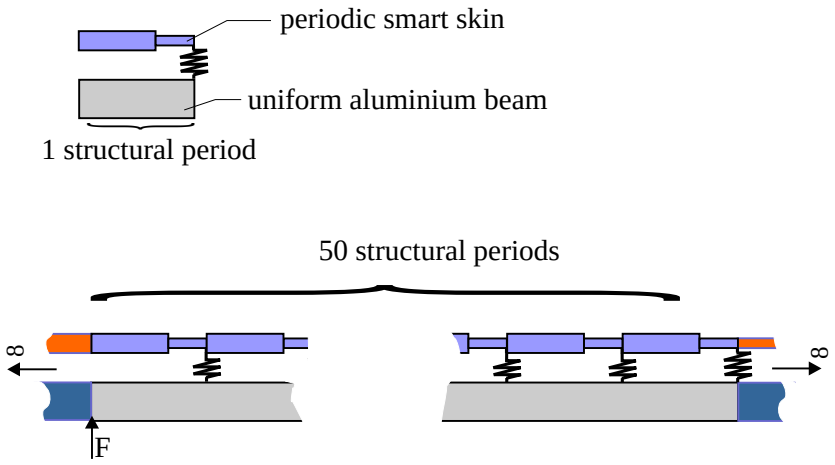


Figure 5.10: Setup for an infinite smart skin simulation

"soft" skin is acoustically very slow and has stopping bands in the [52-65]Hz, [190-230]Hz and [405-525]Hz frequency bands.

Note: A supersonic beam was not investigated in the frequency design band of interest since it would require a large thickness.

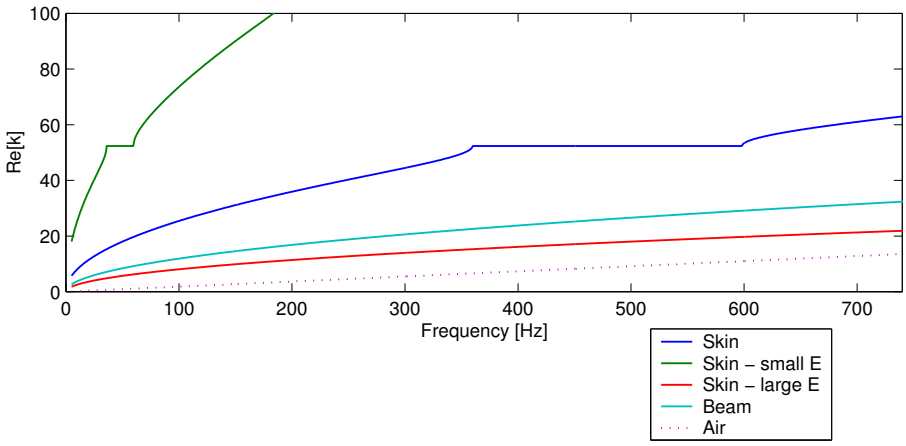


Figure 5.11: Wavenumbers for various infinite structures

### Optical branch wavenumbers

Bending waves are usually reflected from a change of the structural impedance. Thus, in a periodic structure, the wave field is composed of transmitted and reflected waves. If the incoming wave is described by the term $e^{-jk_b}$, the reflected wave is described by a term $Re^{jk_b}$, where R is a complex reflection coefficient ($\mid R \mid < 1$). In addition, a bending wavenumber in a periodic structure is defined *modulo* $2\pi/d$ (see the note page 29. Thus, if the reflected number is $-k_b$, the following also represent the same solution:

$$k_r = -k_b + n \times 2\pi/d \tag{5.5}$$

where $n$ is an integer. The wavenumbers $k_r$ for which $n \neq 0$ are defined as the optical branch wavenumbers [18]. If $n > 0$, $k_r$ can be positive. This is illustrated on figure 5.12.

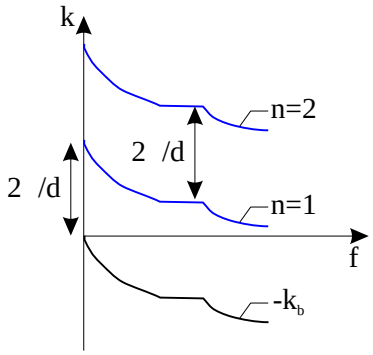


Figure 5.12: Wavenumber optical branch

In a structure, the optical-branch wavenumbers do not physically exist. However, the wavenumber transform of a periodic structure "sees" them since they correspond to existing incident or reflected waves in the structure. In the study case, $d = 0.06$m. Thus, $\frac{2\pi}{d} = 104.7\text{m}^{-1}$. For figures from 5.13 to 5.16, the optical branch wavenumbers are noted $o_+$ and $o_-$ for optical-branch wavenumbers respectively corresponding to the incident waves and the reflected waves.

### Simulations

The different structures were excited by a point force at one end of the beam (see figure 5.8). Simulation results for the bending wavenumber in the different coupled structures are presented from figure 5.13 through figure 5.16. While the $x-$ and $y$-axis respectively represent the frequency and wavenumber spaces, the calibrated color scale indicates the amplitude of the wave in dB (with a reference value of 1). If the skin completely covers the beam, sound radiation is only due to the skin.

The coupled reference case is presented on figure 5.13. Above 70Hz, the beam response ( 5.13-a) has only one dominant wavenumber. This bending wavenumber is equal to the bending wavenumber computed for an infinite beam and presented in figure 5.11. As frequency increases, the amplitude of the wave corresponding to the dominant wavenumber decreases (this is equivalent to the decrease of the transversal displacement envelope of an infinite beam excited with a force of constant norm as the excitation frequency increases). In the skin, two different waves exist: a wave is influenced by the skin dynamics (noted $k_s$ on figure 5.13-b) and to a less extent (i.e. smaller wave amplitude), another wave is forced by the beam dynamics (noted $k_b$). Both of these waves have about the same wavenumbers as the ones predicted for an infinite beam or an infinite skin (see figure 5.11). Thus, the wave corresponding to the skin dynamics does not propagate in the stopping band ([360-598]Hz). Optical branch wavenumbers are also present, one is governed by the skin dynamics, the other one by the beam dynamics. Both of the optical branch wavenumbers have smaller amplitudes than their corresponding ($k_b$ and $k_s$). Below 70Hz, both the skin and the beam have different behaviors than the infinite prediction. This is mainly because of the "stiff" coupling between the two layers.

In the stopping band ([360-598]Hz), the skin normal motion is only governed by the beam bending wavenumber. The waves resulting from the beam bending wavenumber do not have a larger amplitude in that frequency band. Thus, in this region, the coupled structure would be a less efficient sound radiator (if it were supersonic in that region) since only the energy in the wave with the beam bending wavenumber would radiate sound.

### Coupling stiffness sensitivity

Simulations for a weak coupling (springs are $1\text{N.m}^{-1}$) are displayed on figure 5.14. In the beam ( 5.14-a), there is one dominant bending wavenumber. This wavenumber is equal to the one predicted for the infinite case (see figure 5.11). Results show that in the skin ( 5.14-b), there are two different wavenumbers resulting from each layer dynamics as for the reference case. However, the amplitudes of the waves described by these wavenumbers are about 20dB lower than for the reference case (see figure 5.13) while in the beam of the softly coupled structure the levels are higher. Thus, energy does not transfer as easily from the beam to the skin, i.e. the skin does not vibrate as much. If the displacement is reduced, sound radiation is also reduced. Furthermore, the beam response is not affected by the skin at low frequencies, while the skin response remains influenced by both the beam and the skin wavenumbers. This differs from the reference case (see figure 5.13) where below 70Hz, strong coupling occurs.

Ultimately, if the layers are not physically interconnected, one should take into account the effect of acoustically coupling between the two layers. This corresponds to the minimal coupling achievable and it depends on the properties of the fluid enclosed in between the

two layers. It may be possible to construct a skin that encloses a vacuum between it and the beam is acoustic coupling reduces performances.

Finally, if the coupling stiffness is too high, waves will be reflected away from the structure up to a certain frequency as the impedance of the finite structure is too high compared to the one of the infinite ends. In that case, the method for estimating the bending wavenumbers is not appropriate.

### Young's Modulus

By changing the Young's modulus of the skin, the dynamics, and therefore the bending wavenumber of the skin are changed. The bending wavenumber for the uncoupled beam, the "soft" skin and the "stiff" layer are presented on figure 5.11. Figure 5.15 presents the results for a skin with a small Young's modulus ($E = 0.44GPA$) located on a beam. Below 70 Hz, there are coupling effects between the skin and the beam and the dynamics of both the skin and the beam do not follow the wavenumber prediction for the infinite uncoupled structures. Above 70Hz, the beam response ( 5.15-a) is dominated by the waves having the wavenumber of the corresponding infinite beam (see figure 5.11). Above 70Hz, the skin response ( 5.15-b) is a combination of both the wave fields due to the skin and the beam dynamics. The waves propagating due to the skin dynamics are dominant. In addition, there are three stopping-bands ([52-65]Hz, [190-230]Hz and [405-525]Hz) for which the skin dynamics prevent some waves to propagate. Thus, as for the reference case, less sound is radiated in these frequency bands.

Figure 5.16 presents simulations for a beam loaded with a skin with a large bending stiffness (the Young Modulus of the reference skin is multiplied by a factor of 100). As the bending wavenumber in a beam is proportional to $\sqrt[4]{\frac{1}{E}}$, the skin wavenumber becomes lower as $E$ increases and the structure becomes acoustically faster. The beam response (5.16-a) is dominated by the predicted wavenumber of the same infinite beam. However, between 100Hz and 170 Hz, the skin dynamics have a small effect on the beam response, moving some energy at lower wavenumbers in the beam. Thus, this structure is not an interesting arrangement for reducing the radiated sound power since in that frequency band, the beam becomes acoustically faster. The skin response (5.16-b) is a combination of waves resulting from the skin dynamics ($k_s$) and the beam dynamics ($k_b$). However, at all frequencies, the skin is acoustically fast compared to the beam. Thus, energy that leaks from the beam to the skin is transferred to waves in the skin that are supersonic at lower frequencies than the waves in the beam. Thus, this coupled structure is a more efficient sound radiator than the beam alone. Of course, this system may be very useful in one application desired to increase the sound radiation from a structure (a loudspeaker for example).

In general, the results have shown that it appears possible to affect the dynamics of a bare structure with a periodic beam in order to reduce the sound radiation in selected frequency bands.

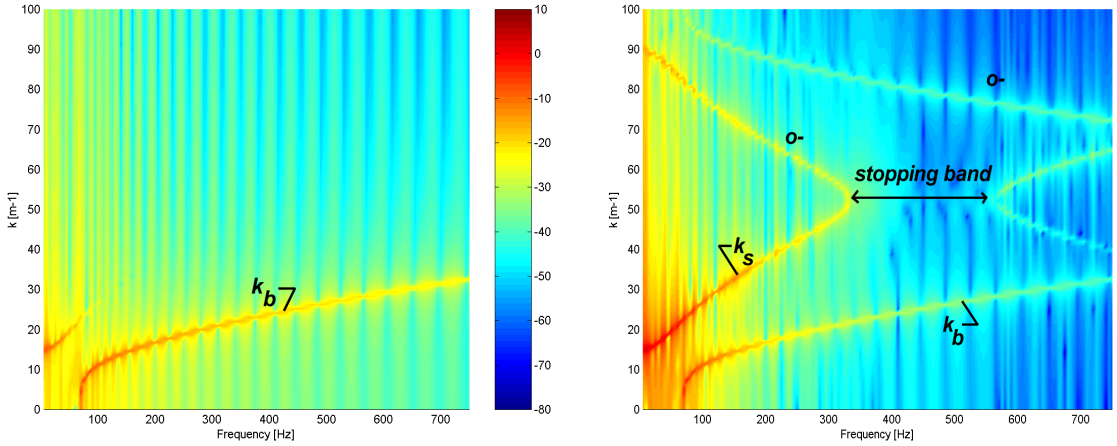


a) Beam b) Skin

Figure 5.13: Wavenumbers estimates for the reference system

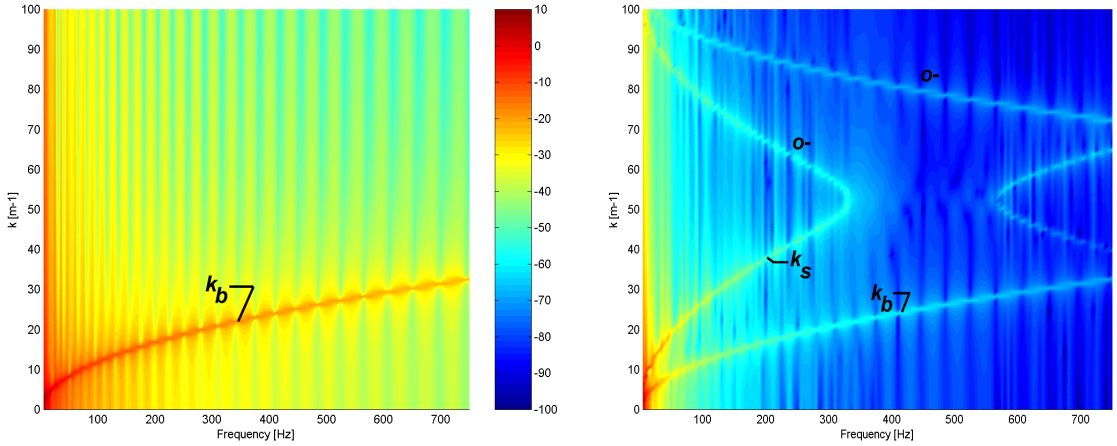


a) Beam b) Skin

Figure 5.14: Wavenumbers estimates for a system coupled with soft springs

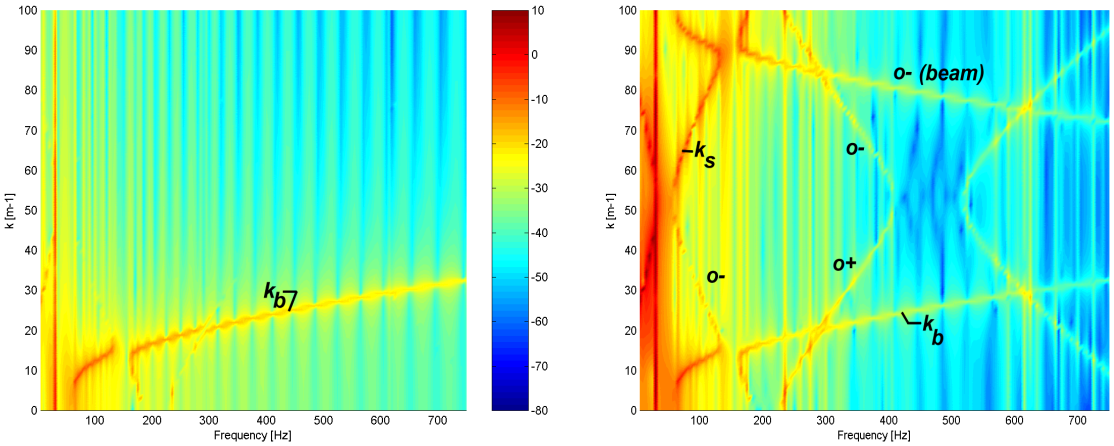


a) Beam b) Skin

Figure 5.15: Wavenumbers estimates for a skin with a "small" Young's modulus

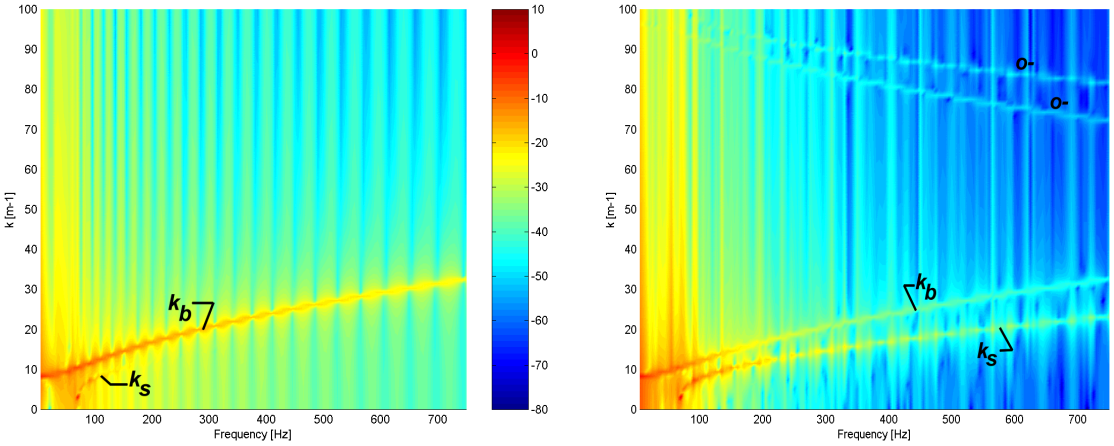


a) Beam b) Skin

Figure 5.16: Wavenumbers estimates for a skin with a "large" Young's modulus

## 5.3 Finite beam with one continuous layer

There are a few cases where structure can be considered infinite. Therefore, we need to address the problem of sound radiation control for finite structures. In this section, we investigate a finite periodic 2-layer structure: a simply supported reference beam is loaded with a periodic smart skin (see figure 5.17). Skins are designed using the genetic algorithm discussed in section 3.2. Since the structure is finite, we try to minimize the radiated sound power $\Pi$ as defined in equation (1.43).

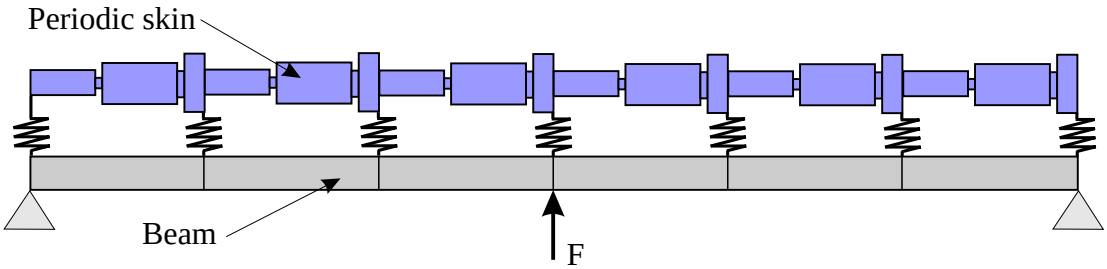


Figure 5.17: Finite beam loaded with a periodic skin

### 5.3.1 Setup

#### Reference beam

The reference setup in this thesis is a simply supported aluminium beam with a rectangular cross section. It has the following properties: Young's modulus $E = 71$GPa, $\rho = 2700$kg.m$^{-3}$, length $L = 1$m, width $b = 0.025$m and thickness $h = 0.003$m.

Note: Damping $\eta$ is assumed to be 0.005, unless specified otherwise.

The modal frequencies of the reference beam are computed using equation (4.3) and presented in table 5.1. The first eight modes are below 500Hz and will be the main concern of this research.

Table 5.1: Beam modal frequencies

| Mode | 1 | 2 | 3 | 4 | 5 | 6 | 7 | 8 | 9 | 10 |
|---|---|---|---|---|---|---|---|---|---|---|
| Modal frequency [Hz] | 7 | 28 | 63 | 112 | 174 | 251 | 342 | 446 | 565 | 698 |

**Skin**

The skin is made of extruded magnesium $E = 44$GPa, $\rho = 1740$kg.m$^{-3}$, with a loss factor of $\eta = 0.0005$. This material was chosen for being less dense than aluminium while being almost as rigid.

**Excitation**

For every simulation, the beam is excited at $x = 0$m, $y = 0m$ by a point force $F$, where $F = 1$ Newton (the coordinate system was introduced in figure 1.7). In that configuration, only odd modes are excited so that attenuation can be made on the most efficient radiating modes.

### 5.3.2 Manual design

The Lee and Ke algorithm was introduced in chapter 2 to predict the wavenumber in infinite structures. The idea is to use this algorithm along with the real-valued genetic algorithm reviewed in section 3.2 to design the skin with a stopping band in the frequency band of concern. This is similar to what is done for infinite periodic beam in section 4.1.2.

The skin is based on a 10-segment sequence with a thickness between 0.0005 and 0.001m. As no infinite structure could be found with stopping bands around the $1^{st}$ and $3^{rd}$ modes, the control region was set around the $5^{th}$ mode (174 Hz). The bending wavenumber estimates for the infinite skin are displayed on figure 5.18. The stopping band is located in the [134-203]Hz band. On the same figure, the wavenumbers in air are also plotted to verify that the skin remains an acoustically slow medium in the design region.

The reference beam is loaded with the designed skin and coupled by springs of 1000N.m$^{-1}$ (this stiffness is arbitrarily chosen for being an intermediate value that does not strongly couple or decouple the skin from the beam). There is a coupling spring at the end of each structural period. One structural period of the structure is presented on figure 5.19. The skin weight is equivalent to 17% of the beam weight.

Simulation of the power radiated by the structure is shown on figure 5.20. The radiated power peak corresponding to the $3^{rd}$ mode of the reference beam is shifted down 7Hz for the coupled skin structure. From 80Hz to 98Hz, the coupled structure is a much more efficient sound radiator than the reference beam. There are no beam modes in this narrow frequency band. Thus, these peaks are a result of the skin dynamics and the coupling with the beam. In the stopping band ([134-203]Hz), the coupled structure always radiates less sound than the reference beam. However, there are no clear signs of a stopping band

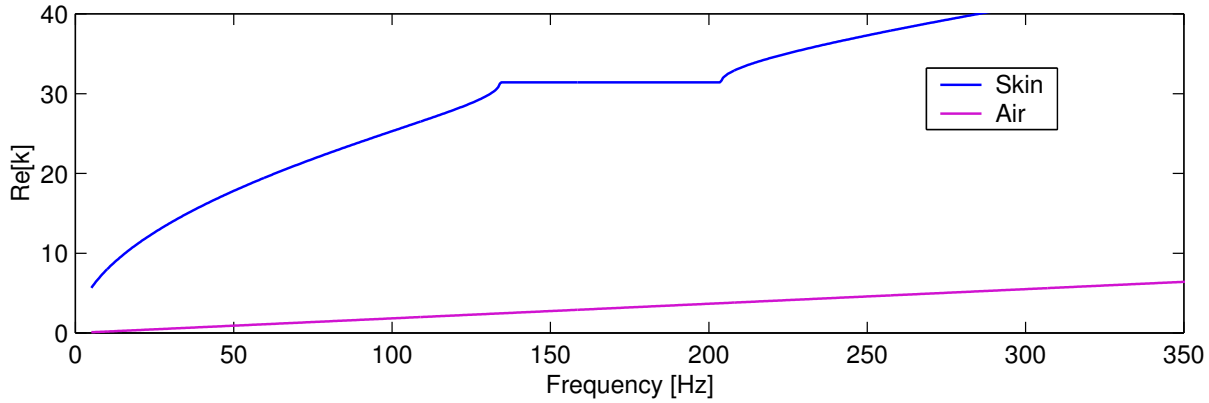


Figure 5.18: Skin wavenumbers - manual design

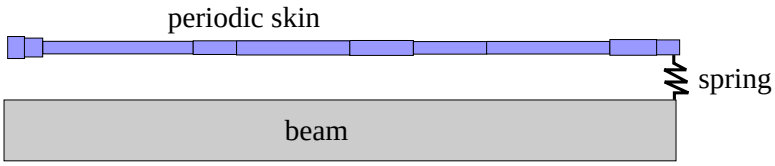


Figure 5.19: Structural period of the beam loaded with the designed skin

on the radiated power plots as for the case of a finite periodic beam (c.f. section 4.2.2). In this frequency band, both power curves have similar trends. From 100Hz to 500Hz, the 2-layer structure power response has no peaks higher than the beam power response, every high order mode being efficiently "controlled".

Vibrational shapes of both the reference beam and the smart skin coupled with the reference beam are presented in figure 5.21 for various frequencies.

- At 90Hz, the coupled structure radiates much more sound than the reference beam. This is due to a larger amplitude of displacement, but also the shape of the skin displacement: the average displacement of the skin is not zero since the displacement close to the position $x = 0$ is positive and much larger than the sum of all the negative displacements. Thus, the net volume velocity on one side of the skin is not zero (as for any odd mode of a simply supported beam). In that case, the skin turns the reference beam into a very efficient sound radiator (this can be an interesting feature only if it is desired to increase the radiated sound power).

- For the $5^{th}$ mode of the reference beam (174Hz), the coupled structure has a smaller displacement value than the reference beam. The displacement of the skin is influ-

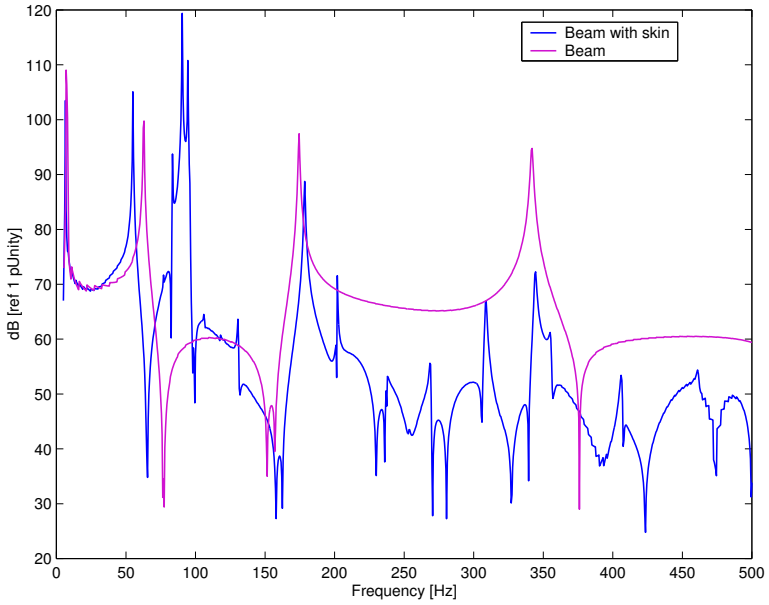


Figure 5.20: Sound power radiated for hand designed skin

enced by the modal behavior of the beam, i.e. the main envelop is based on the modal shape of the 5th mode for a simply supported beam (c.f the curve for the reference beam). However, this modal pattern is disturbed by the skin dynamics and the displacement curve is modified around the peaks of the mode shape (the envelop of each of these peaks is reduced, and thus the net volume velocity is reduced). The reduction of the displacement amplitude and the modification of the mode shape around the peaks yield to a good sound power reduction (28.8dB) at that frequency.

- For the reference beam $7^{th}$ modal frequency (343Hz), the skin does not have a pattern similar to the reference beam. There are more spatial periods in the skin than in the reference beam, i.e. the bending wavenumber in the coupled skin is higher than the bending wavenumber in the reference beam. Thus, the coupled structure is acoustically slower than the reference beam and is a less efficient sound radiator.

Attenuations over various frequency bands are computed in table 5.2. From 100 to 500Hz, the 2-layer structure radiates more than 10dB less than the single beam. In the [0-500]Hz frequency band, the coupled structure is a better sound radiator than the reference beam (8.0dB amplification). Thus, most of the amplification created by the layered structure is concentrated in the [50-100]Hz frequency since in the [5-50]Hz frequency band, the coupled structure radiates less sound than the reference beam.

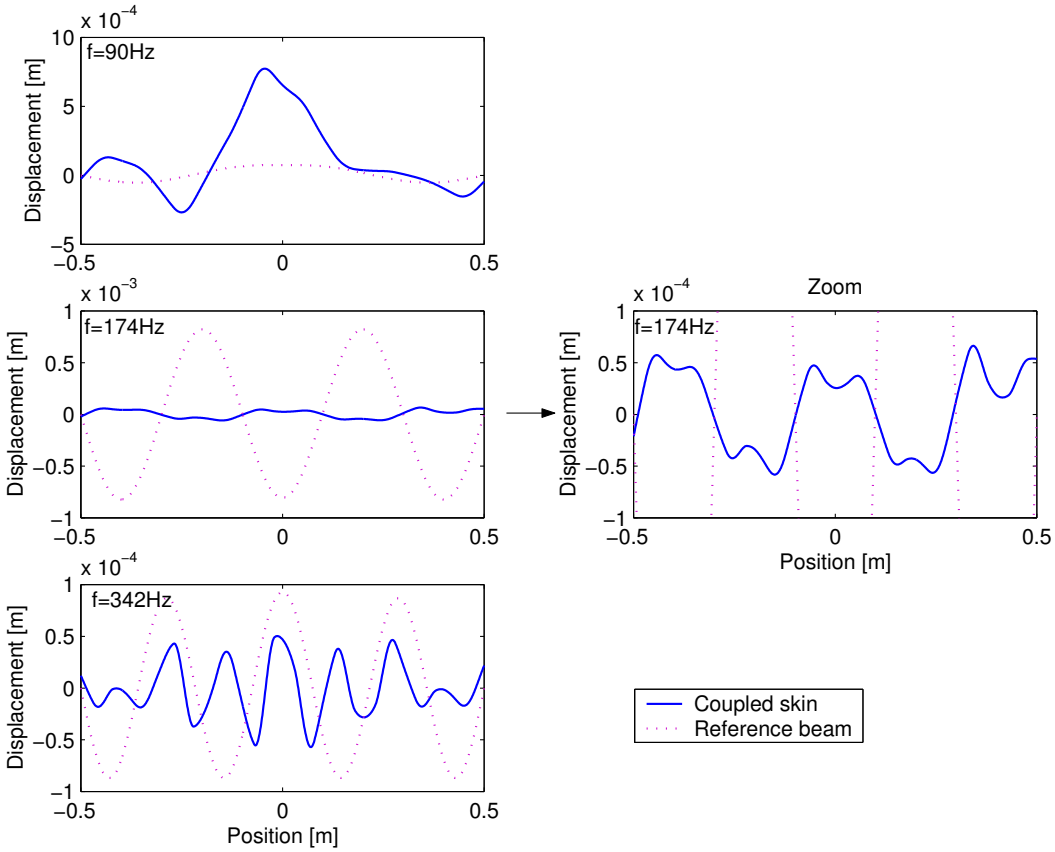


Figure 5.21: Skin displacements at various frequencies (manual design)

Table 5.2: Sound power attenuation for a beam loaded with the "manually" designed skin

| Frequency band [Hz] | 5-50 | 0-500 | 100-500 |
|---|---|---|---|
| Attenuation [dB] | 7.4 | -8.0 | 11.8 |

### Results for an all-mode-excited case

The main setup only takes into account odd modes. Thus, if the cross-section of the skin is symmetric with respect to the excitation point, only odd modes will be excited in the skin. In our case, the manually designed skin does not have a symmetrical pattern (see figure 5.19). To check what happens when both odd and even modes are present in the beam, the structure is excited through the beam at $x = 0.2$.

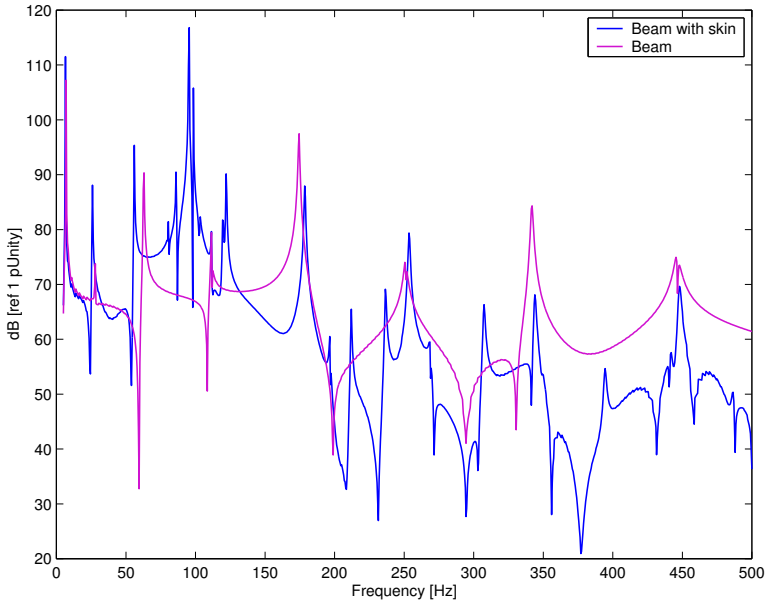


Figure 5.22: Sound power radiated for hand designed skin - all modes excited

Simulation of the power radiated by the structure are presented in figure 5.22. The coupled structure sound radiation is influenced by the modes of the beam as well as the dynamics of the skin. In the skin stopping band ([134-203]Hz), the coupled structure is a less efficient sound radiator than the beam. Around the $5^{th}$ mode (174Hz), the peak of radiated sound power becomes narrower and smaller when the skin treatment is applied. Under 110Hz, the layered structure does not work as well as the middle-excited system as the first four modes become more efficient sound radiators than for a beam. In addition, the coupled system radiates a lot of sound between 75 and 110Hz. Thus, the skin treatment should not be used in that frequency band.

Attenuations over various frequency bands are presented in table 5.3. From 100 to 500Hz, the coupled structure radiates about 4dB less than the single beam. Thus, the structure does not perform as well as for the case where only odd modes are excited in the beam (11.8dB attenuation. See table 5.2). This is a result of the large peak of energy radiated

by the coupled structure in the [70-110]Hz frequency band. If we consider the radiated sound power in [110-500]Hz band, 5.7dB of attenuation can be achieved with the skin. This difference in performance is a result of the difference of behavior in the [175-350]Hz frequency band. For the case where all modes are excited, figure 5.22 shows that the coupled structure behaves closely to the beam whereas for the case of the beam excited at $x = 0$ (see figure 5.20), the coupled system is a less efficient sound radiator than the beam. In the [0-500]Hz frequency band, the coupled structure is a more efficient sound radiator (10dB amplification) than the beam because of the strong peaks of sound radiation below 110Hz.

Table 5.3: Sound power attenuation for a beam loaded with the "manually" designed skin - all modes excited

| Frequency band [Hz] | 100-500 | 110-500 | 0-500 |
|---|---|---|---|
| Attenuation [dB] | 4.0 | 5.72 | -10.3 |

### 5.3.3 Optimized skin

The "manual" design does not take into account the coupling between the beam and the skin (the skin is designed separately). Thus, skins in this section are designed by considering the coupled system and the radiated sound power by the skin. The genetic algorithm (see section 3.2) is used to find the skin structural period. As good sound radiation control can be achieved for frequencies above 100Hz with a "manual" design, structures are only optimized for frequencies below 100Hz.

#### 1-parameter optimization

The design area for sound reduction is set around the first mode of the beam [5-15]Hz. Three different simulations are run in order to see the influence of the following parameters:

- The skin cross-section. The skin is a succession of 10-segment sequences. Each sequence has a length of 0.1m and is connected at its right end to the beam by a spring of 1000N.m$^{-1}$. The overall weight of the skin is kept close (15% lighter) to the weight of a skin that would have a uniform thickness $h = 0.001$m (as in the next two other simulations).
- The spacing between the suspending springs. There is a 1000N.m$^{-1}$ spring at the junction of any sub-elements of the skin.

- The stiffness. The 10-segment based skin is coupled to the beam by springs at each junction of the skin sub-elements. The cross-section of the skin is constant (0.001m thickness).

The radiated sound powers in the design region ([5-15]Hz) ares computed using equation (1.43) in the [5-15]Hz frequency band. Results are presented on figure 5.23. In the design region, there is no significant difference in radiated power levels for the three optimized cases: the coupled structures have shifted down 0.5Hz the peak of radiated power corresponding to the $1^{st}$ mode and they provide about 12dB of attenuation for that peak. Since the skins have approximately the same weight, we conclude that the first mode radiation is mainly controlled by the added mass and not the skin dynamics.

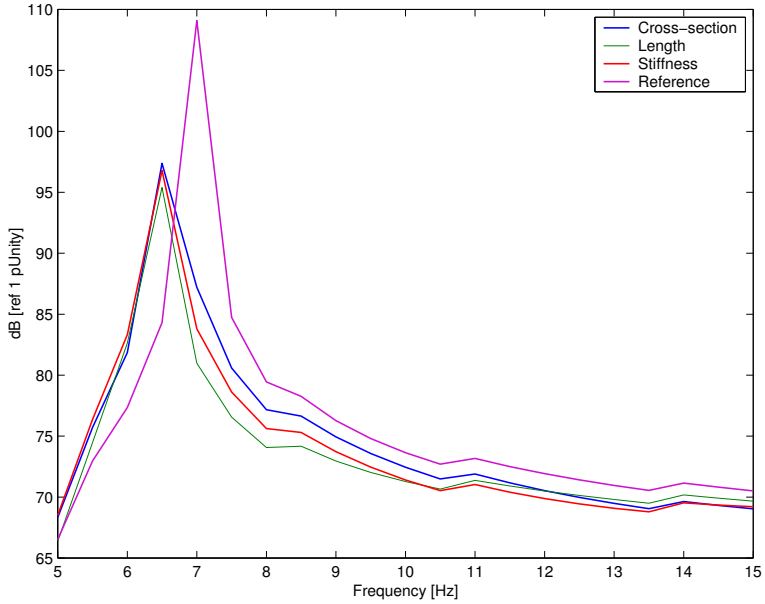


Figure 5.23: Sound power radiated for various 1-parameter optimized cases - design region

Figure 5.24 presents the radiated sound power for the [0-500]Hz frequency band. For frequencies above 50Hz, the sound radiated by the optimized cases have different trends as a result of different skin dynamics. Between 80Hz and 150Hz, each system has high power peaks that do not correspond to any of the beam modal frequencies. Above 150Hz, the length-optimized and the thickness-optimized designs radiate less sound than the reference beam but the beam loaded with the cross-section optimized skin shows more small resonances resulting from the coupling with the beam and the skin resonances. Above the reference beam $5^{th}$ modal frequency (174Hz), the stiffness-optimized design usually radiated less than the reference beam except around 202Hz and 386Hz where two peaks of radiated sound power occur.

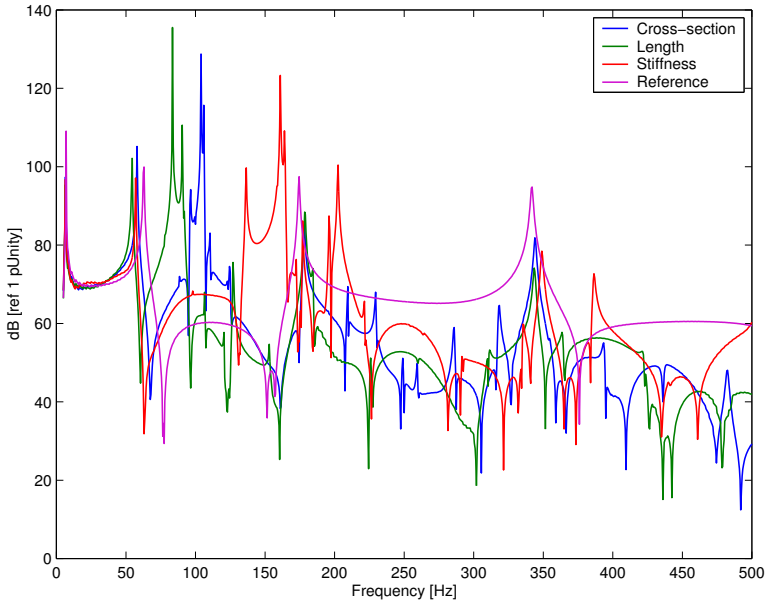


Figure 5.24: Sound power radiated for various 1-parameter optimized cases - 0-500Hz

Table 5.4 summarizes different attenuations. In the design region ([5-15]Hz), the different optimized cases achieve approximately the same reduction of the radiated sound power (for all three optimized cases, the power plot responses are similar). In the [0-500]Hz frequency band, the coupled structures radiates more sound than the reference beam. The structure optimized with spring optimized skin has the smallest amplification (12.7db) mainly because the high level power peak in the [50-200]Hz frequency band was lower than the power peaks of the two other optimized cases in that same region.

Table 5.4: Sound power attenuation for a beam loaded with various 1-parameter optimized skins (10-segment sequence)

| Frequency band [Hz] | 5-15 | 0-500 |
|---|---|---|
| Thickness [dB] | 10.9 | -17.7 |
| Spacing [dB] | 13.0 | -24.1 |
| Stiffness [dB] | 11.6 | -12.7 |

### 3-parameter optimization

The genetic algorithm optimization is now run to reduce the radiated sound power of the structure in the [0-100]Hz frequency band. Skin parameters that can be modified to enhance the response of the system are the sub-element thickness $h_i$, the spacing $l_i$ between two consecutive springs and the coupling stiffness values $s_i$. One structural period of the skin coupled with the reference beam is schematically presented on figure 5.25. The resultant skin is presented on figure 5.26.

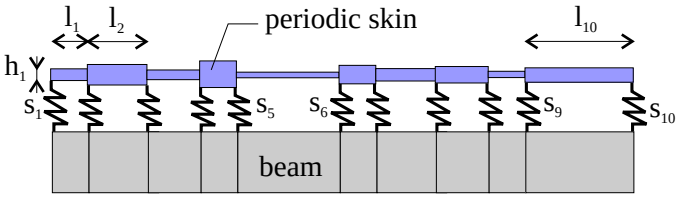


Figure 5.25: Structural period of the beam loaded with an optimized skin

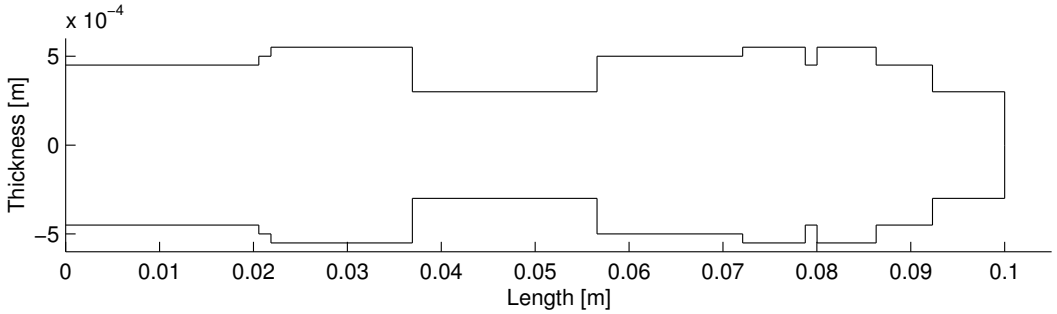


Figure 5.26: Resultant skin - 3-parameter optimization

The radiated sound power in the design region is computed using equation (1.43) and presented on figure 5.27. The sound power at the first mode (7hz) is attenuated by 11.1dB. The reference beam third mode (63Hz) is shifted down 6Hz when the skin is coupled to the beam. Comparing the peak values for with and without the skin, attenuation provided by the addition of the skin is only 1.7dB.

The radiated sound power in the [0-500]Hz frequency band is presented on figure 5.28. The layered structure behaves like the beam up to 200 Hz except that coupled system resonances for the $3^{rd}$ and $5^{th}$ modes are shifted down a few Hertz. In the [200-260]Hz frequency band, the layered structure radiates much more power than the beam. There are peaks of radiated sound power similar to the ones occurring at lower frequencies for the manual design (between 80 and 98Hz) or for the 1-parameter optimization cases (between

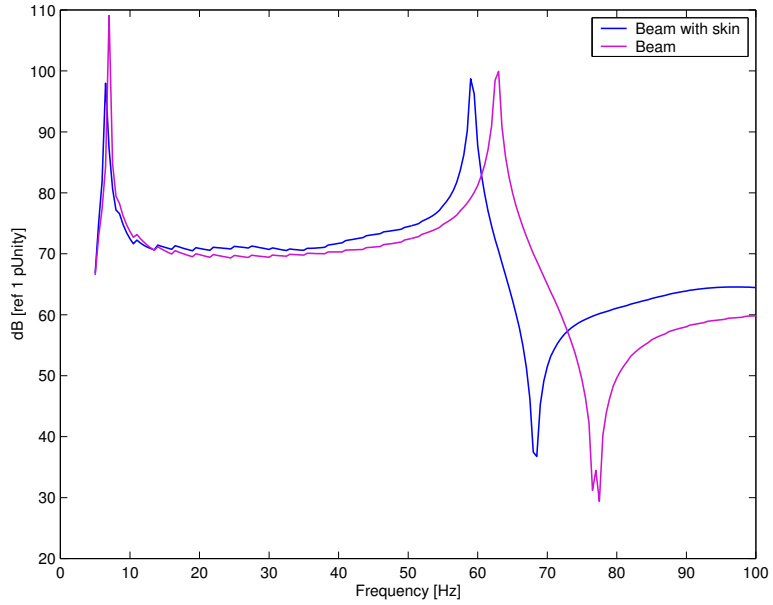


Figure 5.27: Sound power radiated by the coupled structure with a 3-parameter optimized 10-sub-element sequence - [0-100]Hz

70 and 120Hz for the length or the thickness optimized sequences). This confirms that the skins dynamics have an effect on the couple system response above a certain frequency. For frequencies above 300Hz, the coupled structure radiates almost as much sound power than the reference beam.

Vibrational shapes of both the reference beam and the smart skin coupled with the reference beam are presented in figure 5.29 for various frequencies.

- At 7Hz, the coupled structure radiates less sound than the reference beam. The vibrational shapes are identical and sound reduction is only achieved by a lower skin displacement. This is a direct result of the added skin mass.
- At 110Hz, the coupled structure is acoustically slower than the reference beam but since the displacement of the layered structure is much larger than the displacement of the reference beam, the coupled system radiates 5dB more of sound power.
- For the reference beam $7^{th}$ modal frequency (342Hz), both responses have approximately the same displacement amplitude. However, the skin does not have a pattern similar to the reference beam. There are more spatial periods in the skin than in the reference beam, i.e. the bending wavenumber in the coupled skin is higher than the

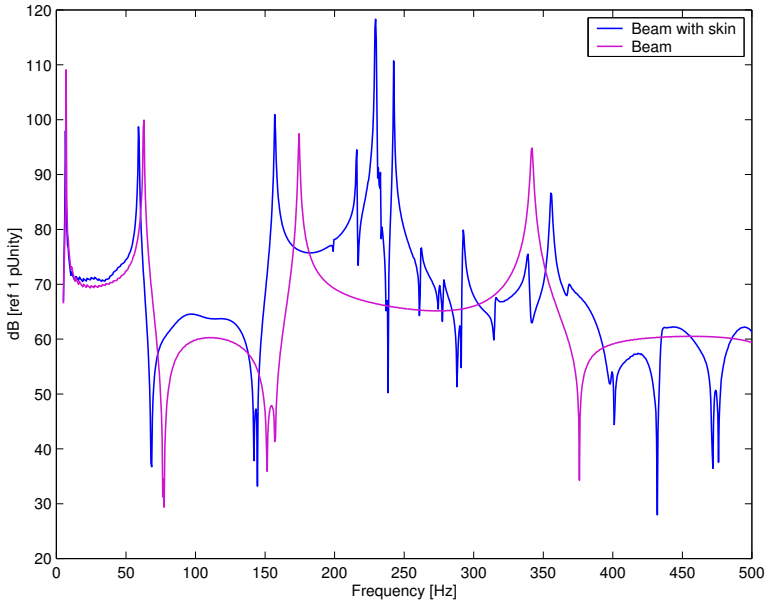


Figure 5.28: Sound power radiated by the coupled structure with a 3-parameter optimized 10-sub-element sequence - [0-500]Hz

bending wavenumber in the reference beam. Thus, the coupled structure is acoustically slower than the reference beam and radiates less sound at that frequency.

Table 5.5 summarizes the radiated sound power in different frequency bands. In the design region ([0-100]Hz), the attenuation is "only" 6.4dB and this is mainly due to the reduction of the power radiated around the first mode (10.4dB). This reduction is on the order of the reduction obtained in the 1-parameter optimization cases. Thus, this attenuation is a result of the added mass by the skin. Overall ([0-500]Hz band), the layered-structure radiates more than the beam (10.9dB amplification) as the layered structure is a very efficient sound radiator in the [150-300]Hz frequency band with pronounced power peaks.

Table 5.5: Sound power attenuation for a beam loaded with a 3-parameter optimized skin (10-sub-element sequence)

| Frequency band [Hz] | 5-15 | 5-100 | 0-500 |
|---|---|---|---|
| Attenuation [dB] | 10.4 | 6.4 | -10.9 |

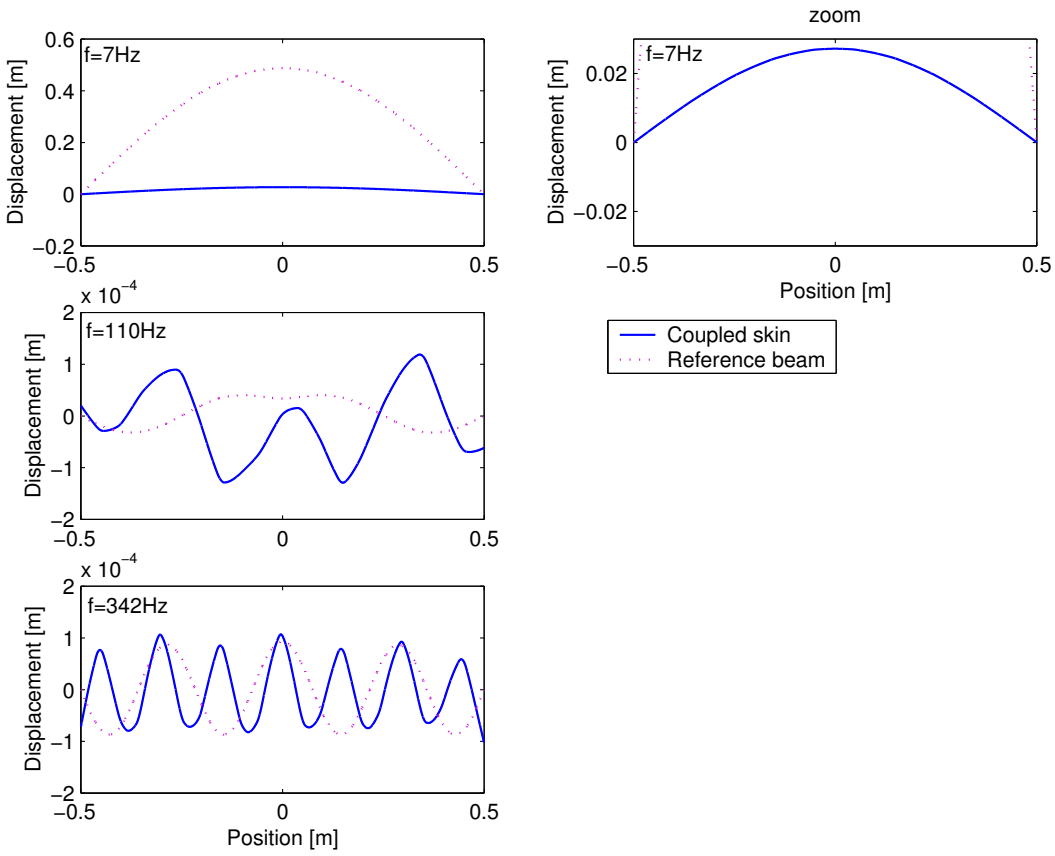


Figure 5.29: Skin displacements at various frequencies (optimized design)

### Remarks

The spring spacings has a critical role at high frequencies. For example, if at a certain frequency, the bending wavelength $\lambda_b$ in the beam is equal to the distance between the suspending springs, the top layer will be excited as a piston, making the structure a very efficient sound radiator (see figure 5.30).

The manual design has shown some very good results in the [100-500]Hz frequency band. Such case could easily be optimized using genetic algorithm. However, computations would require a long processing time (over 1 month of calculations with a 700MHz personal computer in 2001). For frequencies below 100Hz, light periodic smart skins achieved control of the first mode of the beam by adding mass to the overall system. Therefore, smart periodic skins show some encouraging simulation results for sound radiation control above 100Hz, while also reducing the radiated sound power from the first mode by mass-loading effect.

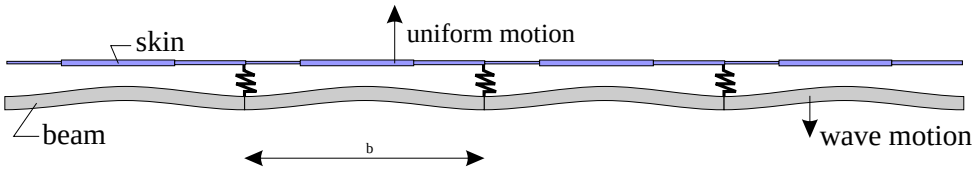


Figure 5.30: Importance of spring spacing in the skin design

# Conclusions and future work

The aim of this work was to investigate the potential of periodic structures, and more specifically subsonic periodic smart skins, in order to achieve sound radiation control for both finite and infinite structures. Theories and numerical tools for predicting the bending wavenumbers in infinite periodic beams were reviewed and an extension was made to consider the case of infinite multi-layered periodic structures (this includes the case of a beam loaded with a periodic skin). Furthermore, two different methods were used to design the sequence defining the periodic structures: Galois sequences and an optimization process using a real-valued genetic algorithm. This optimization technique found the geometry of the structural period that best fits the application. Since sound radiation control is achieved in different ways depending on wether the structure is finite or not, two different objective functions were defined. Finally, various simulations were performed for periodic beams and periodic skins coupled to uniform beams in both finite and infinite configurations in order to study their potential for sound radiation control.

General conclusions drawn from this research can be presented as follows:

- Periodic skins showed very promising results for application to the structural radiation problem for frequencies higher than approximately 100Hz. Approximately 10dB of radiated sound power attenuation was achieved without optimizing the skin performance.
- The structural period defining the periodic structure should be made long and with a large number of sub-element in order to achieve good sound radiation control.
- Galois sequences were successfully used to design periodic structures. These sequences have many wide stopping bands that prevent bending waves to propagate in an infinite structure.
- A simply supported periodic beam is not an efficient sound radiator within its stopping bands. A beam with a structural period based on a Galois sequence showed 10dB and 10.8dB radiated sound power attenuation in its stopping bands, [38-117] Hz and [328-477]Hz respectively.

- The modal frequencies of a simply supported periodic beam are shifted down compared to the modal frequencies of a uniform beam made with the same material and with the same weight.
- A subsonic periodic skin can turn a simply supported beam into a poor sound radiator if the bending wavenumber corresponding to the skin dynamics dominates the response of the skin.
- Sound radiation control provided by periodic light skins below 100Hz is only due to the added mass.

## Recommendations for future work

Recommendations for future work include:

- In order to improve the efficiency of the periodic skin for sound control, one could investigate an active-passive device. This could be done by suspending the skin to the beam with active springs (made with piezoelectric stacks for example). Therefore, if the excitation frequency is known, a variable stiffness would certainly enhanced the structure performance by either coupling or decoupling the moving structure (the beam) from the radiating layer (the skin).
- It may be interesting studying multi-layered structures. The methods presented here allow to build models for structures with more than 2 layers. By superposing many layers, it may be possible to increase control by designing each layer for a different mode of the beam.
- If the coupling between the smart skin and the structure is weak, the enclosed air dynamics between the structure and the skin may largely influence the response of the system. Thus, effects of gas pumping should be included in the model.
- Experimental verification of the simulation results should be carried out.
- The analysis of smart skin should be extended to 2-dimensional structures, e.g. plates.

# Bibliography


[1] Philip A. Nelson and Steve J. Elliott. *Active Control of Sound*. Academic Press, New York, 1992.

[2] S. J. Elliott, I. M. Stothers, P. A. Nelson, A. M. McDonald, D.C. Quinn, and T. Saunders. The active control, of engine noise inside cars. Internoise '88, 1988.

[3] S. Hasegawa, T. Tabata, A. Kinoshita, and H. Hyodo. The development of an active noise control system for automobiles. 1992. Society of Automotive Engineers, Technical paper 922086.

[4] H. Pelton, S. Wise, and W. Sims. Active HVAC noise control systems provide acoustical comfort. *Sound and Vibration*, pages 14–18, July 1994.

[5] D. Gauger. The Bose Headset System: Background, Description and Applications. Bose Corporation, Massachusetts. 1989.

[6] Chris R. Fuller. Experiments on reduction of aircraft interior noise using active control of fuselage vibration. *Journal of the Acoustical Society of America*, 78(S1), 1985.

[7] J. Q. Sun, M. R. Jolly, and M. A. Norris. Passive, adaptive and active tuned vibration absorbers - a survey. *Transaction of the ASME*, 117:234–241, 1995.

[8] M. R. Jolly and J. Q. Sun. Passive tuned vibration absorbers for sound radiation reduction from vibrating panels. *Journal of Sound and Vibration*, 191(4):577–583, 1996.

[9] M. C. Ray, J. Oh, and A. Baz. Active constrained layer damping of thin cylindrical shells. *Journal of Sound and Vibration*, 240(5):921–935, 2001.

[10] Pierre Marcotte, Chris R. Fuller, and Pierre Cambou. Control of the noise radiated by a plate using a distributed active vibration absorber (DAVA). Proc. of Active 99, Fort Lauderdale, Florida, December 1999.

[11] C. A. Gentry, C. Guigou, and C. R. Fuller. Smart foam for applications in passive-active noise radiation control. *Journal of the Acoustical Society of America*, 101(4):1771–1778, 1997.

[12] Brody D. Johnson and Chris R. Fuller. Broadband control of plate radiation using a piezoelectric double-amplifier active-skin and structural acoustic sensing. *Journal of the Acoustical Society of America*, 107(2):876–884, 1999.

[13] Bradley W. Ross and Ricardo A. Burdisso. Low frequency passive noise control of a piston structure with a weak radiating cell. *Journal of the Acoustical Society of America*, 106(1):226–232, 1999.

[14] Miguel C.Junger and David Feit. *Sound, Structures and Their Interaction.* MIT Press, Boston, 1986.

[15] Frank Fahy. *Sound and Structural Vibration.* Academic Press, London, 1985.

[16] A. Berry, J. L. Guyader, and J. Nicolas. A general formulation for the sound radiation from rectangular, baffled plates with arbitrary boundary counditions. *Journal of the Acoustical Society of America*, 88(6):2792–2802, 1990.

[17] C.E. Wallace. Radiation resistance of a baffled beam. *Journal of the Acoustical Society of America*, 51(3):936–945, 1972.

[18] Léon Brillouin. *Wave Propagation in Periodic Structures.* Dover Publications, 2nd edition, 1953.

[19] Charles Elachi. Waves in active and passive periodic structures: a review. *Proceedings of the IEEE*, 64(12):1666–1698, 1976.

[20] Lord Rayleigh. On the maintenance of vibrations by forces of double frequency, and on the propagation of waves through a medium endowed with a periodic structure. *Philosophical Magazine*, XXIV:145–159, 1887.

[21] George W. Hill. *The Collected Mathematical Works of George William Hill.* Carnegie Institute, 1905.

[22] E. E. Ungar. Steady state responses of one-dimensional periodic flexural systems. *Journal of the Acoustical Society of America*, 39:887–894, 1966.

[23] D. J. Mead. Free wave propagation in periodically supported, infinite beams. *Journal of Sound and Vibration*, 11(2):181–197, 1970.

[24] D. J. Mead. Wave propagation in continuous periodic structures: Research contributions from Southampton, 1964-1995. *Journal of Sound and Vibration*, 190:495–524, 1996.

[25] M. A. Hawwa. Reflection of flexural waves in geometrically periodic beams. *Journal of Sound and Vibration*, 199:453–461, 1997.

[26] Eric Tassilly. Propagation of bending waves in a periodic beam. *International Journal of Engineering Science*, 25(1):85–94, 1987.

[27] Sen Yung Lee and Huei Yaw Ke. Flexural wave propagation in an elastic beam with periodic structure. *Journal of Applied Mechanics*, 59:S189–S196, 1992.

[28] D. Bouzit and C. Pierre. An experimental investigation of vibration localization in disordered multi-span beams. *Journal of Sound and Vibration*, 187(4):649–669, 1995.

[29] A. S. Bansal. Free waves in periodically disordered systems: natural and bounding frequencies of unsymmetric systems and normal mode localization. *Journal of Sound and Vibration*, 207(3):365–382, 1997.

[30] Émile Mathieu. *Traité de physique mathématique*, volume 1. Gauthier-Villars, Paris, 1873.

[31] G.Floquet. Sur les équations différentielles linéaires à coefficients périodiques. *Annales École Normale Sup.*, 12:42–89, 1883.

[32] Erwin Kreyszig. *Advanced Engineering Mathematics*. John Wiley, 7th edition, 1993.

[33] Sen Yung Lee and Huei Yaw Ke. Free vibrations of a non-uniform beam with general elastically restrained boundary conditions. *Journal of Sound and Vibration*, 136(3):425–437, 1990.

[34] Manfred R. Schroeder. *Number Theory in Science and Communication*. Springer, Berlin, 3rd edition, 1997.

[35] David E. Goldberg. *Genetic Algorithms in Search, Optimization, and Machine Learning*. Addison-Wesley, Reading, Massachusetts, 1989.

[36] Alden H. Wright. Genetic alogithms for real parameter optimization. In Gregory J. E. Rawlins, editor, *Foundations of Genetic Algorithms*, pages 205–218. Morgan Kaufmann, 1991.

[37] H. Mühlenbein, M. Schomisch, and J.Born. The parallel genetic algorithm as a function optimizer. *Parallel Computing*, 17:619–632, 1991.

[38] Julius S. Bendat and Allan G. Piersol. *Random Data*. John Wiley & Sons, 2nd edition, 1986.

# Appendix A

# Response computation of a finite multi-layered structure

This appendix describes how the normal displacement of each layer of a multi-layered structure can be computed. Considering a finite multilayered structure, the system can be described in a matrix form such that

$$\mathbb{L}\{H\} = \{F\} \tag{A.1}$$

where:

- $\mathbb{L}$ is a matrix built with the equilibrium equations at each sub-element interface in each layer. It takes into account the interactions between the layers (see page 66). $\mathbb{L}$ has the form:

$$\mathbb{L} = \begin{bmatrix} [\mathbb{N}_1 + \mathbb{S}_1] & \mathbb{T}_{2\to1} & \cdots & \mathbb{T}_{n\to1} \\ \mathbb{T}_{1\to2} & [\mathbb{N}_2 + \mathbb{S}_2] & \ddots & \vdots \\ \vdots & \ddots & \ddots & \mathbb{T}_{n\to n-1} \\ \mathbb{T}_{1\to n} & \cdots & \mathbb{T}_{n-1\to n} & [\mathbb{N}_n + \mathbb{S}_n] \end{bmatrix} \tag{A.2}$$

  $\mathbb{T}$ and $\mathbb{S}$ are defined in section 5.2.1 and $\mathbb{N}$ is a matrix describing the continuity

equations along one layer (see page 28). $\mathbb{N}$ has the form:

$$\mathbb{N} = \begin{bmatrix} -\mathbb{E}_1(x_0) & 0 & 0 & 0 & 0 & 0 & 0 \\ \mathbb{E}_1(x_1) & -\mathbb{E}_2(x_1) & 0 & 0 & 0 & 0 & 0 \\ 0 & \mathbb{E}_2(x_2) & \ddots & 0 & 0 & 0 & 0 \\ 0 & 0 & \ddots & -\mathbb{E}_i(x_{i-1}) & 0 & 0 & 0 \\ 0 & 0 & 0 & \mathbb{E}_i(x_i) & -\mathbb{E}_{i+1}(x_i) & 0 & 0 \\ 0 & 0 & 0 & 0 & \mathbb{E}_{i+1}(x_{i+1}) & \ddots & 0 \\ 0 & 0 & 0 & 0 & 0 & \ddots & -\mathbb{E}_n(x_{n-1}) \\ 0 & 0 & 0 & 0 & 0 & 0 & \mathbb{E}_n(x_n) \end{bmatrix} \tag{A.3}$$

- $H$ is a vector regrouping the unknown coefficients $A_i$, $B_i$, $C_i$, $D_i$ (see page (9)) for each sub-element $i$.
- $F$ is a vector describing external excitations to the the finite structure.

Note: If we consider a non-layered structure, e.g. a beam, equation (A.1) is equivalent to equation 2.22.

## A.1 Boundary conditions

### A.1.1 Finite end

Applying the boundary conditions at a finite end of a layer is achieved by removing two "useless" equilibrium equations (this is equivalent to removing the corresponding rows of matrix $\mathbb{L}$). The most common boundary conditions are:

- Free end. The force and the moment created by the beam bending are known. Thus, the displacement and slope equations are discarded.
- Clamped end. The beam displacement and slope are known and cannot be modified. Thus, the moment and force equations are discarded.
- Simply supported end. The displacement and the moment resulting from the beam bending are known. Thus the slope and the force equations are discarded.

### A.1.2 Infinite end

Simulating an infinite end is achieved by adding a semi-infinite uniform element. Since only discontinuities modify propagating and evanescent waves and since no reflection occurs at the infinite side of the semi-infinite element, only waves going in one directions are considered, i.e. the ones coming from the finite side. This is presented in figure A.1 (it is assumed that no wave propagates from the infinite sides). Therefore, adding an infinite end is equivalent to adding four equilibrium equations and only two unknown variables to the matrix $\mathbb{L}$.


Figure A.1: Existing waves in semi-infinite elements

## A.2 System response

Once the boundary conditions are applied at the ends of each layer, $\mathbb{L}$ becomes a square matrix and it can be inverted if and only if $\det \mathbb{L} \neq 0$. In that case, the unknown vector $H$ is found using

$$\{H\} = \mathbb{L}^{-1}\{F\} \tag{A.4}$$

Thus, knowing the $A_i$, $B_i$, $C_i$, $D_i$, one can compute the normal displacement at any point $x$ of a sub-element with

$$w_i(x,t) = [A_i e^{-jk_{b,i}x} + B_i e^{-k_{b,i}x} + C_i e^{jk_{b,i}} + D_i e^{k_{b,i}}]e^{j\omega t} \tag{A.5}$$

where $k_{b,i}$ is the bending wavenumber of the $i^{th}$ sub-element.

# Vita

Arthur Blanc was born at the bottom of the French Alps in May 1977. After graduating with honors from high school in 1995, he joined Université de Technologie de Compiègne (UTC). As part of his curriculum, he spent one year at the Applied Acoustics Laboratories of Chalmers University (Göteborg, Sweden). As Sweden was too dark in the winter, he went to Virginia Tech in the Fall of 1999 while in his last year at UTC. Financial support came from graduate research assistantships provided by the Vibration and Acoustics Laboratories on projects funded by the US Air Force and NASA. In October 2000, he earned his Diplôme d'ingénieur from UTC in Mechanical Engineering with a specialization in acoustics and vibrations. He completed his master of science degree at Virginia Tech in July 2001. Starting Fall 2001, he will pursue a doctorate of philosophy in Mechanical Engineering at Purdue University.